TÉCNICO LISBOA

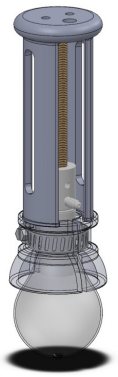

Development of Shape Memory Alloy Actuated Gripper using Jamming Granular Effect

Miguel Santos Ramalho

Thesis to obtain the Master of Science Degree in

Mechanical Engineering

Supervisors: Prof. João Carlos Prata dos Reis
Eng. Ricardo Jorge Torres Marcelino de Oliveira Carvalho

Examination Committee

Chairperson: Prof. Paulo Jorge Coelho Ramalho Oliveira
Supervisor: Prof. João Carlos Prata dos Reis
Member of the Committee: Prof. Mário António Ramalho

September 2020

To my girlfriend, family and friends

Acknowledgments

First of all, I would like to thank all my thesis supervisors. Their availability was extraordinary. Even when they were overwhelmed with work, they always found a slot available for me.
Prof.'s João Reis guidance, patience, experience and out of the box solutions were crucial to the development and conclusion of this work. Eng. Ricardo Carvalho had the ability to calm me down when the results were not as expected. Eng. Ricardo also made sure to give important and constant feedback which proved essential.
Dr. Joana Fonseca proposed out of the box solutions and fast thinking where really helpful especially when I was having trouble giving a hot vapour bath to the 3D printed parts.
I also would like to thank Inês Castro, Luís Oliveira and the Design team (Miguel, Filipe, Paulo and Pedro) that helped and worked alongside me in CENTI's laboratory. At IST's laboratory of control, automation and industrial informatics there are important mentions like Mr. Luís Raposeiro, Eng. Camilo Christo who found the availability to help when I needed.
There were also IST's laboratory colleagues that helped while listening and giving ideas and even finding solutions to latex issues. This group of people include André Pacheco, André Passos, Pedro Outeiro, Guilherme Kano, João Carreira, Mario Torres, Daniel Leite, Rui Assis, Tiago Andrade, André Pires, Luís Duarte, Manuel Morais, Manuel Rego, João Gonçalves.
Finally, I would like thank to my family and my girlfriend support which made all of this possible.

Resumo

Actualmente, a robótica é uma das indústrias mais importantes. A maioria das implementações de garras robóticas usa peças rígidas o que implica várias limitações. Garras baseadas no conceito robótica macia (soft robotics) apresentam soluções para estas limitações. Algumas delas são consideradas garras universais, pois são muito mais versáteis, agarrando com sucesso objetos independentemente da sua forma (e.g. moedas circulares) e até objetos frágeis (e.g. ovos). No entanto, muitos desses projetos dependem da pressão do ar, o que requer a instalação de pesados aparelhos adicionais.

Este trabalho incluiu o projeto, a construção e a validação de um novo mecanismo de atuador para uma garra universal de robótica macia (soft robotics). O conceito desenvolvido baseia-se numa garra que funciona com base no *jamming granular effect*, do mesmo tipo da desenvolvida em [1], mas incorporando um mecanismo de geração de vácuo num circuito pneumático fechado que a torna independente de dispositivos externos. Este mecanismo é leve e usa uma liga com memória de forma (SMA) colocada dentro da garra.

SMAs (Shape Memory Alloys) são materiais leves e ”inteligentes” que têm a capacidade de recuperar a sua forma original quando expostos a um estímulo externo como calor ou campo magnético. Os SMAs já foram usados anteriormente como atuadores em aplicações de robótica macia (soft robotics), mas geralmente não têm a forma de uma mola helicoidal, apesar de esta proporcionar maiores deslocamentos.

Para controlar a mola SMA, foi desenvolvido um sistema baseado num microcontrolador.

O protótipo final da garra universal acionada pelo SMA é leve, compacto e conseguiu agarrar com sucesso objectos de formas diferentes (esfera, moeda, cubo).

Palavras-chave: Robótica Macia, SMA, Controlo, Mola, *Jamming Granular Effect*, Liga com Memória de Forma

Abstract

Robotics is one of the most important industries today. Most of robotic grippers implementations use rigid parts which have limitations. Soft robotics grippers are one of the solutions. Some of them are considered to be universal grippers as they are more versatile, grabbing almost any shape object (e.g. circular coins) and even fragile objects (e.g. eggs). However, a lot of these designs are dependent on air pressure which requires additional external and heavy pumps.

This study involves the design, construction and experimentation of a novel actuator mechanism for a soft-robotics universal gripper. The developed concept is based on a gripper that takes advantage of the granular jamming effect. It is similar as developed in [1], with the exception of incorporating a vacuum generation mechanism in a closed pneumatic circuit, making it independent from external devices. In order to produce this vacuum, a light actuation system uses a shape memory alloy (SMA) placed inside the gripper.

Shape Memory Alloys (SMAs) are light ”smart” materials that have the ability to recover their original shape when exposed to an external factor like heat or magnetic field. SMAs have been previously used as actuator materials in soft robotics applications but usually not in the shape of a coiled spring, despite providing greater displacements.

To control the SMA spring, a system based on a microcontroller was developed.

The final SMA actuated universal gripper prototype is lightweight, compact and it was able to grip successfully objects with different shapes (sphere, coin, cube).

Keywords: Soft Robotics, SMA, Control, Spring, Jamming Granular Effect, Coil, Shape Memory Alloy

Contents

List of Tables

List of Figures

Glossary

BHN Brinell Hardness Number gives a measure of the hardness of the material using a sphere to make an indentation

MOSFET Metal–oxide–semiconductor field-effect transistor is a type of insulated-gate field-effect transistor.

NiTi Nitinol is a shape memory alloy made of nickel and titanium discovered by the US Naval Ordnance Laboratory

PWM Pulse-width modulation is a method to change the average power delivered by an electrical signal. This is done by controlling the frequency of turning on and off the signal.

SMA Shape Memory Alloy is a material that is able to recover its shape when subject to an external environment change like temperature or magnetic field

SME Shape Memory Effect is the ability of a material deformed at a low temperature to recover the deformation when subject to external stimuli (magnetic field, chemical reactions or temperature variation)

Chapter 1

Introduction

1.1 Soft Robotics

As Aristotle described all man seek happiness [2]. With this in mind, every generation worked in ways towards a better life quality. In mechanics field, this meant creating apparatus that could replace and ease some of the day to day tasks. As a branch of mechanics, robotics was created to respond to the need for substitutes that could mimic human interactions with the environment [3]. Nowadays, the robotics field is one of the biggest growing industries, according to studies from [4].

Robotics' applications use discrete mechanisms, usually constructed from a series of rigid links. This is important for many industrial applications where the speed of operation and accuracy are essential. However, there are some limitations like weight/portability and safety concerns. On different situations, other features may provide improved performance. To do so, scientists and researchers have recently turned to nature inspired robots (biomimetism or bio-inspired) [5]. The first robots that somehow fitted this definition were called continuous robots. By definition, these robots combine structures that bend continuously along their length via elastic deformation and produce motion through the generation of smooth curves, similar to the tentacles or tongues of the animals. These robots can be divided into 3 categories, intrinsic, extrinsic and hybrid. The first category includes all robots in which movement is created inside the moving part. Extrinsic devices are activated using a mechanism outside the moving part that is then transferred. Hybrid devices use both [5].

Nowadays the field is known as soft robotics and these ”new” found abilities have materialized in many diverse research fields [6]. Some predictions say most of the applications will be used for home assistance or implants as replacements for human limbs. However, as these opinions about the future are not consensual, the research did not focus on a single objective and resulted in a vast series of applications, each with a different objective.

Some relevant examples of the work done in soft robotics is shown in table 1.1. The OCTOPUS robot (figure 1.1 a) used SMAs as transversally actuation system to create the ability to elongate the arm.

These SMA actuators (figure 1.1 b) along with cables allowed for underwater manipulation. This work faced a variety of challenges and pushed forward related areas of research such as [6]:

- modelling and control of continuum structures;
- study of fluidodynamics in continuum structures;
- morphological computation of continuum structures;
- fabrication of stretchable sensitive skin;
- understanding and implementing the sucker adhesion mechanisms in water;
- study of principles for locomotion and swimming.

GoQBot (figure 1.1 c) showed how shape memory alloys can be used to produce a large amount of force in a small time window. The GoQBot moves similar to the caterpillar, rolls up and propels itself with 9.81 m^2/s acceleration and an angular velocity of more than 200 rpm [7].
However, the largest variety of devices and solutions in soft robotic research has been in grasping. RBO Hand 2 and the universal gripper are also worth mentioning. RBO Hand 2 (figure 1.1 d) used silicone pneumatic-based actuators to mimic a human hand [8]. The universal gripper (figure 1.1 e) is explained in detail in section 1.3.

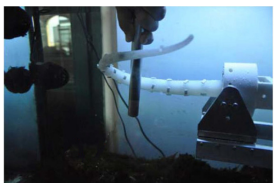

(a) Transverse SMA actuator applied in the OCTUPUS robot (from [9])

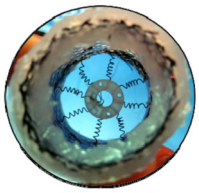

(b) OCTUPUS robot grasping a bar (from [9])

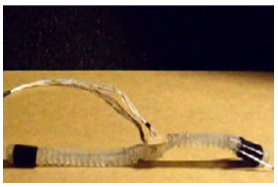

(c) GoQBot actuated in the posterior flex from (from [7])

(d) RBO Hand 2 grasping a round cylinder (from [8])

(e) Positive Pressure Universal Gripper Based on the Jamming of Granular Material (from [10])

Figure 1.1: Resume of important soft robotics applications

.

Table 1.1: Resume of soft robotics advances. Adapted from [6].

Ability	Robot	Technology
Jumping	GoQBot	Fast-contracting SMAs
	Tripedal robot	Pneu-Net powered by combustion
	Hemispheroid robot	Functionally graded and powered by combustion
Peristaltic locomotion	Meshworm	Flexible braided sleeve and SMAs
	Softworm	Flexible braided mesh and tendons
Locomotion through small crevices	Quadrupedal robot	Pneu-Net
	Cockroach-like platform	Origami-style structure
Resilience	Quadrupedal robot	Pneu-Net
Arm elongation and shortening	OCTOPUS robot	Flexible braided sleeve and SMAs
Underwater legged locomotion	OCTOPUS robot	Octopus-inspired pushing by stiffening and elongation Vortex
	PoseiDRONE robot	
Pulsed-jet swimming	PoseiDRONE robot	Vortex rings produced with body squeezing
Stretchability	Sensing skin of crawling robot	HLEC
Climbing	Stickybot	Hierarchical structures, directional adhesion, and control of tangential contact forces
Growing	PLANTOID	Additive manufacturing
Combined bending and stiffening	STIFF-FLOP manipulator	FFAs and granular jamming
Adaptable grasping	RBO Hand 2	PneuFlex actuators
	Universal gripper	Granular jamming phenomenon
Self-deployment	Mechanism	Origami-style structure and shape memory materials HMAs
Morphing, self-reconfigurability Mechanism	Manipulator	HMAs
Self-healing Polyaramid fibers in an elastomeric matrix	Soft pneumatic actuators	DA polymers
Biodegradability and edibility Soft	Actuator	Biodegradable hydrogels

1.2 Shape memory Alloys

1.2.1 Definition

Shape memory alloys (SMA) are materials that are able to recover its shape from large deformation usually performed at lower temperatures (lower than activation temperature). The key difference to other materials is that these deformations can be much larger than the elastic limit of the material. There can be SMA with one-way or two-way memory effect. The one-way memory effect means the shape can only be recovered when heated to higher temperatures. When applied as an actuator, requires an external bias force, either a spring or another SMA, to make the action repeatable. If the two-way memory effect is present the SMA can remember two different shapes. However, their recoverable strain is only about half of the one-way equivalent.

1.2.2 History

Considerable research for modelling the microscopic and macroscopic behaviour of SMAs has been performed in the past fifty years [11].
Authors describe SMAs as a metal alloy that presents shape memory effect (SME). SME was first observed in 1932 in an alloy made of gold and cadmium (AuCd) [12]. Shape memory effect is described as the ability of a material deformed at a low temperature to recover the deformation when subject to external stimuli (magnetic field, chemical reactions or temperature variation) thus producing large strains [13–15].
The breakthrough for engineering applications occurred with the accidental discovery of a nickel-titanium alloy (NiTi-nitinol) by the US Naval Ordnance Laboratory (1961) while investigating materials useful for heat shielding [14, 16–18].
Since the release of the 1965 patent by the US Naval Ordnance Laboratory, the researched blossomed, mostly due to the properties of nitinol [13, 14, 19–21]:

- Inexpensive to produce;
- high force to weight ratio;
- high wear and corrosion resistive;
- large reversible deformations (up to 8%);
- excellent structural and functional properties;
- easy and safer to handle than other SMAs;
- biocompatible and activated with body heat (no external power source);
- compatible with magnetic resonance imaging and computer tomography scanning;
- similarity to biological tissue mechanical response than conventional medical materials.

SMAs properties make them well suitable to applications in controllable shape change, vibration control, and active and semi active damping. As SMAs also have the ability to produce large strains, they have been used as substitutes for piezoelectric materials [13].
Despite all these advantages, SMAs require high currents. They are also difficult to control due to high non-linearity, hysteresis and constraints in frequency. These actuators have limited bandwidth. This means that no high frequencies should be used as they will give non-desirable results. This happens due to the long recovery time from the austenitic phase to the martensitic phase. This slow response is caused by the relatively high heat capacity of the metal [22, 23]. Also, thin SMA wires may pose challenges due to low electrical resistance [24].
In order to cite some of the most important applications of SMAs it easier to lay down some categories: biomedical, aerospace, automotive and robotic.
In biomedical applications, nitinol showed its importance due to the properties mentioned above and

also the ability to perform its function only with body heat (does not require either a power source or external mechanical adjustment) [19]. Some of the most well know applications are orthodontic braces and catheters but new applications of SMA in the biomedical field are still being implemented [19, 25].
Despite all the applications of SMAs in the biomedical industry, one of the earliest implementation of SMAs was in fact in aerospace research industry in 1971. This seems kind of obvious applications because of the alloy's actuation force to weight ratio [21]. Some of the implementations done with SMAs in this field are hingeless ailerons, twistable wings, motors inlet reshapers and motor's noise reduction devices [22, 26].
The automotive industry has mostly used SMAs as low power actuators for comfort and bodywork functions [20]. Some of the implementations are:

- pneumatic valves for lumbar support in car seats;
- actuator to open a hatch vent for easier closing of the trunk lid;
- thermally responsive pressure control valve embedded in automatic transmissions;
- actuated antiglare rear-view (EAGLE) mirror, headlamp actuators, fuel filling lid actuator, and locking mechanism [25].

Finally, another area with SMAs implementations is robotics. Due to all SMA characteristics (biocompatibility, high power to weight ratio, no noise), many robotics implementations take advantages of these alloys abilities as actuators. Some of these systems include artificial muscles, origami robots microscopic grippers and robot prostheses (artificial limbs) [24, 27].
As mentioned above SMA have been used as actuators and even micro-actuators. There are various configurations and shapes such as coil springs, torsion springs, straight wires, ribbons, cantilever strips, and torsion tubes. However, no shapes and or configurations have solved the clamping difficulties [25]. As stated by [28] the coil spring shape provides the largest stroke, thus being preferred in most applications.

1.2.3 Material Phases

SMAs can change between different phases called martensite and austenite. For some specific alloys (eg with iron, cobalt or chromium), another phase called R-phase can also be obtained.
The martensitic phase is a state of the alloy noticeable by its low yield strength compared to its counterpart, the austenitic phase. Similarly, this phase is also characterized by lower shear and Young's modulus. So it is understandable why this phase will transform the same stress applied in a larger deformation of the material than the austenitic phase.
At lower temperatures, the fraction of the material with the martensitic phase is higher and the austenitic fraction phase is lower. In like manner, at higher temperatures, the austenitic fraction is higher and the martensitic fraction (ξ) is lower. The quantity of both phases differs accordantly to the alloy's temperature as we can see by the variation of ξ the with temperature variation in figure 1.2.

Analysing figure 1.2, there are four notable temperature values: M_s, M_f, A_s and A_f. Increasing the temperature above A_s (austenite start temperature) of a fully martensitic sample ($\xi = 1$) increases the austenitic fraction and lowers the martensitic fraction. If the temperature rises above A_f (austenite finish temperature), the sample will enter a fully austenitic state (no martensitic fraction, $\xi = 0$).
On the other hand, decreasing the temperature of a sample in a fully austenitic state below M_s (martensite start temperature) increases the martensitic fraction (ξ) and lowers the austenite fraction. If the alloy's temperature goes bellow M_f (martensite finish temperature), the sample will be only composed by martensite (only martensite fraction, $\xi = 1$).
As can be seen in figure 1.2, this process is non-linear because there is hysteresis between the two previous processes of heating and cooling.

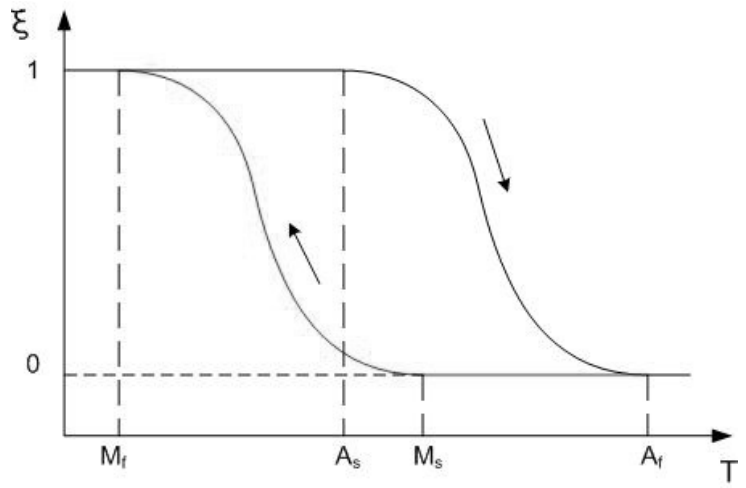

Figure 1.2: Graphic of evolution of martensitic fraction (ξ) with the temperature variation (T). (adaptation from [13])

However, the change in the martensitic fraction is so large with the change of only a few ℃ that we usually consider one temperature called activation temperature (T_{act}) instead of this four temperatures (M_s, M_f, A_s, A_f).

1.2.4 Crystal Structure

Phase changing does not necessarily mean recovering shape. SMA recover from large deformations because of different crystallines structures.

Austenite (β-phase) only has one crystal shape. In contrast, martensite exists in two different crystal structures, twinned (α^+/α^--phase) and detwinned (α^+-phase). Previous to deformation martensite is twinned martensite, after deformation the martensite is called detwinned.

As shown in figure 1.3 the twinned martensite (α^+/α^--phase) is converted in detwinned martensite (α^+-phase) by deformation. In the light of the same figure, it is understandable that upon heating, the martensite (α^+-phase) is replaced by austenite (β-phase). With this temperature rise, the alloy visibly recovers its initial shape before the stress was applied. Again, if the alloy is cooled down the austenite (β-phase) will become detwinned martensite (α^+/α^--phase) without changing the alloy visible macroscopic shape.

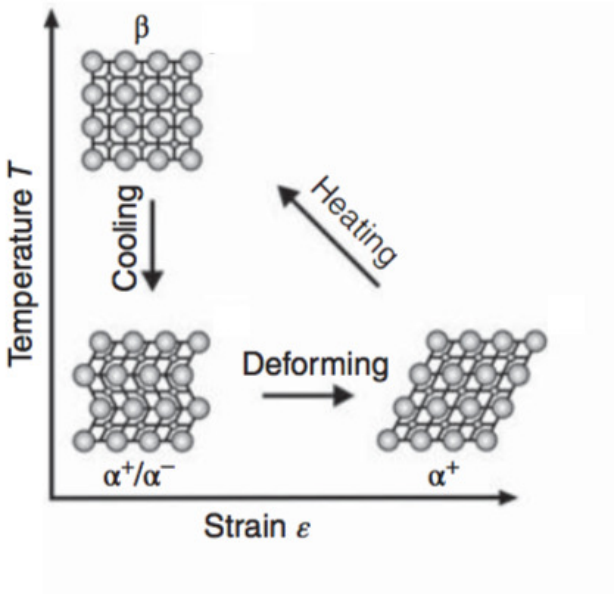

Figure 1.3: Cycle representation of interchanges between the different phase of memory shape alloy due to stress and temperature. (from [14])

1.2.5 Control of Shape Memory Alloys

There have been different approaches to control the highly nonlinear behaviour of an SMA actuator. In [14] a review is made about exploring different techniques like proportional–integral–derivative (PID), fuzzy logics, neural networks, sliding mode control and variable structure control. From this review, it is clear that the main concern is having a good model of the actuator behaviour. As the actuator is subject to variations that occur during the heat treatment, the development of actuator prototypes may require a case by case parameter identification.

As explained in [29], depending on the applications the on-off or ”bang-bang” control can be used to obtain good results. Classical control has been mostly abandoned in research because as stated in [30], the performance is very low and is used for comparison with other control techniques or as the first approach as it was done in [31]. In [32] some work was developed to control the position of a SMA actuator. As most works with this kind of actuation, the actuation is done with pulse width modulation (PWM). The actuator was controlled by a bilinear PID which is a subset of non-linear controllers. BPID is one of the simplest and easiest ways to implement non-linear control techniques. BPID allows to obtain a good system response but at the expense of slightly larger power consumption. BPID imposes greater energy variations that might induce greater functional fatigue decreasing the actuator service life.
In [33] a robot hand similar to the human hand was designed. Each phalanx angular positioning was controlled using SMA with a fuzzy logic based controller. The use of a fuzzy logic control technique does not require detailed knowledge of the elements of the process to be controlled (plant, sensors, actuators, etc.) and is applicable to both linear and non-linear systems. On one hand, fuzzy logic control is quickly implemented at low cost and on the other, it presents characteristics of robustness to uncertainties or parametric variations. The author also describes the errors as permissible for this type of application but still refers to a low response time that could only be solved using a different kind of actuator.
In [34] the author successfully implemented a complex fourth-order strict-feedback nonlinear model which fully describes the system. This alongside an adaptive observer-based output-feedback adaptive neural control method allowed for practical asymptotic stability of the closed-loop system. Experimental results showed superior performance of the proposed SMA actuation control system in terms of tracking accuracy and control bandwidth.
In [35] sliding mode control was used for position control. Results demonstrate that SMC had better tracking capability for a trajectory with higher frequency and less overshoot/undershoot than a simple PID controller. However, due to the highly nonlinear hysteresis effect of SMAs, the response was not completely accurate or fast.
In [23] using variable structure control researchers were able to obtain good positioning accuracy and a high level of stiffness control. VSC is that only requires a few parameters to model the physical system used in the control and is robust to system parameter variation. These properties make VSC a suitable choice for SMA actuators as it is less sensitive to model uncertainties.

1.3 Universal Gripper

In [36] grasping and manipulation are recognized as fundamental functions of robots. In order to overcome the disadvantages of rigid grippers, soft solutions have been developed. With soft grippers it is possible to have more compliance, avoiding damaging shocks between the gripper and object. In this way, it also avoided damage to the desired path and position when manipulating the object. This combined with its simpler mechanic reduces control complexity. On the other hand, the soft grippers cannot house the actuators inside the links as it is done in rigid grippers, increasing the design complexity.

The most commonly used materials in these grippers are elastomers. Silicone rubbers have been the most popular choice because they present ease of fabrication, robustness, low toxicity and relatively low damping. In figure 1.4 it is shown some of the different approaches that have been taken in this kind of grippers.

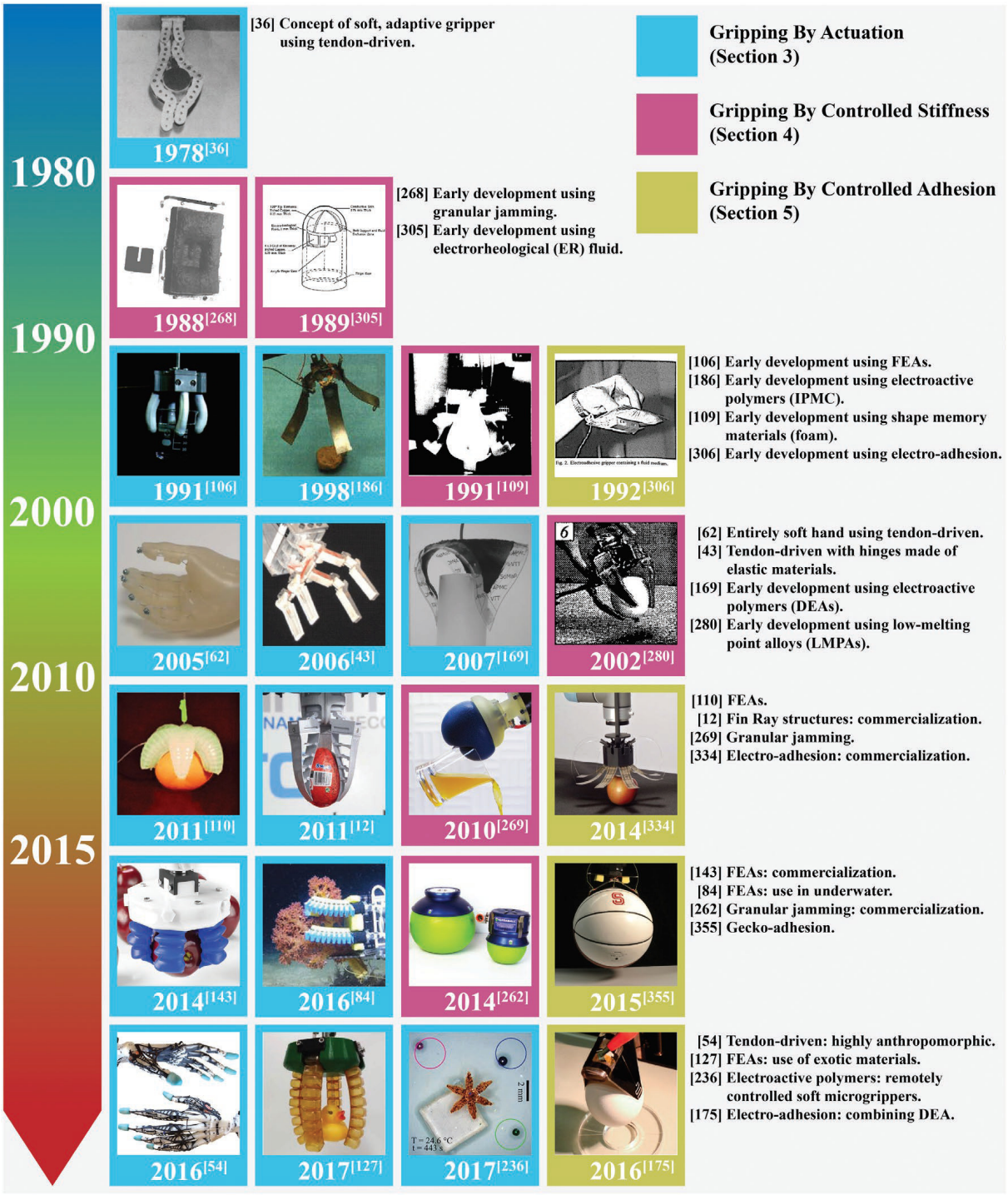

Figure 1.4: Evolution of soft grippers (from [36])

In order to be ready for an industrial market application, a device must prove itself to be reliable and also relatively fast in operation. The main advantage of an universal gripper is to save on precise positioning time when grasping a variety of objects with different shapes, and possibly random orientations. For this advantage to pay off, the operation time of the gripper should not exceed the positioning time of a conventional gripper. Some examples of soft grippers have already reached the market, albeit with different degrees of success. The best examples are the Flexshapegripper® (Festo corporate) and the Versaball® (Empire Robotics). Members of the latter company also published an interesting article about their market experience [37]. Both of them are focused on the idea of a universal gripper, which facilitates compliance, allows to grip a wide variety of arbitrarily shaped object [38].

The origin of the Versaball®is explained in [38]. In 1988, Reinmüller and Weissmantel speculated about the idea of using a single membrane, filled with a material possessing jamming granular properties thus becoming a universal gripper. However, only in 2010 would be shown the high performance of this effect in soft grippers. Some concerns are mentioned in [38] about designing and prototyping Versaball® prototype. The first is design modularity so that the gripper would be easy to replace (service life 1000 grips). In the same manner, all the wear component were included in the head portion of the gripper.

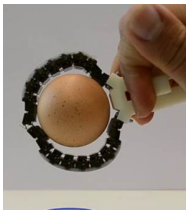

(a) 2017 Tendon-driven origami gripper (from [39])

(b) 2018 Soft pneumatic gripper embedded with stretchable elec–troadhesion (from [40])

(c) 2018 Soft gripper with gecko-inspired adhesive (from [41])

(d) 2019 Vacuum-driven origami gripper (from [42])

(e) 2020 Self-healing gripper with cross-beamed A shaped fingers (from [43])

Figure 1.5: Resume of recent work developed in soft robotics grippers

The second concern was avoiding vacuum pumping systems that may not be available in most industrial facilities. In order to work around this problem, compressed air with a venturi pump was used. Grain size and type also proved to be an important factor. The idea of using an interstitial fluid with grains seemed promising but offered a lot more challenges due to leaks. Further tests proved that gripping is only reliable if the object is between 30 and 70% of the membrane's external diameter. After some research about the size of most industrial application, 9 to 16,5 cm was defined as the most adequate external membrane size diameter.

In [10], the use of both positive and negative pressure on the Versaball® showed increases in both reliability and error tolerance. Some tests with different objects demonstrated the capabilities of this design. Complex gripping problems like picking up flat objects (coins) and fragile objects (eggs) were overcome with this gripper. During this research work, some studies were done to understand the forces involved in keeping the object gripped to the membrane. The main variables in the gripper that affect the grasping capability are the membrane and the granular used inside the membrane. The membrane

used was made of latex (elastomer) as it is easy to buy and provides high friction capability. Different granular materials could be used but the materials like sand would weigh down the gripper or strain the membrane. A lower density material but that still provides the necessary jamming granular effect is milled coffee grains. Some indications about the filling quantity are also provided in the article.

1.3.1 Jamming Granular Effect Gripper

Jamming is the physical process that increases a material viscosity with the increase in density. This physical process is only visible on some mesoscopic materials, such as granular materials, glasses, foams, colloids, and other complex fluids. This phenomenon happens due to the intensification of normal forces between the particles, which results in increased friction amongst the particles [44].
This phenomenon has been proposed as a new phase transition, with similarities to a glass transition. However, it is very different from the formation of crystalline solids [45].
On one hand, the jammed state can resist small applied stresses without plastic deformation. This state is similar to a solid, with a characteristic maximum yield stress. On the other hand, the unjammed state allows flow with low resistance similar to a fluid [44].
As explained in section 1.3 this effect was applied in robotic grippers like [10]. In these grippers, the jamming granular material is closed inside a membrane. While the pressure value inside the membrane is similar to the outside pressure the gripper remains in the unjammed state. When the pressure inside the membrane is lower than the outside pressure, the granular material becomes jammed. An example of the gripping process is shown in figure 1.6.
Accordingly to [10] the grip force occurs due to three gripping modes shown in figure 1.7. The first is static friction from surface contact between the membrane and the object. The second mode depends on the geometric shape of the object, if the object has geometric constraints the membrane will capture the object by interlocking with its shape. The third gripping mode is vacuum suction created when an airtight seal is achieved on some portion of the object's surface.

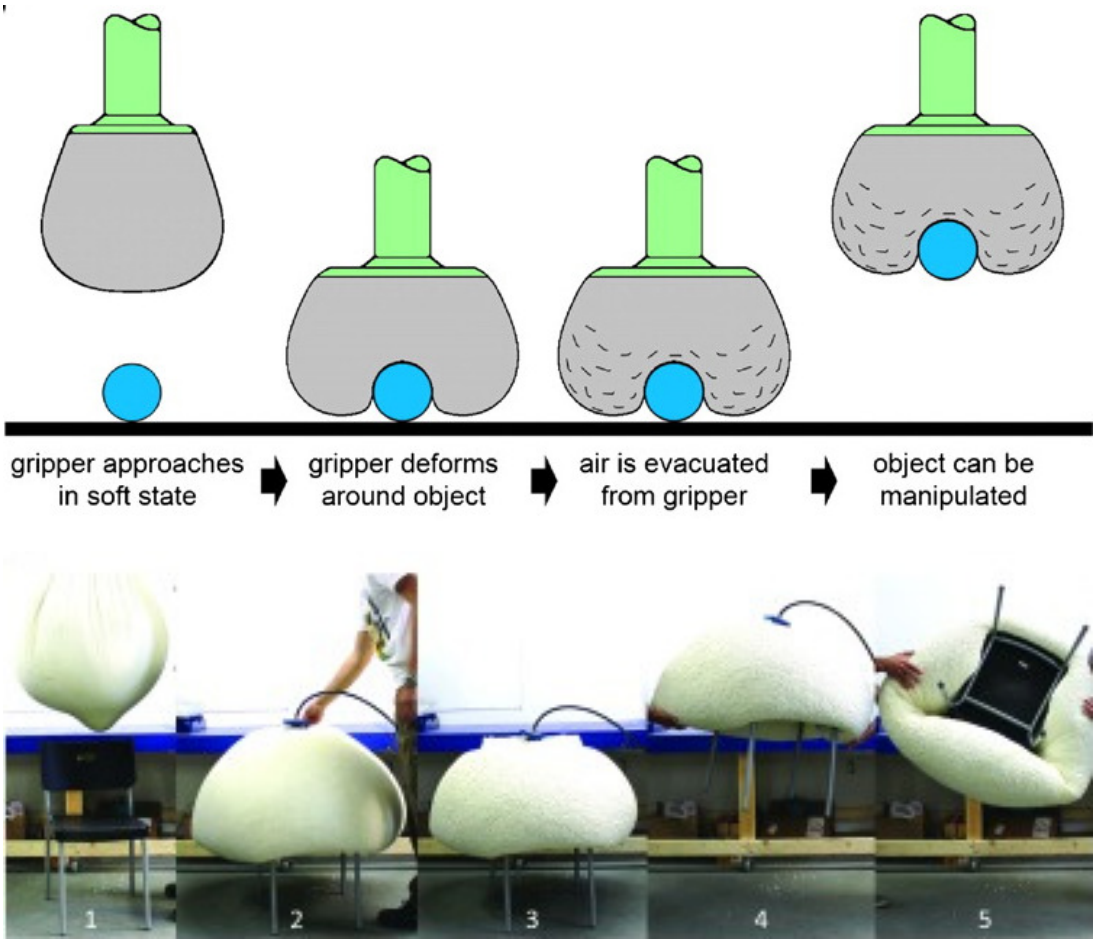

Figure 1.6: Schematic (top) and a very large universal gripper (bottom) gripping an object (from [1] and [38])

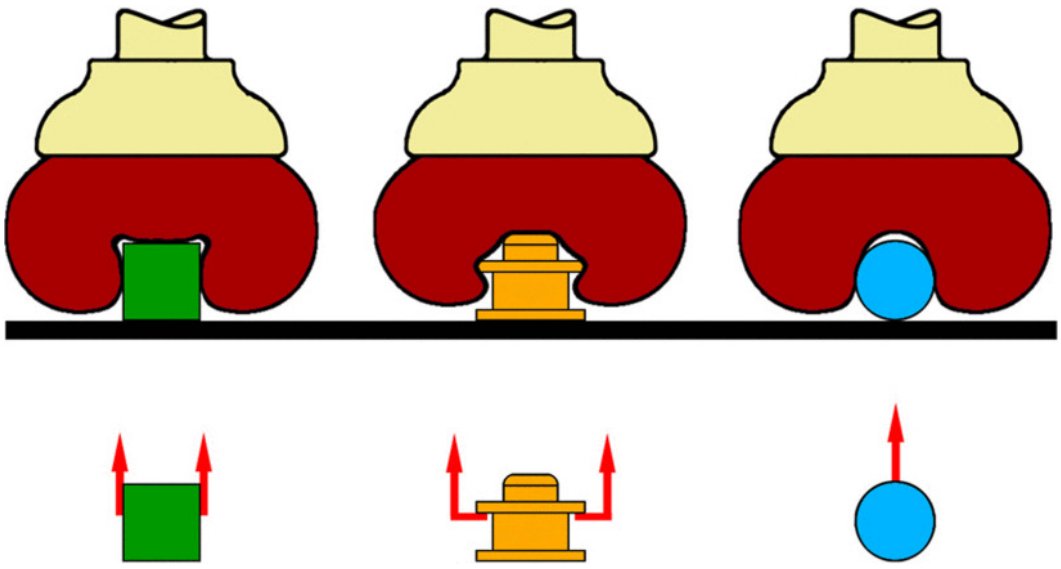

Figure 1.7: Gripping forces applied while gripping an object using a jamming granular effect gripper (from [10]). (Left) static friction on surface contact. (Center) Geometric constraints when interlocked. (Right) Vacuum suction.

1.4 Objectives

The goal of this master thesis is to show the feasibility of a self-contained soft gripper similar to the Versaball® griper described in [38]. Specifically, our version of the gripper contains its own means to produce the required vacuum, eliminating the need for an external vacuum source. This is done with a SMA actuator with only a small increase in the total weight of the gripper. To fulfil this objective the main work was divided into several tasks:

- Choose the best configuration and implementation of a self-contained actuator;
- Design and manufacture the universal gripper;
- Study the best granular material to be applied;
- Design a sensor and actuator control system;
- Test the usability of the gripper.

1.5 Thesis Outline and Contributions

The main contribution is the fact that this gripper needs no external devices and incorporates its own mean of producing the required vacuum, using only volume variation. Showing that a variable volume closed system is a viable approach to this kind of grippers.
In chapter 2, a novel version of an actuation system is presented as well as the process to achieve it. Firstly, the main design goal's are enumerated. Then the selection process of granular material is explained. After this, the design of the novel vacuum system is studied. This chapter also explains the work done to study the actuator properties as well as the fabrication process with tips to produce SMA springs with the minimum pitch. Finally, the chapter ends with the electronics and control system implementation.
Chapter 3 presents the results of the tests done with the prototype gripper and the procedure done to produce these results. Then these results are analysed.
Finally, chapter 4 provides a comprehensive conclusion of the developed work, showing the importance of this work in terms of studying the jamming granular effect, fabricating and applying SMA spring actuators to this kind of devices.

Chapter 2

Design and prototyping

2.1 Design goals

The main objective of this work is to build a self-contained granular jamming gripper that does not need an external compressor. To design a viable option some factors must be taken into account while designing, some of them are weight, size, modularity and easy part replacement.
The final SMA spring actuator should have the least amount of weight while keeping the maximum force and maximum elongation length and also respecting the functional fatigue constraint (strains lower than 4%).

2.2 Design

2.2.1 Jamming Granular Effect

As explained in section 1.3.1 this phenomena requires an increase in density which is done by negative pressure inside the membrane. Therefore, some tests were conducted to find out the order of magnitude of the minimum pressure that would allow a reasonable grabbing. These tests also allowed to identify potential issues and better understand how this effect worked in practice.
For these preliminary tests a version of the universal gripper was assembled using part of a PET bottle, a latex balloon and coarse grains of sodium chloride (commonly known as kitchen salt) applied as the granular material. This gripper was used to grab a 7/16" open end wrench (39 g) (see figure 2.1). The vacuum was created by a 60 ml syringe creating a maximum stable vacuum of 3×10^4 Pa (figure 2.1). The pressure values along time were also recorded.
The first test, consisted of grabbing the object with the max pressure and slowly decreasing the pressure until the object fell off the gripper. The average result was 10^4 Pa.
As for the second test, the objective was trying to pull the object when the pressure was the same as the average obtained on the first test. This would serve as validation and ensure that the grip was successful and not only due to friction between the membrane and the test object.

This confirmed that the minimum acceptable vacuum pressure would be 10^4 Pa. These preliminary tests also showed that air leaks were an important issue to address.

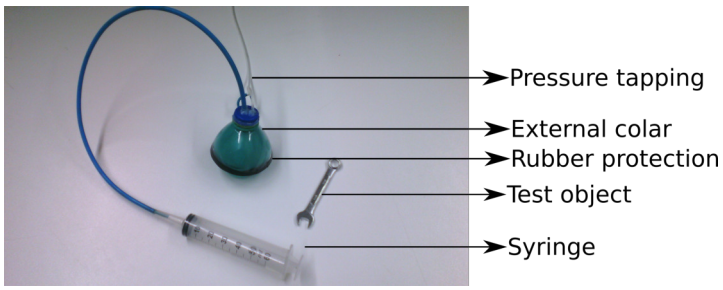

Figure 2.1: Minimum pressure test montage

2.2.2 Selection of Granular Material

The granular material must have three characteristics:

- High Yield strength during the jammed phase;
- Low friction resistance during the unjammed phase;
- Low density.

The first ensures that the grip will keep the shape of the object during the low pressure phase. Low friction resistance during the unjammed phase is very important as it allows grains to slip between each other to involve the object to increase the contact surface and taking full advantage of the geometry of the object. This will enhance the 3 modes of gripping explained in section 1.3.1. Low density is also important to add the less weight possible to the gripper.

As there are many granular materials available, 5 different materials were chosen for comparison: fine grains and large grains of sodium chloride (commonly known as kitchen salt), expanded polystyrene grains (commonly known as Styrofoam™), milled coffee and sand. All granular materials were chosen from [10] and [1], except for the expanded polystyrene that was chosen due to its low density. Also, different size grains of sodium chloride was used as a control because [38] mentions that smaller grains are able to grip better than bigger grains.

Currently, no reliable mathematical models to simulate the yield strength of the jammed phase seem to be available in literature so it was necessary to devise a repeatable and reliable test to chose the right granular material for the gripper prototype. The solution was to perform some sort of a hardness test. The first experiment was a Vickers hardness test, which showed no visible indentation due to diamond size and the elastomer properties of the membrane. Doing a Shore hardness test also proved impossible as the results would be about the latex and not the granular element inside. As the Brinnel hardness test uses a sphere as an indenter, the results would be easily measured and less prone to errors. However using normalized sizes was not possible due to the small sphere diameter, so a manual hardness testing apparatus (figure 2.2) was designed and built. The sphere used in this apparatus had a diameter of 17×10^{-3} m. This gripper version also used a latex balloon as a membrane but no external

collar was used. The seal was improved in comparison to the gripper version used in section 2.2.1. The improvement consisted in using a thicker rubber tube to connect the syringe to the balloon and a plastic zips ties were used to ensure a tight seal.

The experiment consisted of placing this gripper on a lifting platform, and then pulling the syringe's plunger creating a volume variation (measured in the markings on the syringe). After this, the spindle of the lifting platform was turned until the indentation was made and the dynamometer achieved the expected value of force. Then the spherical indentation was measured using a caliper. A picture of one of the hardness tests is shown in picture 2.2.

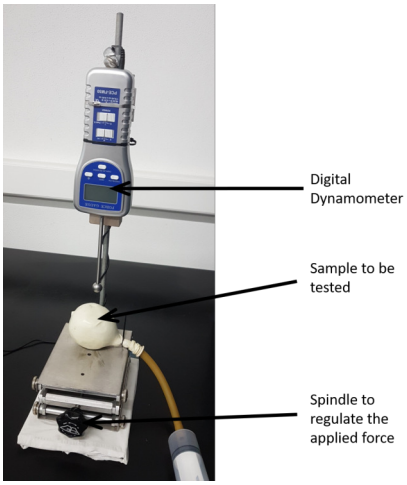

Figure 2.2: Picture of a Brinnel hardness test assembly

The hardness tests where done using 2 different forces (5 and 10 N) and 2 different volume variations of the syringe (5 ml and 24 ml). This combination allowed the middle of the sphere to stay above the balloon while making a visible indentation. The results of this hardness tests are presented in table 2.1. The hardness number was obtained using the equation (from [46]):

$$\mathrm{BHN} = \frac{2P}{\pi D(D - \sqrt{D^2 - d^2})} \tag{2.1}$$

where BHN is the Brinell Hardness Number, P is the applied load in kgf, D is the diameter of the indenter in mm, d is the diameter of the indentation in mm.

When comparing different grain sizes of sodium chloride, higher hardness values are obtained with smaller grain size as expected. The results were confirmed by what was seen when gripping objects with these materials at this stage. The only unexpected result was the low BHN of expanded polystyrene. This substance showed great results when picking up objects. This might be explained by the capability of the material to deform and better involve the grip object.

As for the low friction resistance during the unjammed phase, almost all of them proved to be fully reliable. The only granular material that had some problems was the milled coffee as it absorbed moist. After being exposed too long to air the fine coffee grains were subject to a high friction force between each other requiring a higher force to conform the gripper to the test objects.

The density of each material is presented in table 2.1. The tests to calculate the density were done with the granular materials at atmospheric pressure and at rest.

Table 2.1: Brinnel test

Granular Material		Sodium Chloride				Expanded polystyrene		Milled Coffee		Sand	
		Fine Grains		Coarse Grains							
Volume (m^3)		7×10^{-5}									
Mass (g)		113.74		126.4		16.79		40.06		126.4	
Density (10^3 Kg/m^3)		1.62		1.81		0.24		0.57		1.81	
Volume variation 5ml	Force (N)	10	25	10	25	10	25	10	25	10	25
	indentation (10^{-3} m)	10	13	12	16	22	25	9	10	6	9
	BHN (10^6 Pa)	0.122	0.175	0.083	0.109	0.019	0.025	0.151	0.305	0.348	0.379
Volume variation 24 ml	Force (N)	10	25	10	25	10	25	10	25	10	30
	indentation (10^{-3} m)	7	9.5	10	14	14	16	6	10	5	7.5
	BHN (10^6 Pa)	0.254	0.301	0.122	0.148	0.059	0.109	0.348	0.305	0.504	0.663

Based on these results the expanded polystyrene and coffee were chosen as the granular materials to be used in the design. These materials were both lightweight and had high gripping capacity.

2.2.3 Vacuum solutions

Using the volume variation of syringes was a fast initial solution. However as the syringe size and diameter were fixed, there would not be enough freedom to adjust the dimensions and the force required to keep the desired pressure. So other solutions were attempted. The first solution was using industrial suction cups (figures 2.3) as a low friction device to generate vacuum. Despite the high diversity of this suction cups with detailed data sheets, these are not intended to be used extended when subject to negative pressure which meant they were incapable of keeping its shape while subject to lower inner pressures. Then using the concept of rolling lobe air a different idea emerged. The rolling-lobe or reversible sleeve air (figure 2.4) is a concept based on air springs. It is used in many applications such as web tensioners, dancer, roll tensioners, roll loaders, valve actuators, accumulators, positioners and impact absorbers. It is considered to be a low-friction actuator [47]. During compression, the rubber walls of this type of spring roll over a piston [48].

Figure 2.3: Picture of the suction cups initially tested for this project

This idea was implemented according to the scheme in figure 2.4 (b). Here it is already visible the chosen SMA actuator shape attached to the piston. This spring shape was chosen due to the larger stroke (chapter 1.2.2). On the left, the pressure inside the membrane (represented in green) is the atmospheric pressure, keeping the material in the unjammed state. The spring is not actuated and is fully extended. When the spring is contracted, the piston is pulled, increasing the volume and decreasing the pressure. This decrease changes the material to the jammed state as represented on the right side of figure 2.4 (b). The outer tube was added to keep the piston centered and to avoid the collapse of the membrane. To pull the piston back to the initial position, it is necessary another force. This could be a compression spring but it would easily buckle and interfere with the temperature sensors that need to be implemented. The springs could also conduct unwanted currents, so the extension springs were not the solution. So the force necessary to help bring the piston to its initial shape was done by rubber bands. As the intended pressure was at least 10^4 Pa, the piston diameter and length variation was designed using Boyle–Mariotte law ($P_1V_1 = P_2V_2$) and assuming air as an ideal gas.

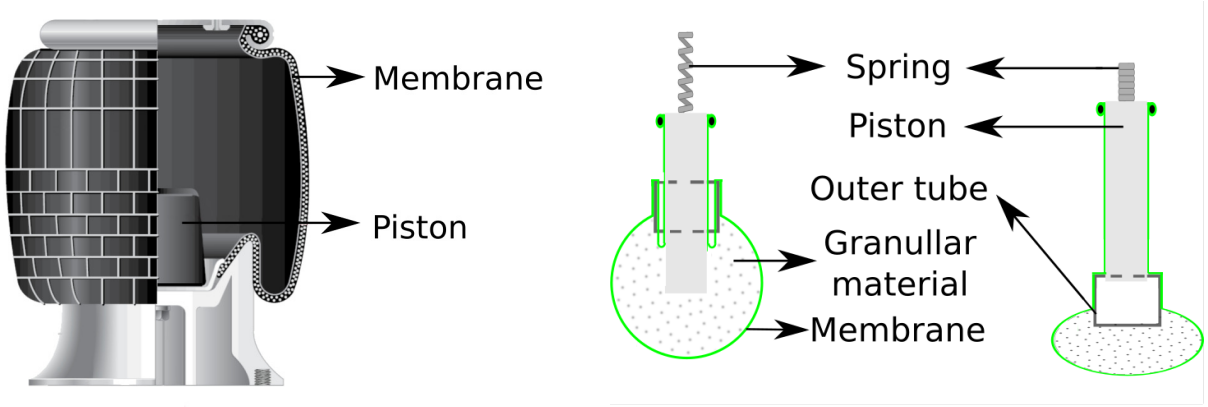

(a) Rolling lobe adapted from [49]

(b) Schematic of the gripper developed

Figure 2.4: Vacuum System

2.2.4 Design of Structural Elements

The next step of the design was to find a solution for clamping of the NiTi wire mentioned in [25] (Chapter 1.2.2). This was done by placing each of the end coils of the spring between 2 flat copper plates as shown in picture 2.5. The pressure is done with two bolts that also secure the electric wire to make sure the electric contact is secure. In the upper region of the image, this implementation is done with nuts. In the lower region of the same figure, this is done with screws against the piston wall represented in gray. In order to make sure that this prototype had the desired dimensions and a secure way of gripping the spring it was mainly modelled in the software Solidworks® and later printed in a high density ABS 3D printer available at CENTI. During the design, some concerns were taken into account like avoiding rough edges and the precision of the printer 0.5×10^{-3} m. The part which was subject to the higher force is shown in figure 2.6. As one of the major concerns was removing parts weight some questions

were raised whether it would resist the pressure. So a tensile analysis was made to this part using finite elements as it can be seen in figure 2.6. As the highest von-Mises tensions (approximately 10^6 Pa) were much smaller than the Yield strength (approximately 3×10^6 Pa), no further analysis was needed.

In figure 2.7 is presented the final version of the 3D design and the prototype.

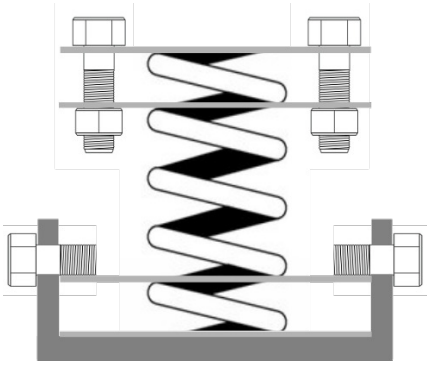

Figure 2.5: SMA clamping method applied. At each end of the spring, the last coil is pressured between two metal plates represented in gray lines.

Also, this part has some magnets underneath that are attracted to magnets also placed in the external collar to help when assembling the prototype (check figure 2.8 a).

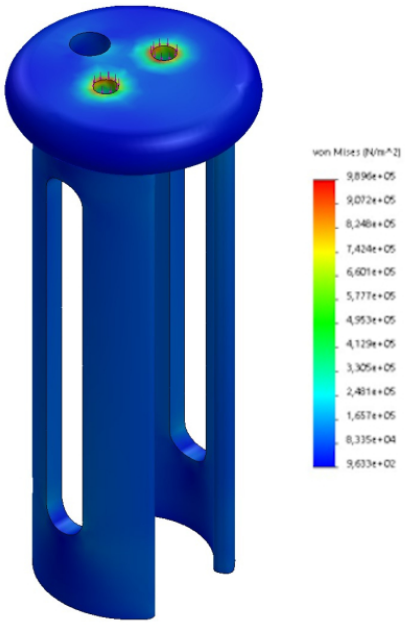

Figure 2.6: Finite element analysis

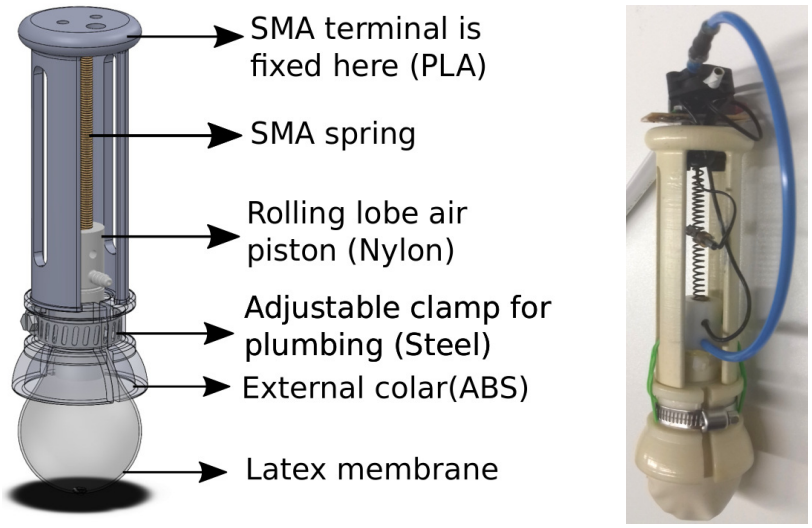

(a) Complete 3d gripper Design

(b) Gripper prototype

Figure 2.7: Final 3D design and physical Prototype

The next phase was ensuring that there was no air leakage so that the pressure inside the membrane remains stable. There were two techniques used to identify air leaks. The first consisted of submerging the gripper in water and increasing the pressure inside the membrane. This technique allowed to identify the leaking spots, which where:

- the surface of the piston;
- the contact circumference where the membrane meets the piston (”groove for membrane” in picture 2.8 b);
- the connection of the pressure tube to the piston (”pressure tube connection” in picture 2.8 b);
- the connection of the pressure tube to the pressure sensor.

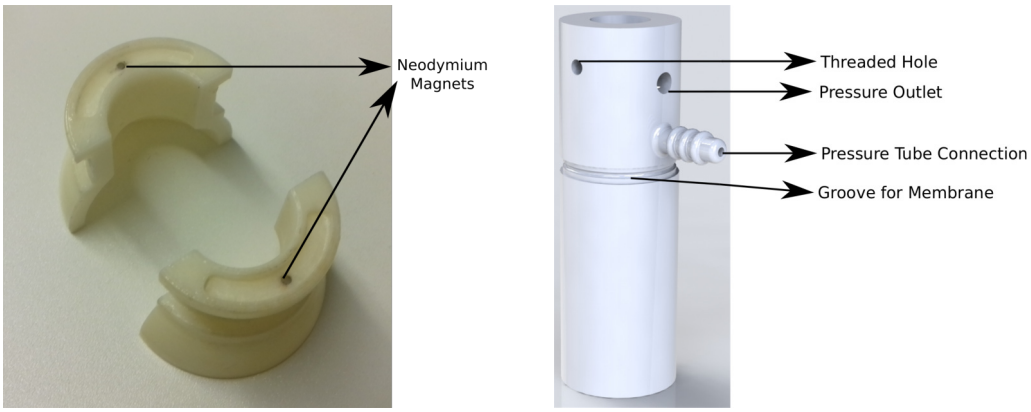

(a) Complete 3d gripper Design

(b) Gripper prototype

Figure 2.8: External Colar and Piston

After some iterations where leaking spots were fixed, another technique was used. This technique was applying dish soap and water in the previously identified leaking spots and increase the pressure inside the membrane. This second technique was easier as there was no need to fully submerge the gripper and the locations of the leaking spots were more visible.
Obviously, the Fused Deposition Modeling technique used to print parts had micro holes that made the parts porous, letting air pass through. In order to correct this problem, two solutions were applied. First, the part was subject to a bath of hot acetone vapor (($CH_3)_2CO$), this reacts with the external layers of the ABS parts resulting in a liquid mixture which fills some of the smaller holes. Secondly, ABS was coated with a layer of epoxy. To make sure no air would enter the system, a grove was made on the outside of the piston. The open end membrane was placed around this grove. Over the membrane, a higher diameter rubber ring was pressured using a zip tie. Finally, the part was submerged in water to check for any air leakages. However, there were still visible air leaks so as a final solution the piston was replaced by manually machined nylon piece.

2.3 Actuator development

2.3.1 SMA Helical Springs

Helical springs are divided into three big groups, compression, extension and torsion springs. The first two convert the linear motion of the spring into a torsion strain on the wire. Compression springs are projected to resist compression forces whereas extension springs are used to carry tensile loading. The torsion springs are made to resist and deflet under torsional loads [50]. For the purpose of this gripper design, extension springs were chosen as the most suitable type.
When designing SMA springs some mathematical relations are relevant. First, the actuator has 3 working modes and lengths (represented in figure 2.9):

- The first is the phase which the actuator is not subject to any force and the material temperature is lower than the activation temperature ($T<T_{act}$), so it has all coils close together. The spring size in this working mode is identified as Li. Normally this is the spring in its state before being assembled into the system;
- The second is the spring subject to the maximum force and keeping the material in the martensitic phase (($T<T_{act}$)). This is the maximum length that spring will achieve and it is identified as Lm;
- The third is the spring subject to the maximum force and happens when the actuator has been active for a while ($T>T_{act}$). This is the length that spring will achieve when it is in its austenitic phase and it is identified as La.

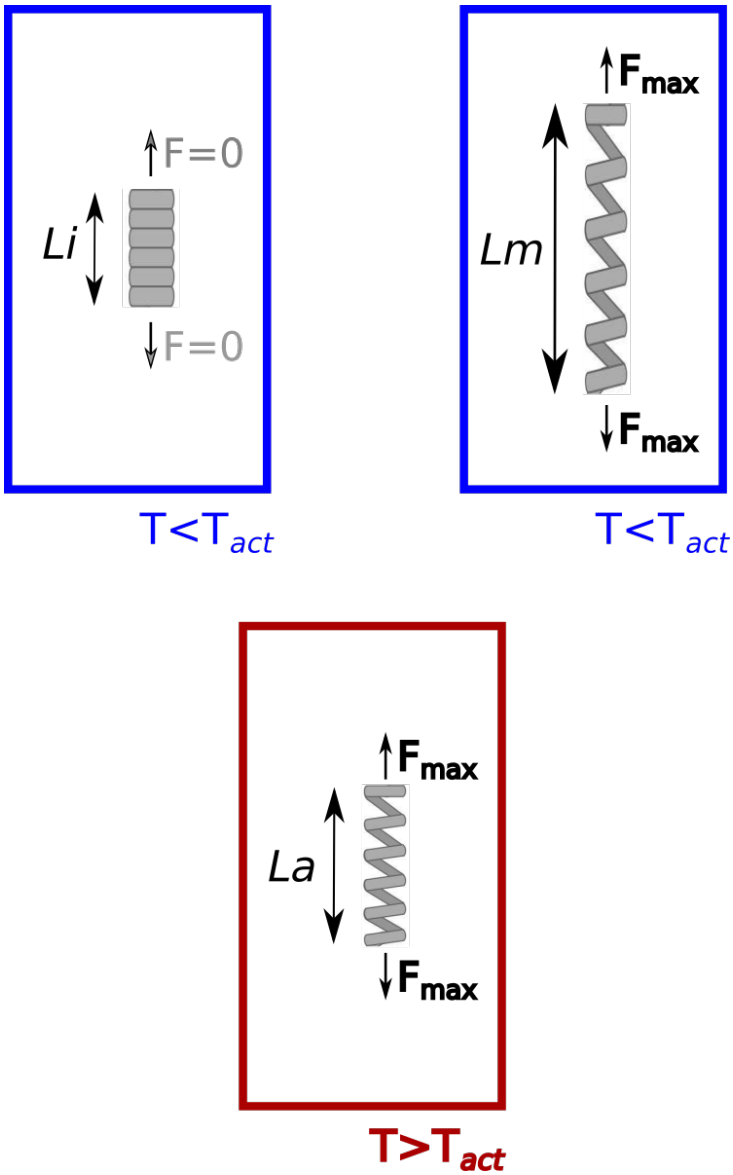

Figure 2.9: Different sizes of the SMA spring actuator during a working cycle

The total strain can be obtained from the Castigliano's theorem from [50]. In this way, total deflection can be derived from the total strain (u) using the applied force (F) as the differentiation variable:

$$y = \frac{\partial u}{\partial F} = \frac{8FD^3N}{d^4G} + \frac{4FDN}{d^2G} \tag{2.2}$$

where y is the spring displacement during an elongation without phase change (in m), N is the number of active coils, F is the force in N, d is the wire diameter in m, G is the shear modulus in Pa, D is the mid diameter given by the outer diameter of the spring minus the wire diameter. The shear modulus is different for martensite and austenite thus this equation can only be applied to the same phase state of the SMA (austenitic or martensitic).

Considering an ideal linear spring the Hooke's law can be applied with equation 2.2:

$$\frac{F}{y} = k = \frac{d^4 G}{8D^3 N + 4DNd^2} \tag{2.3}$$

where k is called the spring constant.

The helicoidal spring elongation δ is related to the shear strain γ at the external radius of the wire cross section ([14]):

$$\delta = \frac{\pi N D^2}{d}\gamma \tag{2.4}$$

where δ is the spring displacement (not dependent on SMA phase state) and γ represents the shear strain.

Considering only shear forces, the maximum residual equivalent strain (Lagrangian) ϵ_{eq} is stated in [14] as:

$$\epsilon_{eq} = \sqrt{\frac{4}{3}\gamma^2} \tag{2.5}$$

where ϵ_{eq} represents the equivalent strain.

Applying the equivalent strain (2.5) and total deflection (2.2) alongside the Hooke's law on the maximum elongation of the SMA spring:

$$\delta = Lm - Li = \frac{\pi N D^2}{d}\frac{\sqrt{3}}{2}\epsilon_{eq} \tag{2.6}$$

Equation 2.6 and 2.3 can now accommodate constraints like the 4% tensile strain mentioned in the literature to avoid functional fatigue. The δ can be considered $Lm - Li$ as this will be the maximum elongation and strain.
Using these equations it is possible to design and predict SMA spring behaviour, respecting requirements such as functional fatigue durability, force and maximum elongation.

2.3.2 Fabrication of the Actuator

To develop a spring linear SMA actuator, it was required to shape the nitinol wire into a spring (cold-working) and then apply a heat treatment called annealing followed by quenching. The wire was acquired from the companies Nexmetal Corporation and Kellogg's Research Labs.

One of the most popular ways to give the wire the helicoidal shape is to wound it around a screw thread, with the same pitch as the wire's diameter. To achieve this a drilling machine, illustrated in figure 2.12, was used. This meant that when using normalized threaded rods, the wire diameter needed to be the same as the pitch. Also, the wire should be wound in the clockwise direction (right hand rule) so that the wire would fit the thread profile when rotating. In theory, the rod should rotate in the counter-clockwise direction.

During the experiments, it was found that better results (less spaced coils) were obtained if the wire was wound in the counter-clockwise direction (Left hand-rule). This can easily be explained by the geometric shape and friction effect that the thread profile exerts on the wire. As the thread coils make an obtuse angle with the spring, the coils are pushed closer to each other due to increased friction. Figure 2.10 shows a representation of how the wire should be wound up.

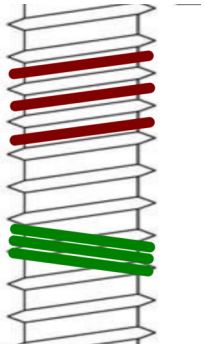

Figure 2.10: Wounding SMA direction. The red lines represent the SMA wire being wound up in the clockwise direction. The green represent the SMA wire being wound up in the counter-clockwise direction, giving less spaced coils.

This discovery opened new possibilities as every diameter size normalized threaded rod could produce springs with the minimum pitch using any diameter wire.

Some other conclusions were taken from this process. The first would be a solution to clamp the wire to the rod. The best approach was using an adjustable clamp for plumbing but smaller diameters are not easy to find. So the best alternative is using steel rope clamp (figure 2.11 b). Other important findings include the alignment the wire is held (horizontal) and doing the first turn by hand. Also after testing several diameters wire it was found that wire with diameters bigger than 1×10^{-3} m were too difficult to bend and would often break.

The full procedure is called training the SMA. The steps are described next:

1. Clamp the wire to the threaded rod using a wire rope clip;
2. Fasten the assembly (rod+clamped wire) to the drill chuck, make sure the wire is also clamped by the machine;
3. Manually twist the wire to make sure the wire will be wound up in direction intended;
4. Chose the rotation mode to be counterclockwise;
5. Hold the wire perpendicularly to the apparatus, while switching on the machine;
6. Let the wire descend while keeping pressure on the wire;
7. Switch off the driller while keeping pressure on the wire;
8. Use a curved jaw locking plier to hold the spring in place, avoiding unwinding;
9. Cut the excess wire, leaving at least 0.07 m excess;
10. Clamp the end of the wire with the help of a wire rope clipper;
11. Make sure the furnace is at 500 ℃;
12. Heat the constraint spring in the furnace for 900 s (15 min);
13. Rapidly cool the spring in a bucket with cold water and ice for 60 s.

Figure 2.11 shows the apparatus during the training procedure after step 12 and a spring before going into the furnace.

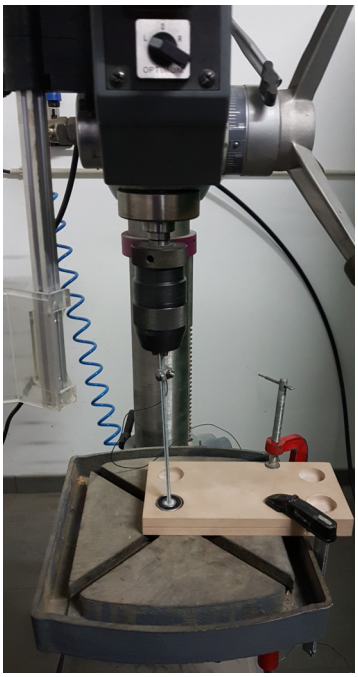

(a) Training procedure before turning on the driller(step 5)

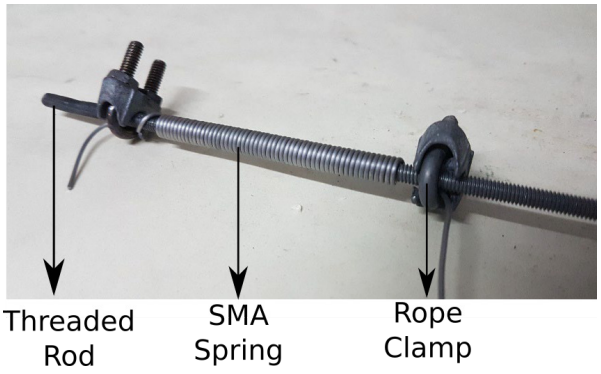

(b) Assembly with spring before heat treatment (step 12)

Figure 2.11: SMA spring fabrication

2.3.3 Spring Design

In order to design an adequate spring, it was necessary to find the shear modulus (G). Consequently, tensile tests were made. In this section, the results respecting the determination of the austenite shear modulus G are presented.

To evaluate this constant it was necessary to produce different springs. In this work, threaded rods with a nominal major diameter of 4×10^{-3} m, 5×10^{-3} m and 6×10^{-3} m (M4, M5 and M6) were selected to produce springs with outer diameters of 5.7×10^{-3} m, 6.7×10^{-3} m and 7.7×10^{-3} m, respectively. The diameter of the wire used should be as high as possible accordingly to equation 2.6 from section 2.3.1 to provide the biggest force. The biggest wire diameter applicable is 10^{-3} m (reasons explained in the section 2.3.2). However, a smaller diameter of the spring is much more important to create large force spring. Then the springs were placed in the assembly of figure 2.12. This assembly allowed to test the clamping system mentioned above in chapter 2.2.4 (figure 2.5). The system did work as expected but it was important to ensure the two metal plates were tight or the spring might still slip. With this assembly, values for spring elongation and applied force on the spring were collected. During this test, an infrared thermographic camera was used to ensure the spring was between 80 and 90 ℃, avoiding too much functional fatigue while keeping the spring in the fully austenitic phase. It was noticeable during this tests that if the temperature was too high the spring would not fully recover its initial shape, whereas if the spring was stretched over the limit of functional fatigue no immediate decrease in shape recover was visible.

The applied voltage was 1.1 V, being the current value 6.3 A. The results of these tests are presented also in figure 2.13. The maximum force of 34 N and 2.4×10^{-2} m displacement were obtained.

As these results show some error, three measurements with 60 s interval were taken for each displacement. Approximating the values with a linear function, the spring elastic constant (k) was found. From this value and using equations 2.2 and 2.3, the shear modulus for each spring was found. Using weighted arithmetic with the weights error (R^2) from each linear approximation, the value of 13.09$\times 10^9$ Pa was obtained which is the same order of magnitude than the values in [51].

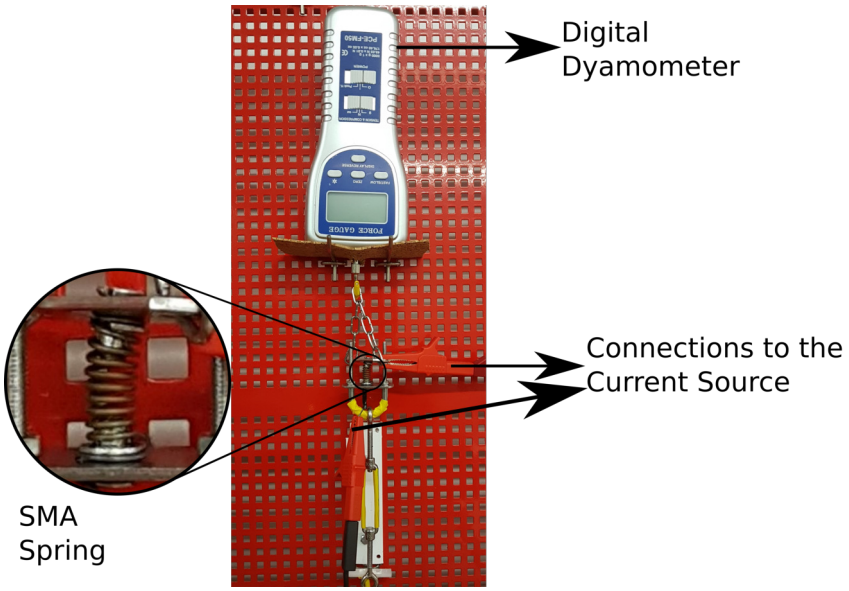

Figure 2.12: Tensile tests assembly

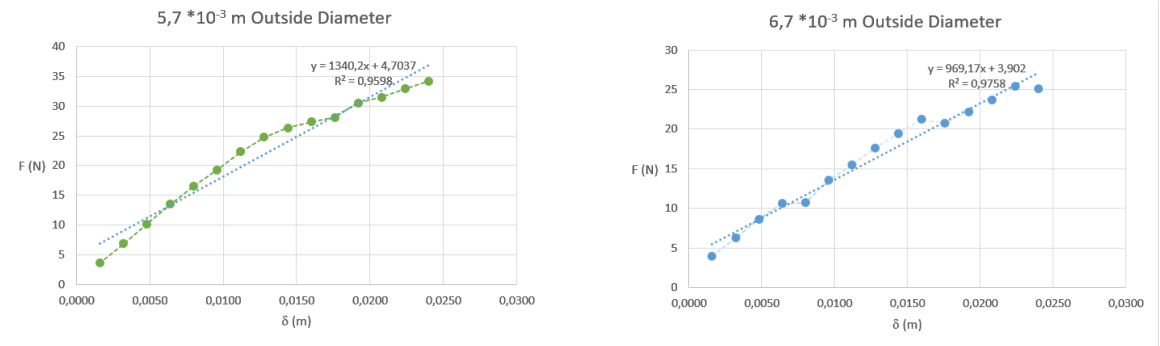

(a) (b)

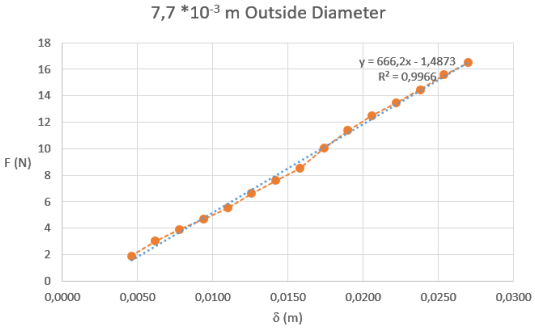

(c)

Figure 2.13: Graphics of tensile tests

As there are fewer constraints than the number of variables of a spring measurement it is difficult to find the best spring dimensions that prove the most effective for each application. With this in mind, it was necessary to develop a calculation design tool that uses generalized reduced gradient non-linear solving method to find the best result.

This tool had a small database of shear modulus since it was only tested with the wire that came from the company Nexmetal Corporation and Kellogg's Research Labs. The Nextmetal Corporation wires tested had 3 different shear modulus values as they had 3 different activation temperatures (40, 45 and 80 ℃).

So the final version of this calculator had 4 user input variables: maximum displacement, maximum force exerted, maximum wire elongation (ϵ) allowed and type of wire chosen from the database (activation temperature).

The variables were the diameter of the springs (limited to the threaded rods available) and the number of coils. The objective function to minimize was:

$$f(x) = w_1(\frac{\pi N D^2}{d}\frac{\sqrt{3}}{2}\epsilon_{eq} - y + La - Nd)^2 + w_2(F - \frac{d^4 G}{8D^3N + 4DNd^2}(La - Li))^2 + \\ + w_3(N - N_{rounded})^2 + w_4(D - D_{rounded})^2 + w_5 La + w_6\frac{La}{Li} \tag{2.7}$$

Variables:

- D - spring diameter;
- d is the wire diameter in m;
- N - number of active coils.

Constraints:

- w_1 - weight of functional fatigue restriction (equation 2.6);
- w_2 - weight of the Castigliano's theorem (equation 2.2);
- w_3 - weight of the integer precision;
- w_5 - weight of the La size importance;
- w_6 - weight of the La size in respect to the Li importance;
- ϵ_{eq} - equivalent tensile strain;
- La - size of the spring when fully extended in martensitic phase (in m);
- F - force in N;
- G is the shear modulus in Pa;
- Li - size of the spring when fully compressed (in m).

Obtained from the solution:

- y - spring displacement during elongation in martensitic phase (in m);
- $N_{rounded}$ - number of active coils rounded to integers;
- $D_{rounded}$ - spring diameter rounded to integers.

For the weights the best values based on the speed of calculation and best results were found to be $w_1 = 0.8$, $w_2 = 0.9$, $w_3 = 1$, $w_4 = 100$, $w_5 = 1000$ and $w_5 = 0.5$.
As constraints we admitted that the number of coils could only be bigger than 1, the size of coils could only be of a size that threaded rods could produce, La could only be bigger than Li, and that the first and second term of the objective function could not bigger than 0.09. A figure of this design tool can be seen in the picture 2.14

	Mola	cm/ºC/GPa/g/N	SI
Input	d - Diâmetro do fio	0,1	0,001
	T - Temperatura de activação	80	353,16000000
	dx - Deslocamento efectivo que a mola faz	3	0,0300000000
	F (N) - Força de actuação a ser aplicada	20	20
	ε máx - Extensão máxima	4,00%	4,00%
Dados mola	G - Módulo de corte/ shear	13,09022616	1,31E+10
	K (N/m) - Rigidez da mola em fase austenítica	——	5,79E+02
	D - Diâmetro da hélice	0,467795559	0,004670924
	C -Índice da mola	4,677955593	4,677955593
	N - Nº de espiras	27,08942998	27,08942998
	Lfio - Comprimento de fio necessário para a mola	39,81125187	0,398112519
	δ - Elongamento máximo (s/ corrente nem peso)	6,45	0,065
	Lm - Comprimento máximo da mola esticada - Não ultrapassar	9,160321937	0,0916032194
Output	La - Comprimento da mola austenítica c/deformação	6,16	0,062
	OD - Diâmetro exterior da mola	0,567795559	0,0057
	Dveio - Diâmetro do veio de fabrico	0,397795559	0,0040
	Li - Comprimento da mola s/deformação	2,7089430	0,027
	Massa - Massa suportada	2038,74	2,04

Figure 2.14: Spring design tool

2.4 Sensors and Control

To control and study the behaviour of this prototype, some sensors needed to be implemented. This prototype has three sensors: pressure, current and temperature. The SMA spring is actuated with a n-channel MOSFET. The control, analogue reading, analogue to digital conversion is made using an Arduino® Uno. A schematic of all the connections is shown in figure 2.15 and a picture of the implementation is shown in figure 2.16.

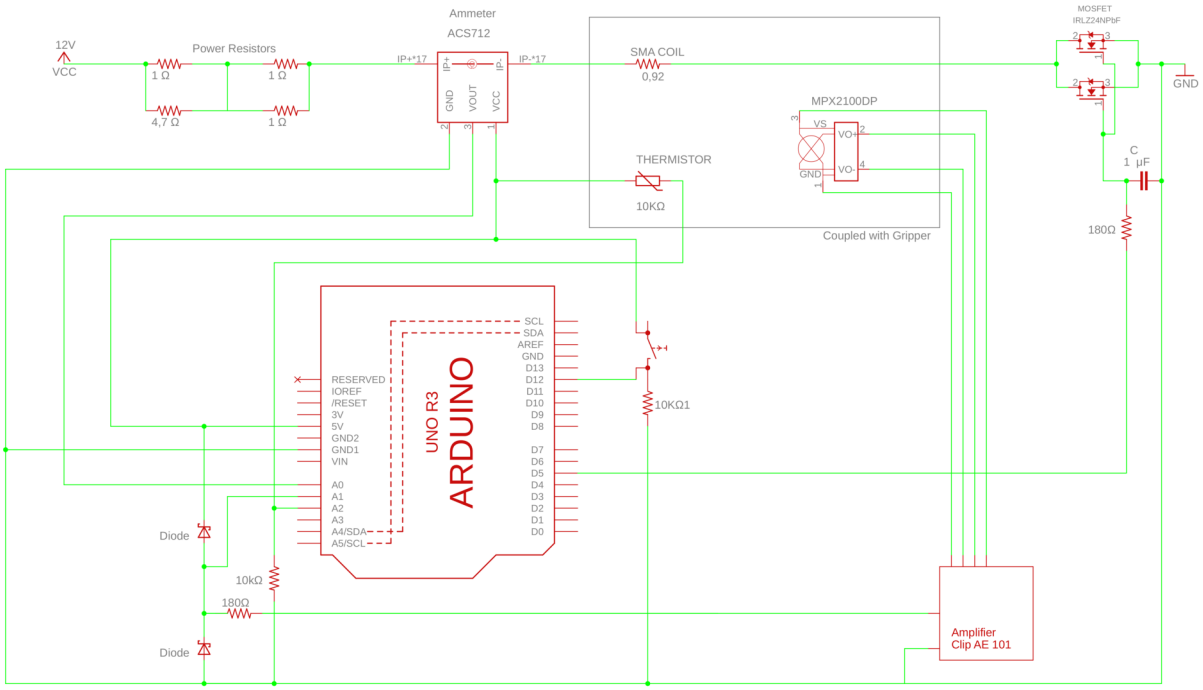

Figure 2.15: Schematic of the electrical connections

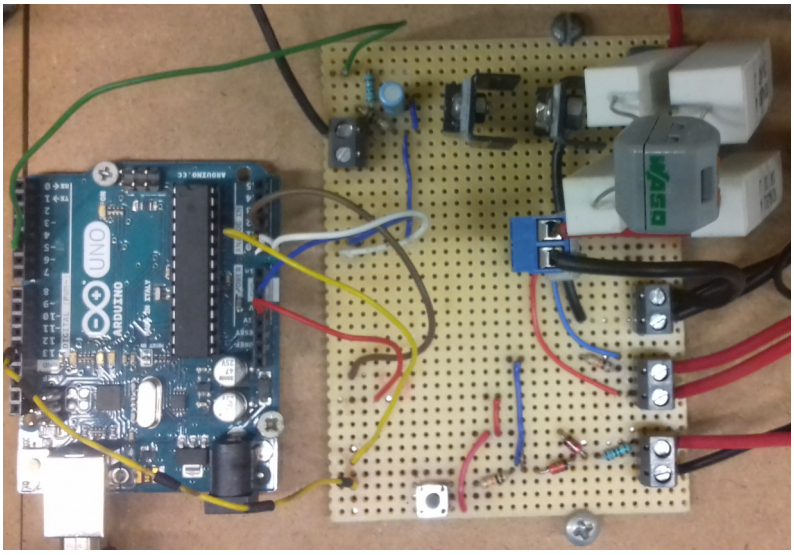

Figure 2.16: Picture of the control and sensor system implemented

Despite the use of a heatsink and a cooler fan, the conductivity of the MOSFET was not as expected from the manufacturer data, so due to immediate availability, a decision was made to use two of the same model in parallel. Also, the MOSFET did have a tendency to stay open even if the signal of the Arduino® was 0 but as the PWM from the Arduino® made interference with the power supply, the problem was solved using an RC filter to flatten the signal.

The resistance of the SMA is very low and power resistors were added to increase the circuit resistance, limiting the current and avoiding damage the power supply. However, the SMA is clamped to the wire with 2 metal plates, so the pressure clamping these plates should be ensured to guarantee a good connection.

For the pressure sensor a MPX2050DPH was used. This sensor has a small output of 0 to 0.004 V and the analogue port of the Arduino® measures only from 0 to 5 V. This required an amplification, as the sensor is based on a Wheatstone bridge, a Clip Electronic Amplifier AE101 was used to amplify the signal with a gain of K = 493.4. Because the amplified signal could be outside the range accepted by the Arduino® if the input signal would go outside the expected values, a protection circuit was needed. In order to implement this circuit 5.1 V zenner diodes and $10^3\ \Omega$ were used.

To control the temperature to avoid any functional fatigue to the SMA a 100 Ω thermistor and a ACS712 current sensor were used.

A control of the type on-off was implemented. The spring was heated until the temperature was 75℃ as this would avoid an overshoot over the 80 ℃ affecting the functional fatigue. After this, the current would only be turned on if the spring temperature would lower bellow 60 ℃.

A schematic of the complete prototype with its electrical connections is shown in figure 2.17.

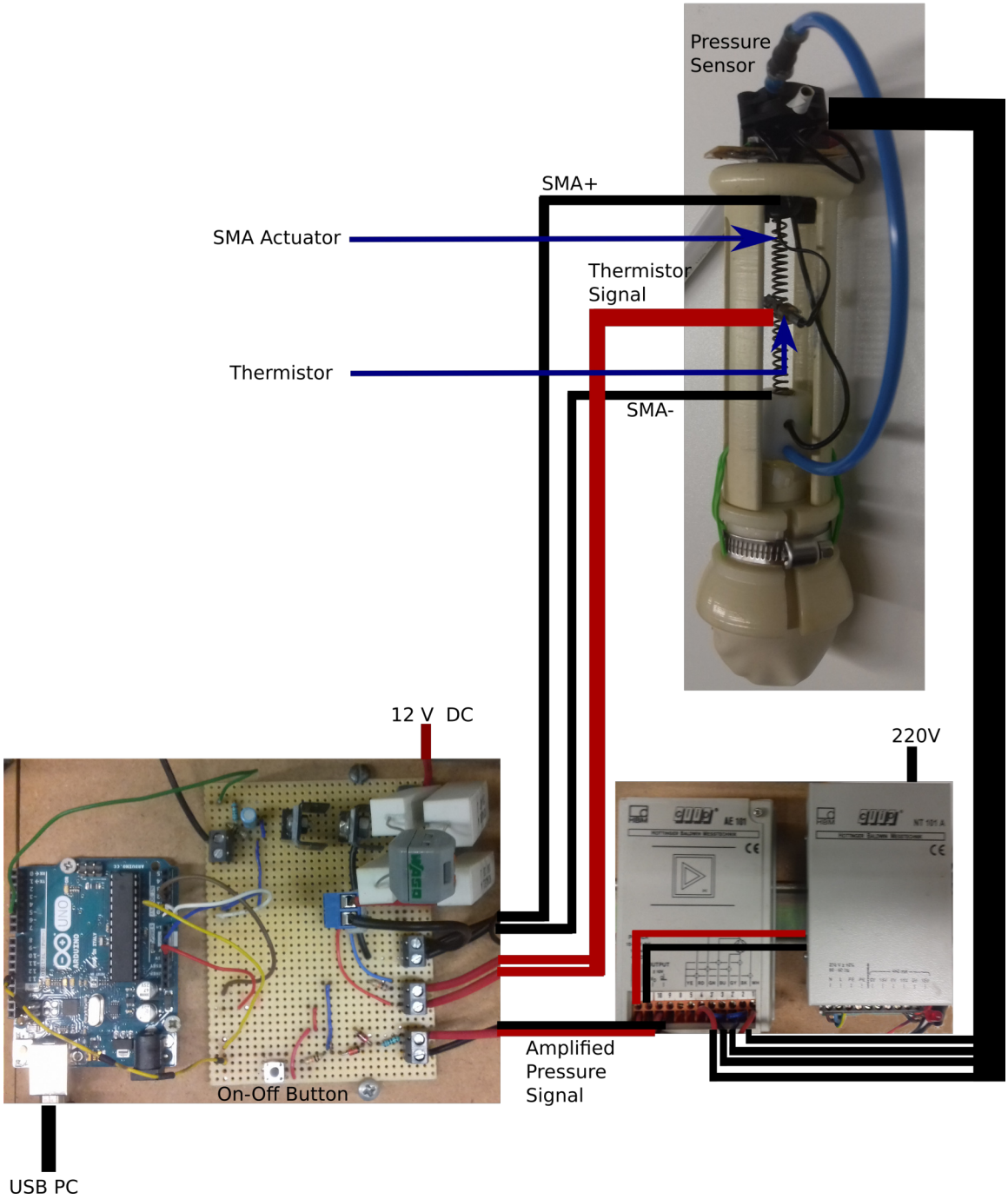

Figure 2.17: Experimental setup and components.

Chapter 3

Experimental Procedure and Results

3.1 Experiments

There was a need to test if the prototype did work similar to [1, 10, 38, 52] and also find its limitations. This included several questions:

- When choosing a granular substance to produce the jamming granular effect, is the hardness tested in section 2.2.2 the most important factor?
- Did this mechanical design create an admissible vacuum?
- Does the hysteresis effect of the SMA create any problems when grabbing objects?
- Is an on-off control enough to control this system?
- How universal is this gripper?
- Which moments of the action of gripping are visible using the 3 sensors available?
- How do temperature and pressure relate?
- Using different granular materials or gripping different objects produce different sensor readings?

The first step to obtain these answers was to collect the sensor data during a full activation and relaxation of the actuator without using the gripper to grip any object. This data includes recording the pressure, the temperature, the current, and the PWM signal.
The next tests consisted of doing grip success tests. In order to do this test there was the need to chose different objects. So 4 different shapes were chosen based on [1]. These 4 shapes were a coin, a pyramid a sphere and a cube. This choice included two difficult to grip parts (pyramid and coin) and two parts that are considered easy to grip (cube and sphere), according to [1]. As [1] mentioned the importance of the size test objects, this work used objects that were not too big (bigger than gripper size) or not too small that would be too easily gripped. So the size of the test objects chosen were 50% and 75% of the gripper membrane diameter (approximately 4×10^{-2} m), giving a total of 8 test objects. Euro

coins were used for the coin shapes, these were 5 cents and 50 cents coins. As for the other shapes, a PLA (Poly Lactic Acid) 3D printer was used. The weights and a picture of these 8 objects are shown in table 3.1 and figure 3.1, respectively.

Originally, the test consisted of grabbing the object 7 times and checking whether the object stayed gripped during at least 20 s. However, after verifying that the results were always the same, it was chosen to do only 1 grip test for each object, using 3 different granular materials: small sphere of polystyrene (3×10^3 m diameter), couscous (2×10^3 m diameter) and milled coffee. A total of 24 experiments were done.

The last important step in this experiment was to register the time at which these important actions occurred:

- Gripper is pushed against test object;
- Gripper is lifted;
- Test object falls down.

The protocol used consisted on:

1. Measure 5×10^{-2} ml of filler material;
2. Assemble Gripper;
3. Check for air leakage;
4. Begin Data Acquisition;
5. Push the gripper against the test piece;
6. Register elapsed time since the beginning of data acquisition;
7. Register initial temperature;
8. Turn on the Arduino® control;
9. After the second peak in temperature, lift gripper;
10. Register elapsed time since the beginning of data acquisition;
11. If the test object falls, register time since the beginning of data acquisition;
12. After 120 s shut gripper off;
13. When test object fells, register elapsed time since the beginning of data acquisition;
14. Wait until the temperature is the same as the initial temperature;
15. Stop data collection.

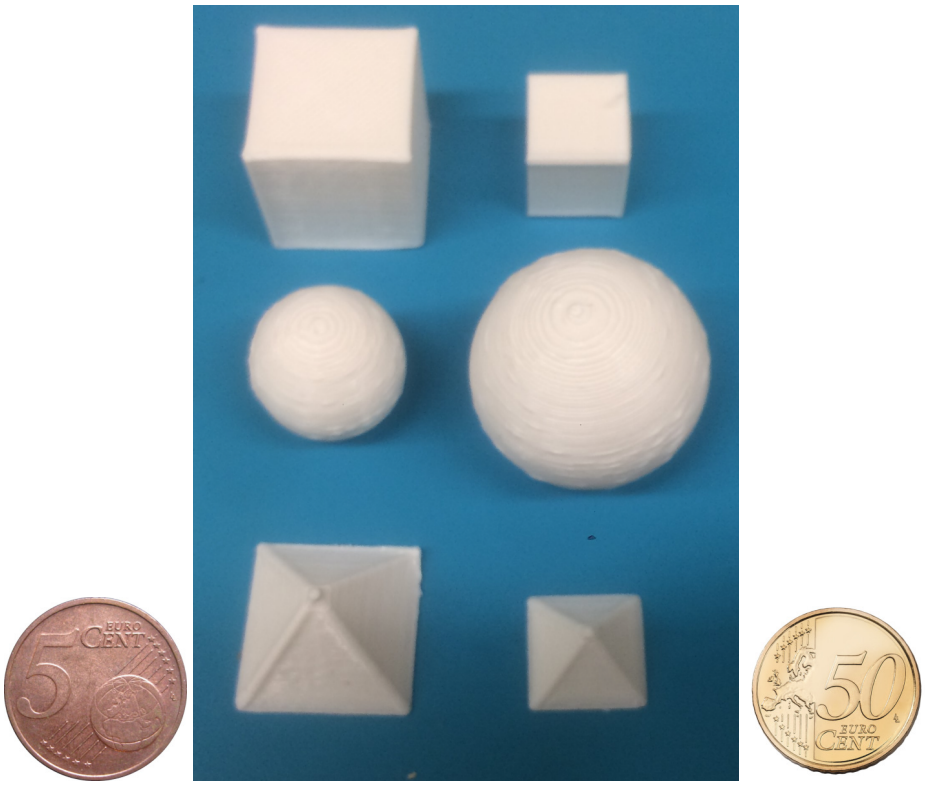

Figure 3.1: Objects used for gripping tests

Table 3.1: Gripping tests Pieces

Object	Weight (g)	
	50% gripper size	75% gripper size
sphere	1.82	4.92
cube	4.15	1.65
pyramid	1.48	0.61
5 cent coin	3.92	
50 cent coin	7.80	

3.2 Results

3.2.1 Cycle analysis

The first experiment that consisted of only activating the actuator produced the results shown in figure 3.2:

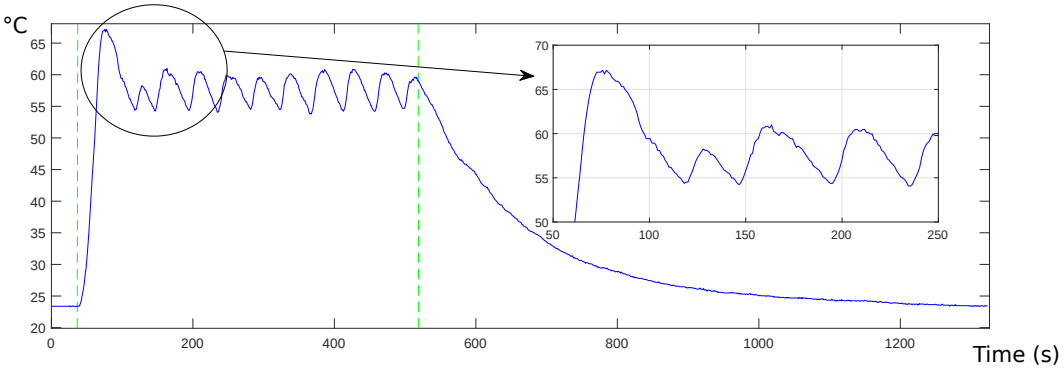

(a) Readings from the temperature sensor in ℃ along the time in s

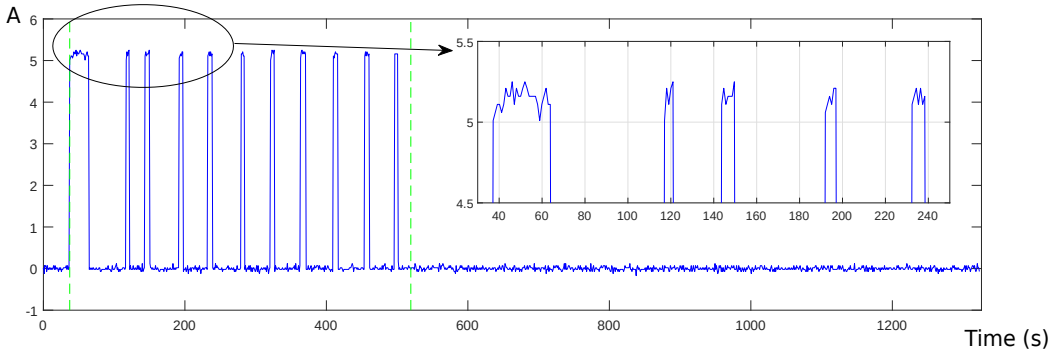

(b) Readings from the current flow sensor in A along the time in s

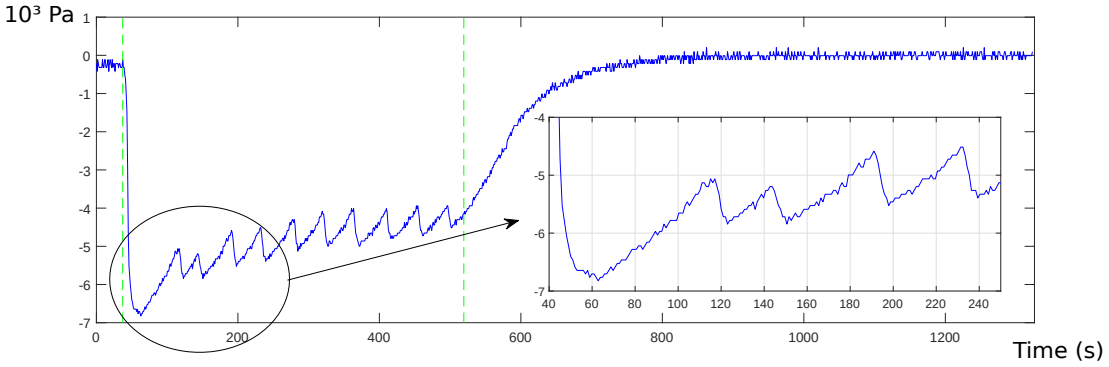

(c) Readings from the pressure sensor in 10^3 Pa along the time in s

Figure 3.2: Readings from the temperature sensor (top), current flow sensor (middle) and pressure sensor (bottom) during a full actuation and de-actuation cycle. The x-axis is time and the y-axis is temperature, current and pressure, respectively.
The first green dashed line represents the moment when the gripper was activated and the second is the time it was turned off.

It is visible that the delay between turning the switch on (marked as a green dashed line) and the current flow being detected is lower than 1 s. This means that the time elapsed between pushing the on-off button and to open the transistor and the current beginning to flow is lower than 1 s.

There is an overshoot of the temperature, 15% reaching 67 ℃ after 38 s of the initial activation period to heat the SMA. This period is 29 s long. The next activation period is only given after 51 s, when the temperature is below 55 s. The next activation does not last longer than 5 s keeping the temperature between 54 and 61 ℃, which is enough to keep the SMA with a low martensitic fraction (ξ). This value of ξ is enough to maintain a vacuum pressure suitable for gripping objects.

The current did show a direct relation with temperature and pressure. When the PWM signal was at 0 V it is noticeable the immediate increase in temperature and the immediate decrease in pressure. On the other hand, when the PWM signal was at 5 V the effects on temperature and pressure were slower. This is expected as this is a thermal system using only natural convection.

As expected this system takes more time to lower its temperature than to increase it. After the moment it was turned on (1st vertical green dashed line) it only took 39 s to reach the desired temperature values but it took 398 s to retrieve the initial temperature value after the moment it was turned off (2nd vertical green dashed line). As for the pressure, it took a similar amount of time to reach the desired pressure as to reach the desired temperature (26 s) but took a lot lesser time than the temperature to recover the original value (297 s). This might be explained by the loss of vacuum due to small leaks.

However, the relation between the temperature and the pressure is visible. As the temperature rises, the pressure lowers and vice versa. So a transformation function, that scales and moves the pressure across the vertical axis can be found so this similarity can be studied. This function was:

$$Transformed\ Values = -\frac{(max\ ℃) - (min\ ℃)}{(min\ Pa) - (max\ Pa)}(original\ Pa\ values + max\ Pa) + min\ ℃ \quad (3.1)$$

This transformation is shown in figure 3.3 (a). In this figure it is noticeable across all the response, turning on the current produces an immediate effect on the pressure sensor readings, which shows that the Joule effect is an effective way of actuating an SMA spring.

Another representation of the data is shown in figure 3.3(b), instead of showing the evolution across time this graphic shows the pressure in function of the temperature. It is visible a series of circles between 54 and 63 ℃ and between -3.5$\times$10³ and -6$\times$10³ Pa. These circles happen because we are avoiding to reaching the 0% martensitic fraction associated with functional fatigue. These circles are caused by the control turning on and off the actuator, changing the martensitic fraction. This is not a single cycle because there are the pressures losses, sliding each circle as the negative pressure is lost. It is noticeable that activating the gripper to grip a part is a lot faster than recovering its original pressure to be able to grip another part.

In this test, it became clear that the system worked and could create the minimum pressure to grab an object during a reasonable amount of time. Also, this type of control proved to be effective in maintaining a pressure value.

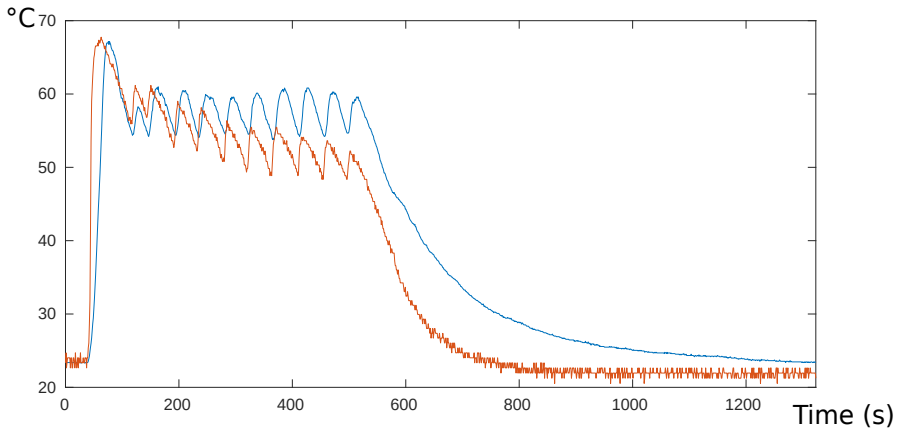

(a) Readings from the current pressure sensor in red and adjusted readings from the pressure sensor in blue along the time in s

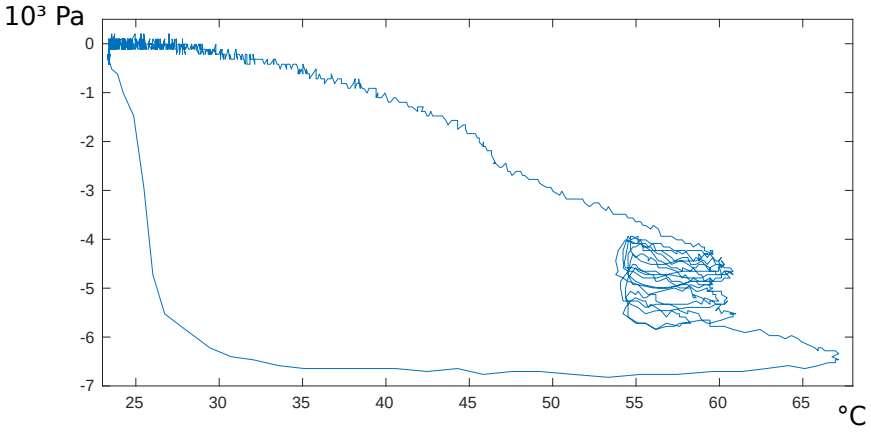

(b) Evolution of pressure (the vertical axis) with the temperature (horizontal axis)

Figure 3.3: In the top graphic is presented the readings from the temperature sensor as blue line along with adjusted pressure sensor readings (equation 3.1) as a red line.
The bottom graphic represents the change in pressure as the temperature changes.

3.2.2 Gripping Tests

The next test was a grip success test with 7 trials for each object. This was done filling the membrane with 30 ml of granular material (polystyrene for the first tests) which presented low gripping capabilities. Even using the spheres and cubes the successful grips were between 3 and 4 successes out of 7 trials. So after some testing, the filling was changed to 50 ml of granular material and this time the success rate was always the same as presented in table 3.2. So 50 ml filling was used to do all 24 tests across all different objects and granular substances.

As stated in table 3.2 the only parts that the gripper could not grab with success where the pyramids and the 50 cent coin. This is in accordance with the holding force measured in [1], pyramids and coin have low holding force.

There were experiments where the initial pressure was not zero, some of these experiments did not reach pressures lower than -5$\times$10³ Pa. These experiments were not considered in the final results, but nevertheless showed an interesting fact. Despite the smaller vacuum, the gripper could still be used to

grip successfully the smallest objects (50% of the gripper size).
The polystyrene seemed to grip the part better because even in the case of misalignment the part was grabbed as in the other fillers they would mostly fall out. Also, it was the only granular material that was able to lift the 50 cent coin from the surface despite not holding for the 20 s stated. The pyramids could only be gripped if the base edge was facing upwards instead of the top. It was also tested to see whether any other external force would make the object fall and the test object did not ungripp unless it was firmly pulled. Examples of some of these tests are shown in figure 3.4

Table 3.2: Success rate on 7 trial experiment with 50 ml polystyrene as filler material

Object	Successful grip	
	50% gripper size	75% gripper size
sphere	7/7	7/7
cube	7/7	7/7
pyramid	0/7	0/7
5 cent coin	7/7	
50 cent coin	0/7	

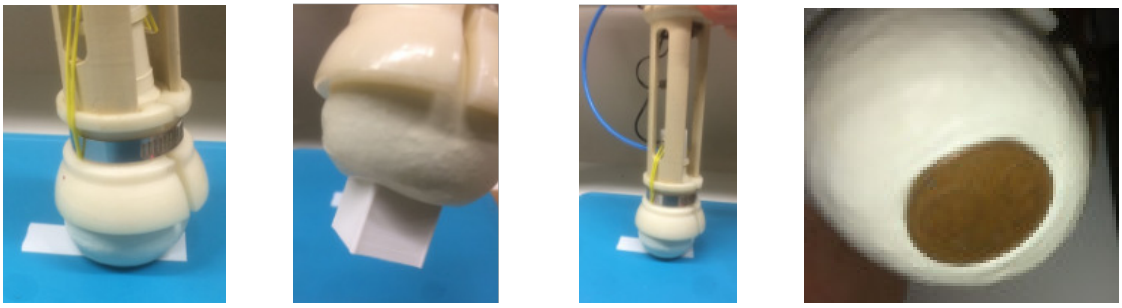

(a) (b) (c) (d)

Figure 3.4: Examples of some of the gripping tests performed

As most of this data is very similar, in this section only 3 tests are presented (figures 3.5, 3.6, 3.7) each with a different filler material and the rest can be found in appendix A. The first fact that must be reported is the similarity of these figures with figure 3.2. One difference is the moment the gripper touches the part, producing a slight increase in pressure (cyan circle). The second difference is the moment that the piece is lifted from the plane (green circle), producing a slight increase in pressure. In some cases, this smaller difference is not visible due to the sensor noise. As for the moment the object falls off the gripper, no change is visible in any of the sensors values. There are variations in current and temperature visible when executing a gripping test. During these experiments, it was possible to see that this system is very slow to recover its original state of high martensitic fraction.
As explained in [1], positive pressure after a grip is important to get a better grip on the next object so a full recovery of the initial pressure is needed.
One of the difficulties of this experiment is the force done while pushing the gripper against the object. As the granular material might not be exactly in the same position the force applied has to be regulated by the increase in pressure.

It was also noticeable in every test, with the exclusion of the experiment with polystyrene and 50 cents coin, if the test object stayed gripped within the first 20 s it stayed gripped till the gripper was turned off.

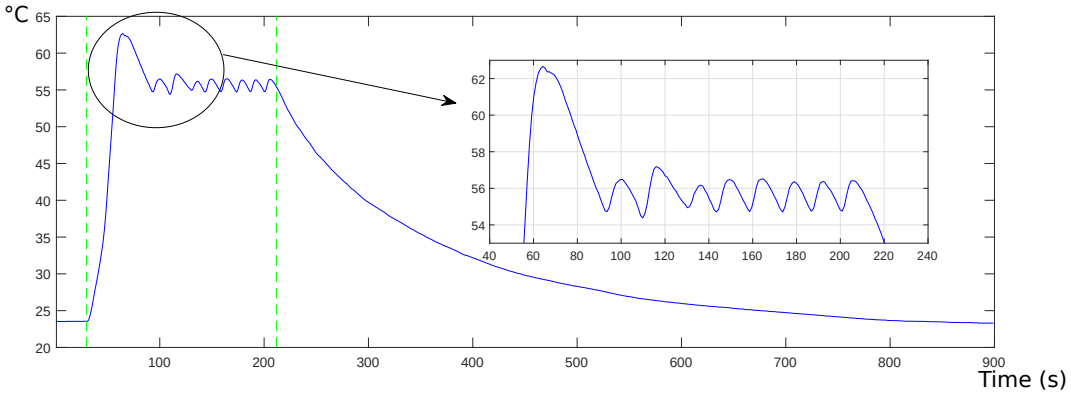

(a) Readings from the temperature sensor in ℃ along the time in s

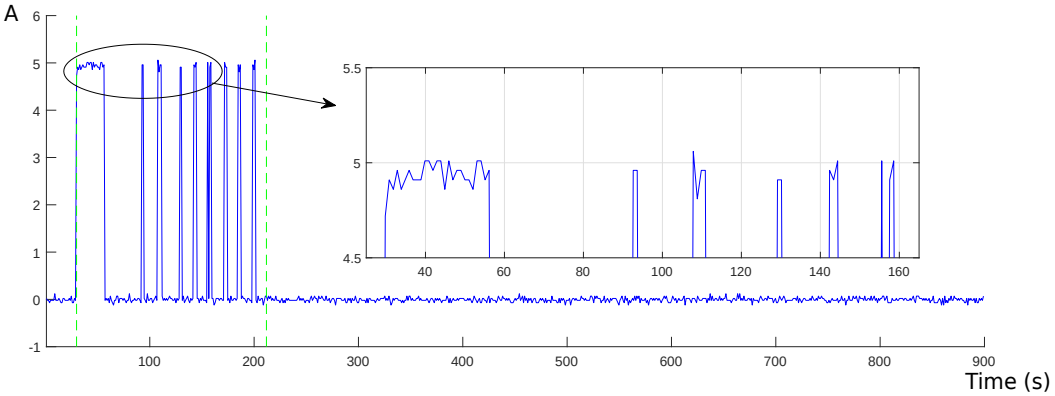

(b) Readings from the current flow sensor in A along the time in s

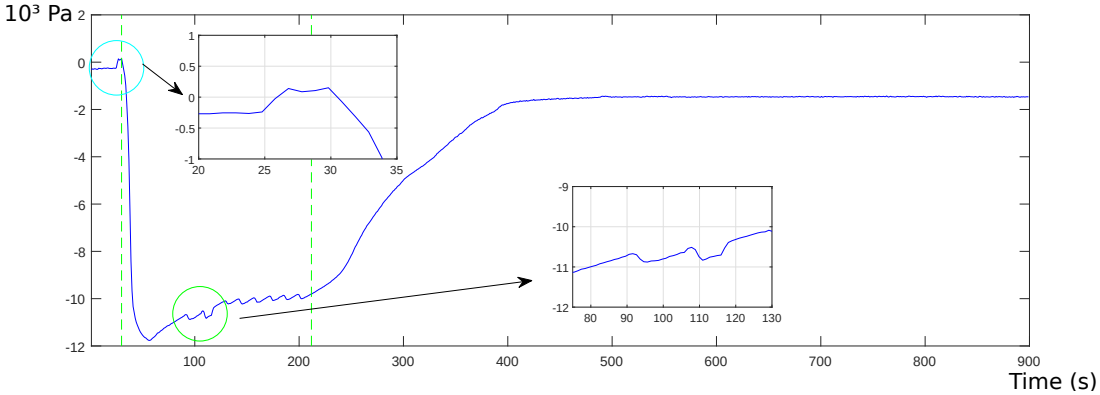

(c) Readings from the pressure sensor in 10^3 Pa along the time in s

Figure 3.5: Readings from the temperature sensor (top), current flow sensor (middle) and pressure sensor (bottom).
The 50% sized sphere was grabbed using polystyrene as grip filler. The x-axis is time and the y-axis is temperature, current and pressure, respectively.
The first green dashed line represents the moment when the gripper was activated and the second the time it was turned off. The cyan and green circles represent the following moments: gripper touches the object and gripper is lifted from the table.

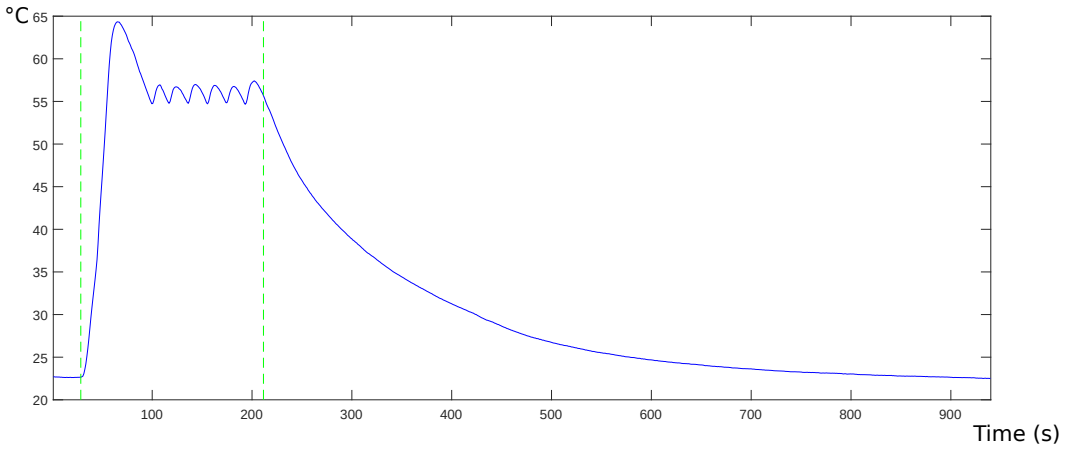

(a) Readings from the temperature sensor in ℃ along the time in s

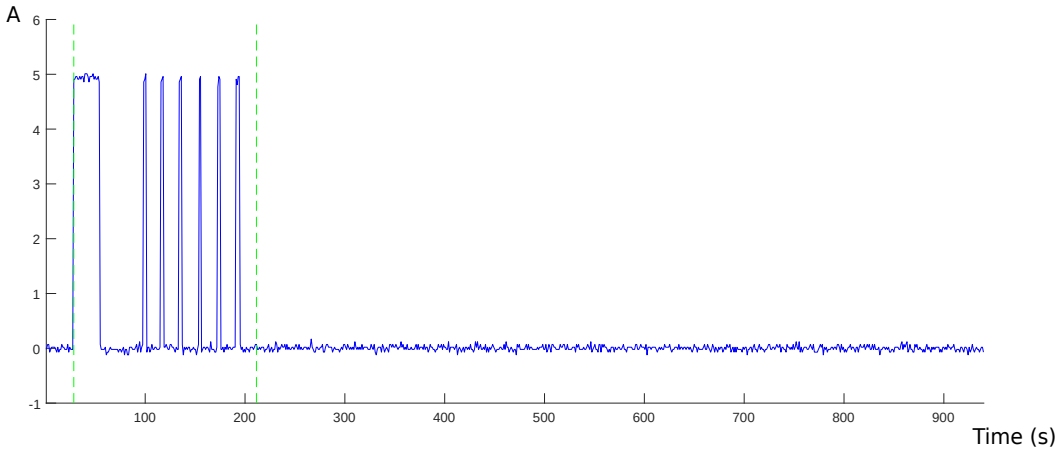

(b) Readings from the current flow sensor in A along the time in s

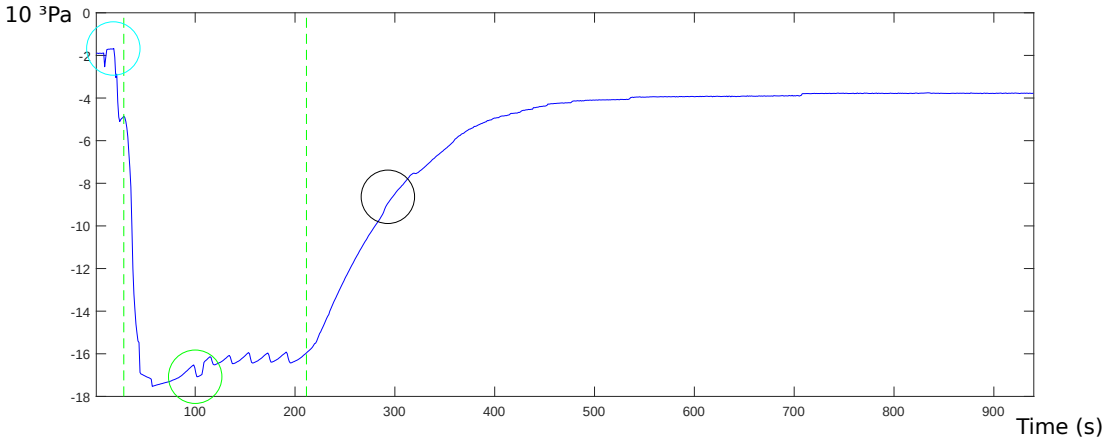

(c) Readings from the pressure sensor in 10^3 Pa along the time in s

Figure 3.6: Readings from the temperature sensor (top), current flow sensor (middle) and pressure sensor (bottom).
The 75% sized cube was grabbed using couscous as grip filler. The x-axis is time and the y-axis is temperature, current and pressure, respectively.
The first green dashed line represents the moment when the gripper was activated and the second the time it was turned off. The cyan and green circles represent the following moments: gripper touches the object and gripper is lifted from the table.

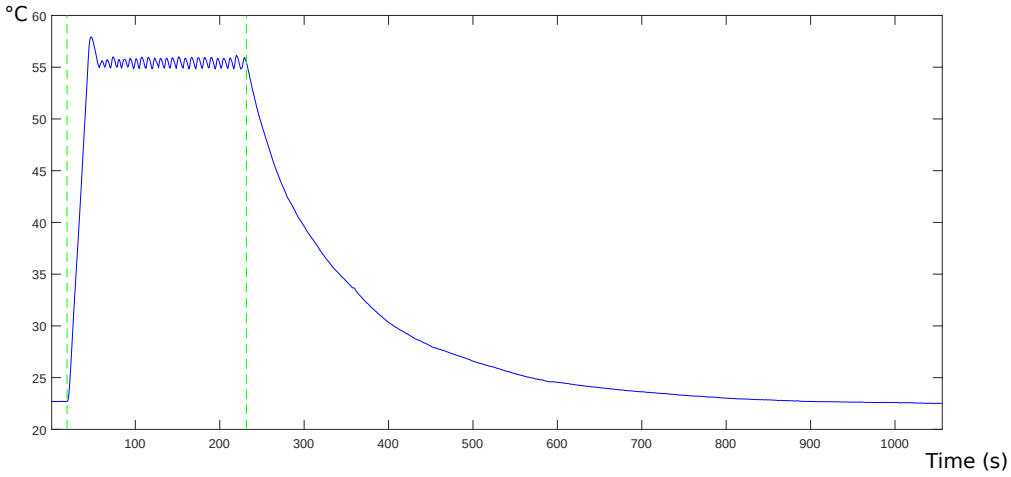

(a) Readings from the temperature sensor in ℃ along the time in s

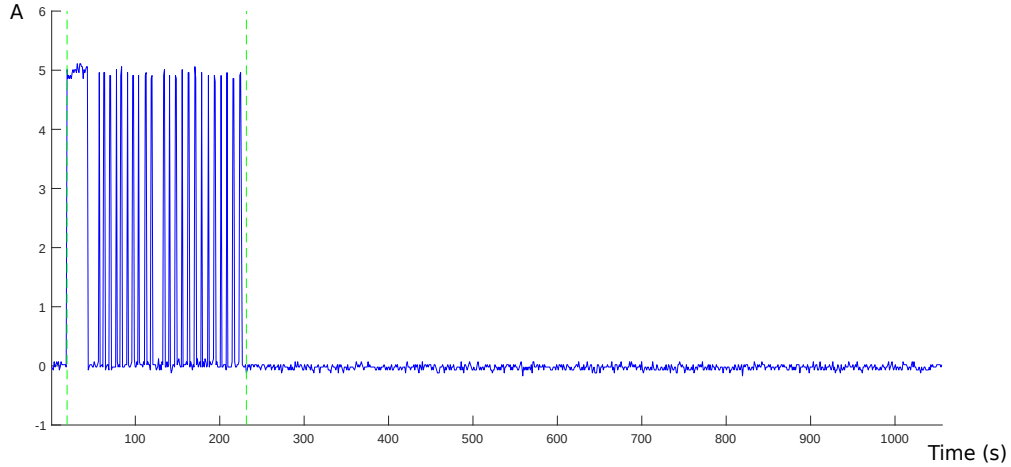

(b) Readings from the current flow sensor in A along the time in s

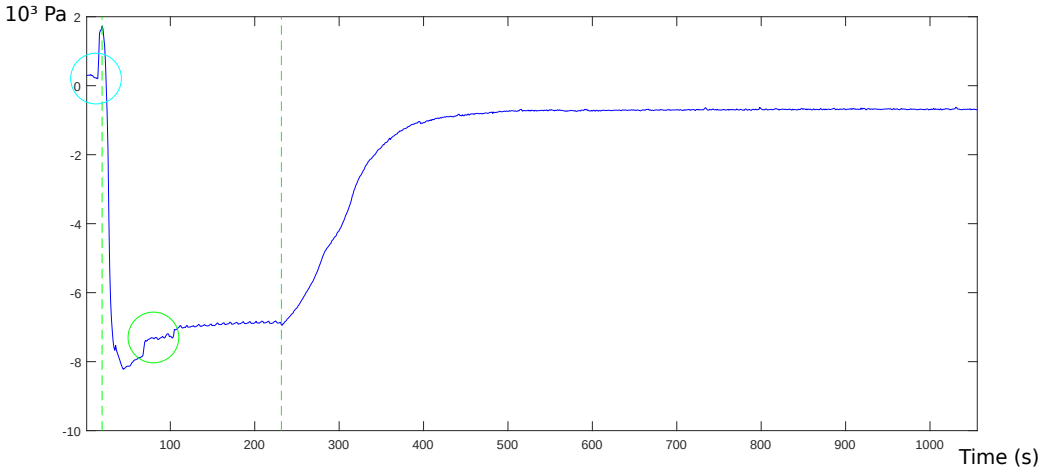

(c) Readings from the pressure sensor in 10^3 Pa along the time in s

Figure 3.7: Readings from the temperature sensor (top), current flow sensor (middle) and pressure sensor (bottom).
The 5 cent euro coin was grabbed using coffee as grip filler. The x-axis is time and the y-axis is temperature, current and pressure, respectively.
The first green dashed line represents the moment when the gripper was activated and the second the time it was turned off. The cyan and green circles represent the following moments: gripper touches the object and gripper is lifted from the table.

Chapter 4

Conclusions

The proposed design and prototype make use of a self-contained SMA actuation system to drive a fully closed vacuum system. It was demonstrated that a variable volume closed system is a viable approach to generate the vacuum pressure required to drive a granular jamming gripper. So the main objective of this work was achieved.

A new method (hardness tests) to select granular materials was also proposed. This method is meant to give a good first analysis of the jamming granular effect efficiency, and it did show that granular substances with bigger grains would produce a less desirable effect, in accordance with [1]. However, this experiment along with the experiments of gripping objects shows that a certain degree of deformability may be desirable to optimize the application of jamming granular effect to gripping objects. This was demonstrated when expanded polystyrene did show the most flexibility with gripper and test object misalignment, despite having a smaller BHN than milled coffee used in [38]. It also made the gripper lighter and avoided the humidity sensibility present in coffee.

While developing the SMA actuator it was essential the creation of a design tool as it sped the work and made it less prone to errors. This allowed the production of springs that could exert the needed force to create negative pressure inside the membrane. This pressure was verified in chapter 3.2.2 so it can be asserted that austenitic shear modulus was correctly estimated during the tensile tests. The wire diameter and the outer spring diameter are the most important factors as it influenced the actuation force. Despite of that, the choice of diameters is limited to the torque of the drilling machine and the tensile strength of the wire. In this work, the limit was the torque of the drilling machine.

After several attempts, the method of producing spring was perfected so that tightly springs without spacing between coils were obtained. So there is a reasonable degree of certainty in the fact that this method of producing springs is a good alternative to the lathe machine. Here it is important to point out the importance of wounding the wire in the direction opposing the screw thread.

As for the last experiments, it was proven that a PWM actuation with an on-off control is efficient in this application and did not produce any detectable functional fatigue of the actuator. The sensor system was able to provide the necessary data pressure and temperature to show that the system is very fast to activate but slow to recover to its initial condition. The recorded time to full recovery of the original

pressure value was close to 600 s, which is not acceptable for a practical application of the device, but more can be done to improve recovery time.
In the analysis of the experiment, it was found a relation between the temperature and pressure and it was observed that the actuator was working in a safe zone where the martensite fraction was not zero.
Finally, as in [1], some gripping tests were made, showing to some extent the universality and capabilities of the gripper. Also, it was demonstrated that a self-contained actuator is a viable answer to solve issues such as weight, noise, compactness and additional compressors or electric motors.

4.1 Future Work

There is still work to be developed and further investigation of these areas is needed.
As for the granular effect, it would be very important to model and predict correctly its behaviour.
The Brinell hardness test might give a good first analysis of the jamming granular effect efficiency but further studies should be done to find the optimal Brinell hardness number. Brinnel tests should be done with different materials, followed by grip success tests to find the number that characterizes the optimal deformability and holding force. There are also some issues to be addressed like small variations in pressure due to air leaks, the difficulty in measuring the indentation due to elastic properties of the membrane and precision of the measurement done with a caliper.
In order to improve the slow cooling time of the actuator maybe a fan could be used to generate forced convection instead of natural convection of the surrounding air. Also, the implementation of a magnet used alongside the rubber bands could be studied. However, cautions must be taken to avoid interference with the control board, sensors and the object being gripped. If this addition is possible, it could extend the spring faster improving the cooling time.
During this work, one of the major concerns was making sure that the pressure inside the membrane was always the same when the actuator was turned on. One of the main issues with the technique used for printing plastic (fused deposition modeling) is that it creates small fissures which air can pass through. In this prototype the solution was to replace the printed part with a part machined from a nylon blank. However, using a 3D stereolithographic printer could be another interesting solution to make lighter but still airtight parts.
Improving the sealing could also allow for better employment of higher vacuum pressure after grips, increasing the next grip success probability even in the case of misalignment.

Bibliography

[1] E. Browna, N. Rodenberga, H. L. , John Amendb , Annan Mozeikac , Erik Steltzc , Mitchell R. Zakind, Jaegera, and H. M. Universal robotic gripper based on the jamming of granular material. *IEEE Transactions on Robotics*, 28(2):341–350, 2010. ISSN 15523098. doi: 10.1109/TRO.2011.2171093.

[2] Aristotle. *Nicomachean Ethics*. 2014. ISBN 9781624661174.

[3] B. Siciliano, L. Sciavicco, L. Villani, and G. Oriolo. *Robotics: Modelling, Planning and Control*. 2009. ISBN 9781846286414. doi: 10.1007/978-1-84628-642-1. URL http://books.google.com/books?hl=en{&}lr={&}id=jPCAFmE-logC{&}oi=fnd{&}pg=PR8{&}dq=Robotics+-+Modelling+Planning+and+Control{&}ots=3TMi0jIsuu{&}sig=VoMpDiIASZGcrAg7juLabQszoqE.

[4] International Ffederation of Robotics artcles and news. https://ifr.org/ifr-press-releases/news/robots-double-worldwide-by-2020. Accessed: 2019-07-23.

[5] J. D. G. Robinson. Continuum Robots - A State of the Art. *Conference on Robotics and Automation*, (May):2849–2854, 1999.

[6] C. Laschi, B. Mazzolai, and M. Cianchetti. Soft robotics: Technologies and systems pushing the boundaries of robot abilities. *Science Robotics*, 1(1):eaah3690, 2016. ISSN 2470-9476. doi: 10.1126/scirobotics.aah3690. URL http://robotics.sciencemag.org/lookup/doi/10.1126/scirobotics.aah3690.

[7] H. T. Lin, G. G. Leisk, and B. Trimmer. GoQBot: A caterpillar-inspired soft-bodied rolling robot. *Bioinspiration and Biomimetics*, 6(2), 2011. ISSN 17483182. doi: 10.1088/1748-3182/6/2/026007.

[8] R. Deimel and O. Brock. A novel type of compliant and underactuated robotic hand for dexterous grasping. *International Journal of Robotics Research*, 35(1-3):161–185, 2016. ISSN 17413176. doi: 10.1177/0278364915592961.

[9] B. Mazzolai, L. Margheri, M. Cianchetti, P. Dario, and C. Laschi. Soft-robotic arm inspired by the octopus: II. from artificial requirements to innovative technological solutions. *Bioinspiration and Biomimetics*, 7(2), 2012. ISSN 17483182. doi: 10.1088/1748-3182/7/2/025005.

[10] J. R. Amend, E. Brown, N. Rodenberg, H. M. Jaeger, and H. Lipson. A positive pressure universal

gripper based on the jamming of granular material. *IEEE Transactions on Robotics*, 28(2):341–350, 2012. ISSN 15523098. doi: 10.1109/TRO.2011.2171093.

[11] M. H. Elahinia and H. Ashrafiuon. Nonlinear Control of a Shape Memory Alloy Actuated Manipulator. *Journal of Vibration and Acoustics*, 124(4):566, 2002. ISSN 07393717. doi: 10.1115/1.1501285. URL http://vibrationacoustics.asmedigitalcollection.asme.org/article.aspx?articleid=1470452.

[12] S. C.-g. Alloys. Cadmium-Gold Alloys Solid. 337(1906), 1932.

[13] D. J. L. Leo. *Engineering Analysis of Smart Material Systems*. 2007. ISBN 9780471684770. doi: 10.1002/9780470209721. URL http://doi.wiley.com/10.1002/9780470209721.

[14] M. Elahinia. *Shape Memory Alloy Actuators: Design, Fabrication and Experimental Evaluation*. 2016. ISBN 1118359445. doi: 10.1002/9781118426913. URL https://books.google.com/books?id=hJAvCgAAQBAJ{&}pgis=1.

[15] D. Zrinscak. *Study and design of a bioinspired actuation system for a soft robotic total artificial heart*. PhD thesis, POLITECNICO DI TORINO, 2018.

[16] W. J. Buehler and R. C. Wiley. United States Patent Office. *U.S. Code*, 157(35):75–170, 1961. URL https://patentimages.storage.googleapis.com/60/57/80/e5941b87509929/US3174851.pdf.

[17] C. Fi. Case fi l copy. *NASA Technical Memorandum*, 1-16-59L(L-144), 1959. URL http://ntrs.nasa.gov/archive/nasa/casi.ntrs.nasa.gov/19980232082.pdf.

[18] P. K. Kumar and D. C. Lagoudas. Shape Memory Alloys. 1, 2008. doi: 10.1007/978-0-387-47685-8. URL http://link.springer.com/10.1007/978-0-387-47685-8.

[19] F. Auricchio, E. Boatti, and M. Conti. *SMA Biomedical Applications*. Elsevier Ltd, 2014. ISBN 9780080999210. doi: 10.1016/B978-0-08-099920-3.00011-5. URL http://dx.doi.org/10.1016/B978-0-08-099920-3.00011-5.

[20] J. M. Jani, M. Leary, and A. Subic. Shape Memory Alloys in Automotive Applications. *Applied Mechanics and Materials*, 663:248–253, 2014. ISSN 1662-7482. doi: 10.4028/www.scientific.net/AMM.663.248. URL http://www.scientific.net/AMM.663.248.

[21] K. Ikuta. Micro/miniature shape memory alloy actuator. *Proceedings., IEEE International Conference on Robotics and Automation*, pages 2156–2161, 1990. doi: 10.1109/ROBOT.1990.126323.

[22] D. J. Hartl and D. C. Lagoudas. Aerospace applications of shape memory alloys. *Proceedings of the Institution of Mechanical Engineers, Part G: Journal of Aerospace Engineering*, 221(4):535–552, 2007. ISSN 09544100. doi: 10.1243/09544100JAERO211.

[23] A. Hadi, A. Yousefi-Koma, M. Elahinia, M. M. Moghaddam, and A. Ghazavi. A shape memory alloy spring-based actuator with stiffness and position controllability. *Proceedings of the Institution of*

Mechanical Engineers. Part I: Journal of Systems and Control Engineering, 225(7):902–917, 2011. ISSN 09596518. doi: 10.1177/2041304110394570.

[24] M. M. Kheirikhah, S. Rabiee, and M. E. Edalat. A Review of Shape Memory Alloy Actuators in Robotics. pages 206–217, 2011.

[25] J. Mohd Jani, M. Leary, A. Subic, and M. A. Gibson. A review of shape memory alloy research, applications and opportunities. *Materials and Design*, 56:1078–1113, 2014. ISSN 18734197. doi: 10.1016/j.matdes.2013.11.084. URL http://dx.doi.org/10.1016/j.matdes.2013.11.084.

[26] J. N. Kudva. Overview of the DARPA smart wing project. *Journal of Intelligent Material Systems and Structures*, 15(4):261–267, 2004. ISSN 1045389X. doi: 10.1177/1045389X04042796.

[27] B. a. Trimmer, A. E. Takesian, B. M. Sweet, C. B. Rogers, D. C. Hake, and D. J. Rogers. Caterpillar locomotion : A new model for soft- bodied climbing and burrowing robots. *7th International Symposium on Technology and the Mine Problem, Monterey, CA May 2-5, 2006*, (April 2002):1–10, 2006.

[28] T. Ishii. *Design of shape memory alloy (SMA) coil springs for actuator applications*. Woodhead Publishing Limited, 2011. doi: 10.1533/9780857092625.1.63. URL http://dx.doi.org/10.1533/9780857092625.1.63.

[29] K. S. Kuang, S. T. Quek, and W. J. Cantwell. Active control of a smart composite with shape memory alloy sheet using a plastic optical fiber sensor. *Sensors and Actuators, A: Physical*, 201: 182–187, 2013. ISSN 09244247. doi: 10.1016/j.sna.2013.06.024. URL http://dx.doi.org/10.1016/j.sna.2013.06.024.

[30] P. A. Gédouin, E. Delaleau, J. M. Bourgeot, C. Join, S. Arbab Chirani, and S. Calloch. Experimental comparison of classical PID and model-free control: Position control of a shape memory alloy active spring. *Control Engineering Practice*, 19(5):433–441, 2011. ISSN 09670661. doi: 10.1016/j.conengprac.2011.01.005.

[31] N. Keshtkar and K. Röbenack. Unstructured uncertainty based modeling and robust stability analysis of textile-reinforced composites with embedded shape memory alloys. *Algorithms*, 13(1), 2020. ISSN 19994893. doi: 10.3390/a13010024.

[32] Á. Villoslada, N. Escudero, F. Martín, A. Flores, C. Rivera, M. Collado, and L. Moreno. Position control of a shape memory alloy actuator using a four-term bilinear PID controller. *Sensors and Actuators, A: Physical*, 236:257–272, 2015. ISSN 09244247. doi: 10.1016/j.sna.2015.10.006. URL http://dx.doi.org/10.1016/j.sna.2015.10.006.

[33] A. Silva, S. De Oliveira, A. Ries, S. A. Silva, and C. Souto. A Fuzzy Logic Control System for a Robotic Hand Driven by Shape Memory Alloy Wires. *European Journal of Engineering Research and Science*, 4(10):173–178, 2019. doi: 10.24018/ejers.2019.4.10.1599.

[34] Y. Pan, Z. Guo, X. Li, and H. Yu. Output-Feedback Adaptive Neural Control of a Compliant Differential SMA Actuator. *IEEE Transactions on Control Systems Technology*, 25(6):2202–2210, 2017. ISSN 10636536. doi: 10.1109/TCST.2016.2638958.

[35] J. Li and H. Tian. Position control of SMA actuator based on inverse empirical model and SMC-RBF compensation. *Mechanical Systems and Signal Processing*, 108:203–215, 2018. ISSN 08883270. doi: 10.1016/j.ymssp.2018.02.004. URL https://doi.org/10.1016/j.ymssp.2018.02.004{%}0Ahttp://linkinghub.elsevier.com/retrieve/pii/S0888327018300633.

[36] J. Shintake, V. Cacucciolo, D. Floreano, and H. Shea. Soft Robotic Grippers. *Advanced Materials*, 1707035(May), 2018. ISSN 15214095. doi: 10.1002/adma.201707035.

[37] J. Amend, N. Cheng, S. Fakhouri, and B. Culley. Soft Robotics Commercialization: Jamming Grippers from Research to Product. *Soft Robotics*, 3(4):213–222, 2016. ISSN 2169-5172. doi: 10.1089/soro.2016.0021.

[38] J. Amend, N. Cheng, S. Fakhouri, and B. Culley. Soft Robotics Commercialization: Jamming Grippers from Research to Product. *Soft Robotics*, 3(4):213–222, 2016. ISSN 2169-5172. doi: 10.1089/soro.2016.0021. URL http://online.liebertpub.com/doi/10.1089/soro.2016.0021.

[39] A. Firouzeh and J. Paik. Grasp Mode and Compliance Control of an Underactuated Origami Gripper Using Adjustable Stiffness Joints. *IEEE/ASME Transactions on Mechatronics*, 22(5):2165–2173, 2017. ISSN 10834435. doi: 10.1109/TMECH.2017.2732827.

[40] J. Guo, K. Elgeneidy, C. Xiang, N. Lohse, L. Justham, and J. Rossiter. Soft pneumatic grippers embedded with stretchable electroadhesion. *Smart Materials and Structures*, 27(5), 2018. ISSN 1361665X. doi: 10.1088/1361-665X/aab579.

[41] P. Glick, S. A. Suresh, D. Ruffatto, M. Cutkosky, M. T. Tolley, and A. Parness. A Soft Robotic Gripper with Gecko-Inspired Adhesive. *IEEE Robotics and Automation Letters*, 3(2):903–910, 2018. ISSN 23773766. doi: 10.1109/LRA.2018.2792688.

[42] S. Li, J. J. Stampfli, H. J. Xu, E. Malkin, E. V. Diaz, D. Rus, and R. J. Wood. A vacuum-driven origami 'magic-ball' soft gripper. *Proceedings - IEEE International Conference on Robotics and Automation*, 2019-May:7401–7408, 2019. ISSN 10504729. doi: 10.1109/ICRA.2019.8794068.

[43] E. Roels, S. Terryn, J. Brancart, R. Verhelle, G. Van Assche, and B. Vanderborght. Additive Manufacturing for Self-Healing Soft Robots. *Soft Robotics*, 00(00):1–13, 2020. ISSN 2169-5172. doi: 10.1089/soro.2019.0081.

[44] D. Bi, J. Zhang, B. Chakraborty, and R. P. Behringer. Jamming by shear. *Nature*, 480(7377):355–358, 2011. ISSN 00280836. doi: 10.1038/nature10667. URL http://dx.doi.org/10.1038/nature10667.

[45] G. Biroli. Jamming: A new kind of phase transition? *Nature Physics*, 3(4):222–223, 2007. ISSN 17452481. doi: 10.1038/nphys580.

[46] J. P. Davim and A. G. Magalhães. *Ensaios Mecânicos e Tecnológicos*. Publindústria, 2010. ISBN 9789728953546.

[47] IInterautomatika datasheets. http://interautomatika.lt/download/Diaphragm%20Air%20Cylinders%20datasheet_ENG.pdf, . Accessed: 2020-04-10.

[48] M. N. Fox, R. L. Roebuck, and D. Cebon. Modelling rolling-lobe air springs. *International Journal of Heavy Vehicle Systems*, 14(3):254–270, 2007. ISSN 1744232X. doi: 10.1504/IJHVS.2007.015603.

[49] Globalspec database. https://www.globalspec.com/learnmore/mechanical_components/springs/air_springs, . Accessed: 2019-07-23.

[50] R. Budynas and K. Nisbett. *Shigley's Mechanical Engineering Design*. McGraw-Hill Education, 2010. ISBN 9780073529288. URL https://books.google.pt/books?id=eT1DPgAACAAJ.

[51] Globalspec database. http://www.matweb.com/search/datasheettext.aspx?matguid=44afc7d3c6eb4829bc2df27884fd2d6c. Accessed: 2020-07-10.

[52] E. Brown, N. Rodenberg, J. Amend, a. Mozeika, E. Steltz, M. R. Zakin, H. Lipson, and H. M. Jaeger. From the Cover: Universal robotic gripper based on the jamming of granular material. *Proceedings of the National Academy of Sciences*, 107(44):18809–18814, 2010. ISSN 0027-8424. doi: 10.1073/pnas.1003250107.

Appendix A

Gripping Tests

A.0.1 Polystyrene Grain as Filler Material

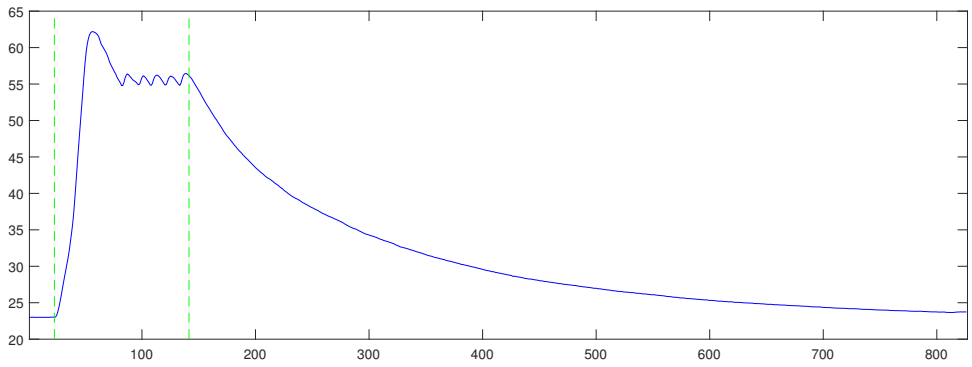

(a) Readings from temperature sensor in °C along the time in s

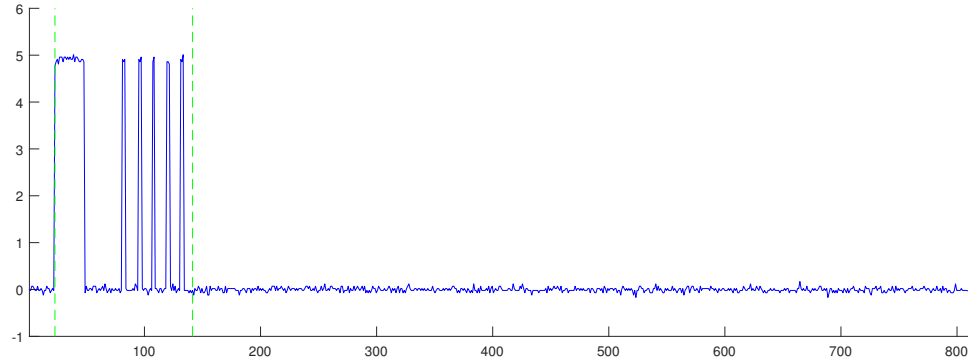

(b) Readings from current flow sensor in A along the time in s

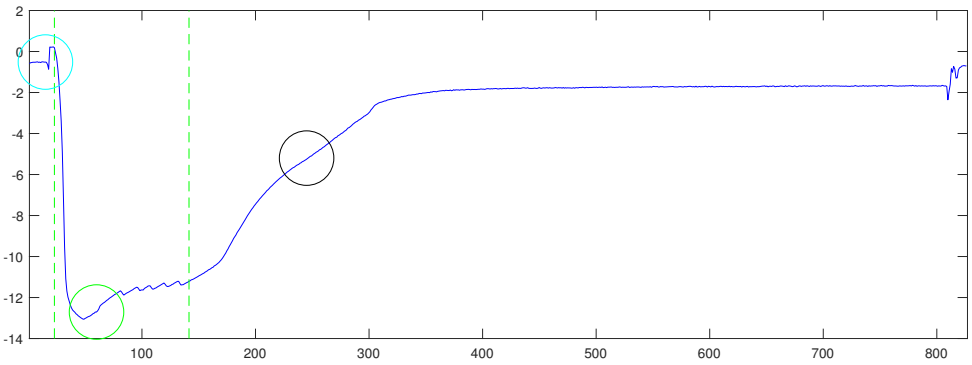

(c) Readings from pressure sensor in 10^3 Pa along the time in s

Figure A.1: Readings from temperature sensor (Top), current flow sensor (middle) and pressure sensor (bottom).
The 75% sized sphere was grabbed using polystyrene as grip filler. The 5 cent euro coin was grabbed using coffee as grip filler. The x-axis is time and the y-axis is temperature, current and pressure, respectively.
The first green dashed line represents the moment when the gripper was activated and the second the time it was turned off. The cyan and green circles represent the following moments: gripper touches the object and gripper is lifted from the table

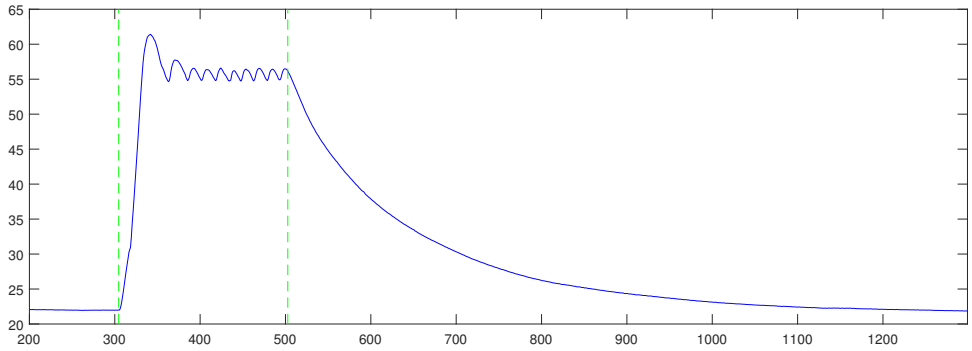

(a) Readings from temperature sensor in ℃ along the time in s

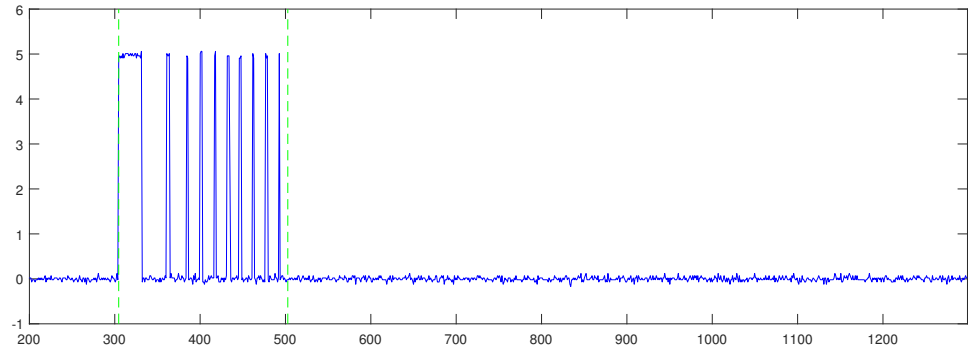

(b) Readings from current flow sensor in A along the time in s

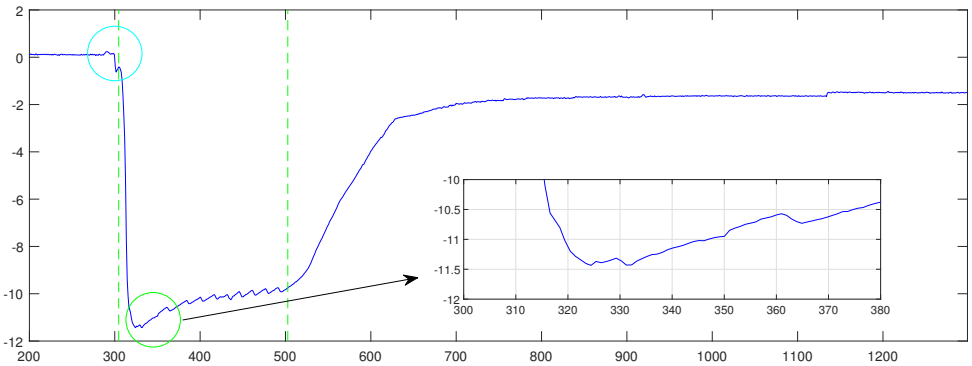

(c) Readings from pressure sensor in 10^3 Pa along the time in s

Figure A.2: Readings from temperature sensor (Top), current flow sensor (middle) and pressure sensor (bottom).
The The 50% sized cube was grabbed using polystyrene as grip filler. The x-axis is time and the y-axis is temperature, current and pressure, respectively.
The first green dashed line represents the moment when the gripper was activated and the second the time it was turned off. The cyan and green circles represent the following moments: gripper touches the object and gripper is lifted from the table

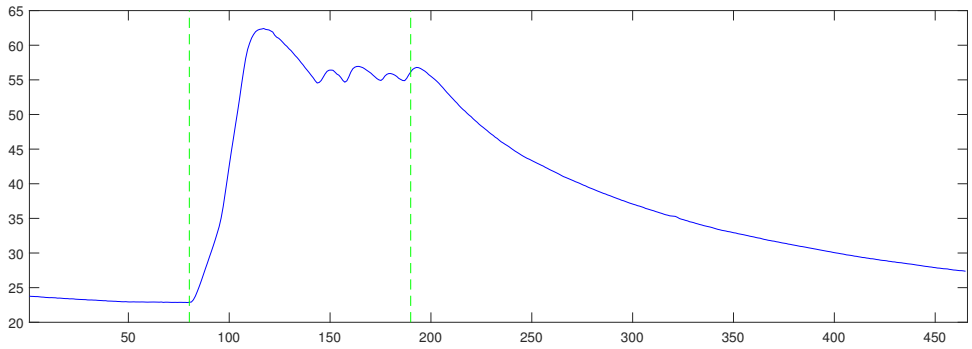

(a) Readings from temperature sensor in ℃ along the time in s

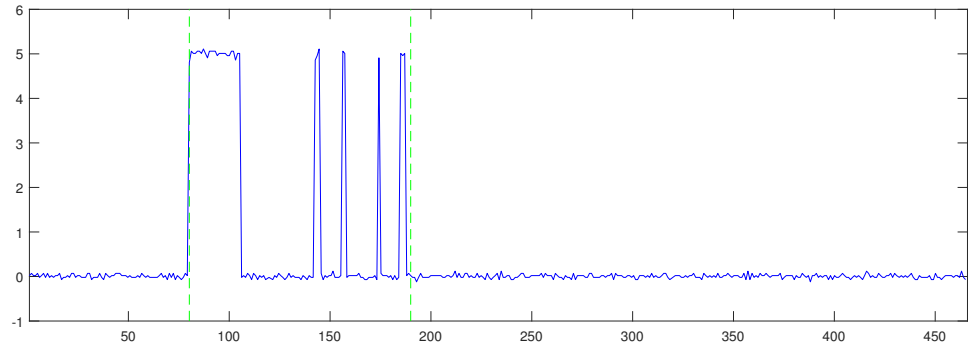

(b) Readings from current flow sensor in A along the time in s

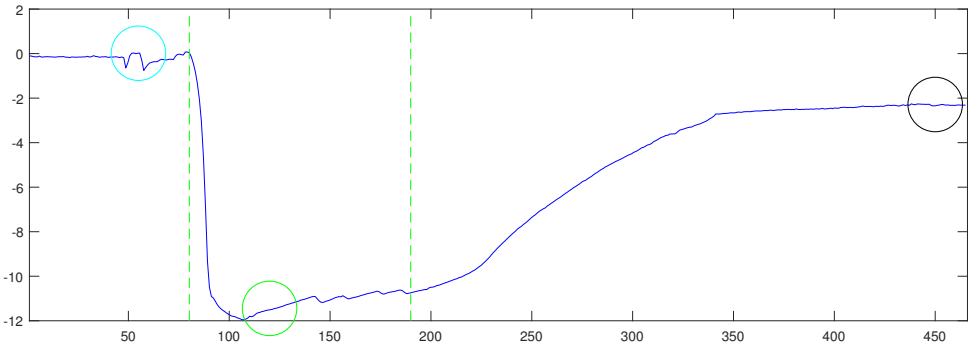

(c) Readings from pressure sensor in 10^3 Pa along the time in s

Figure A.3: Readings from temperature sensor (Top), current flow sensor (middle) and pressure sensor (bottom).
The The 75% sized cube was grabbed using polystyrene as grip filler. The x-axis is time and the y-axis is temperature, current and pressure, respectively.
The first green dashed line represents the moment when the gripper was activated and second the time it was turned off. The cyan and green circles represent the following moments: gripper touches the object and gripper is lifted from the table

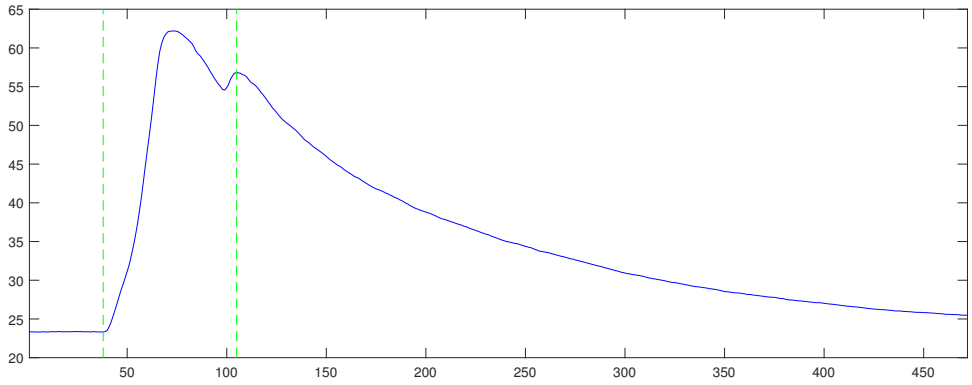

(a) Readings from temperature sensor in ℃ along the time in s

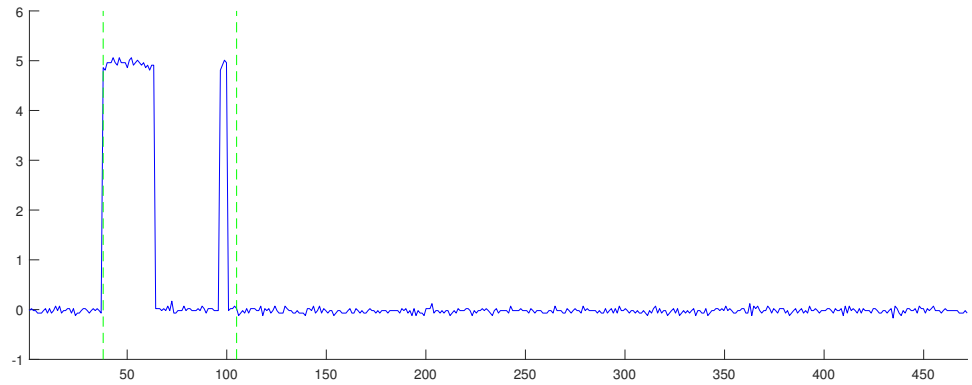

(b) Readings from current flow sensor in A along the time in s

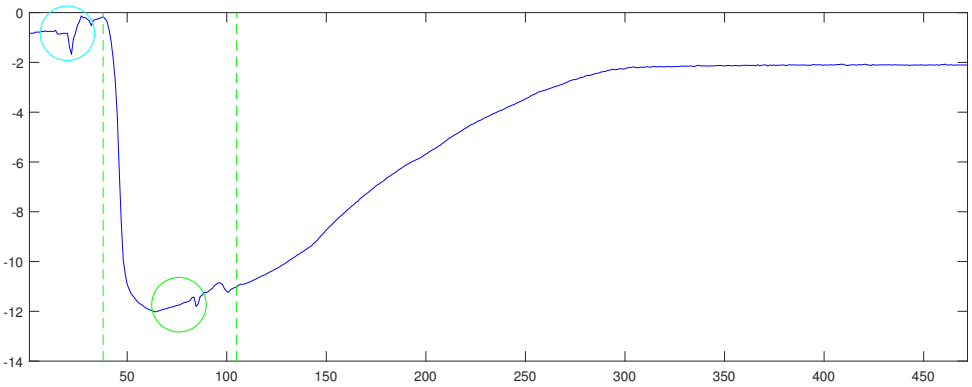

(c) Readings from pressure sensor in 10^3 Pa along the time in s

Figure A.4: Readings from temperature sensor (Top), current flow sensor (middle) and pressure sensor (bottom).
The 50% sized pyramid was grabbed using polystyrene as grip filler. The x-axis is time and the y-axis is temperature, current and pressure, respectively.
The first green dashed line represents the moment when the gripper was activated and the second the time it was turned off. The cyan and green circles represent the following moments: gripper touches the object and gripper is lifted from the table

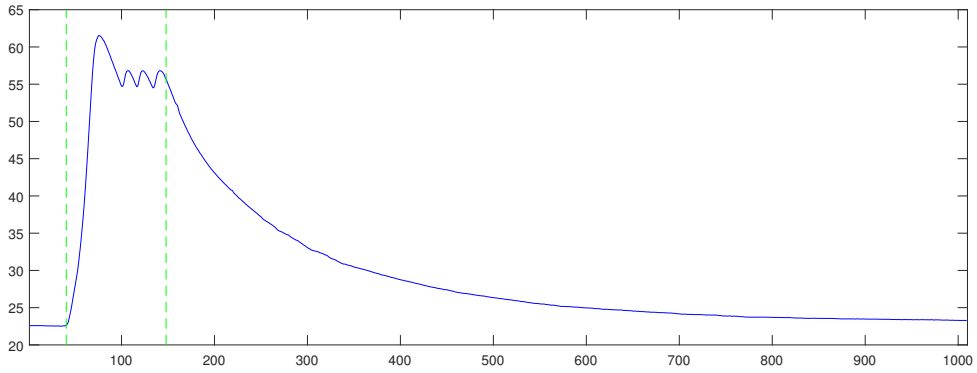

(a) Readings from temperature sensor in ℃ along the time in s

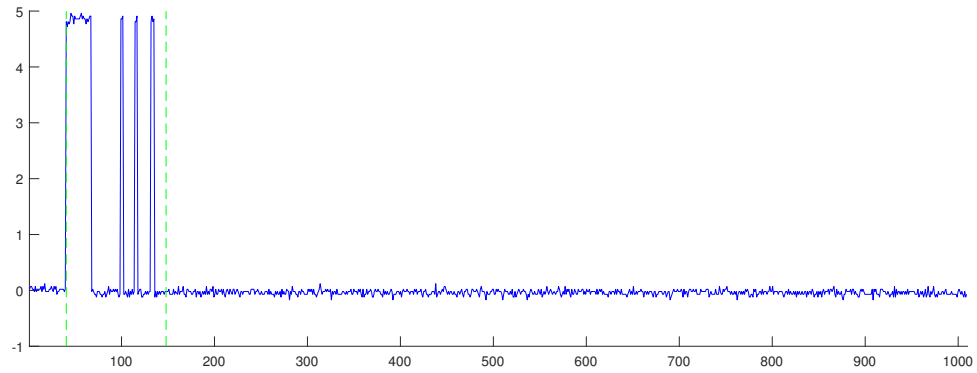

(b) Readings from current flow sensor in A along the time in s

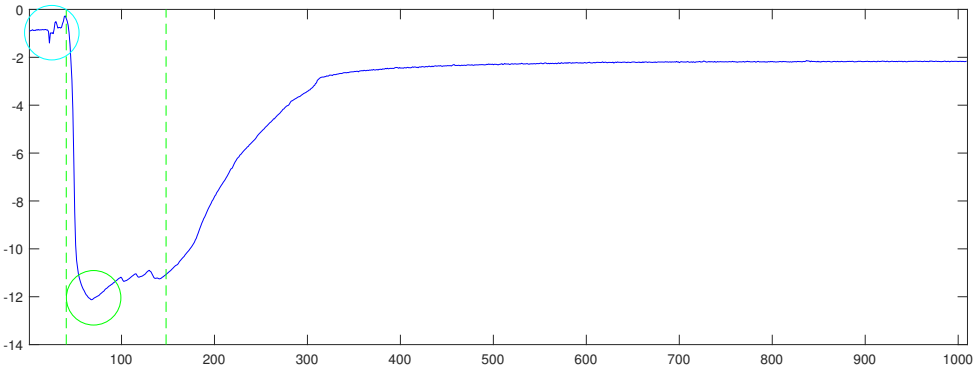

(c) Readings from pressure sensor in 10^3 Pa along the time in s

Figure A.5: Readings from temperature sensor (Top), current flow sensor (middle) and pressure sensor (bottom).
The 75% sized pyramid was grabbed using polystyrene as grip filler. The x-axis is time and the y-axis is temperature, current and pressure, respectively.
The first green dashed line represents the moment when the gripper was activated and the second the time it was turned off. The cyan and green circles represent the following moments: gripper touches the object and gripper is lifted from the table

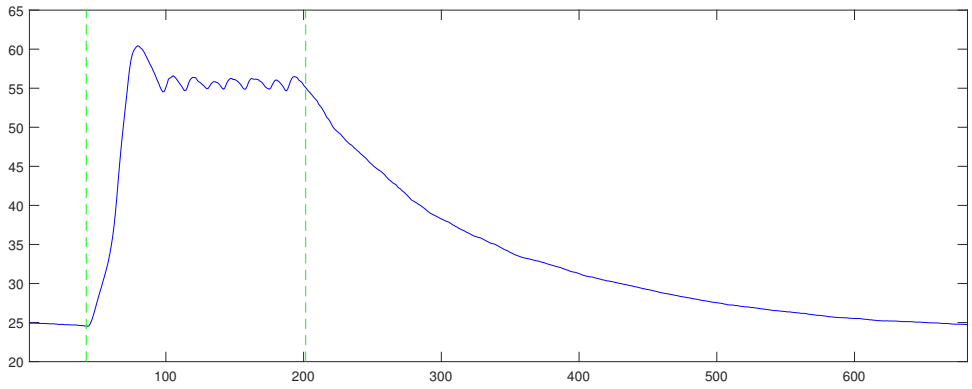

(a) Readings from temperature sensor in ℃ along the time in s

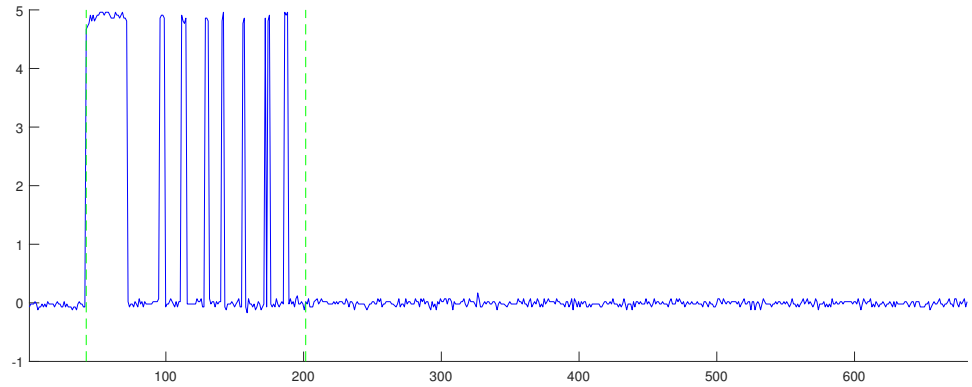

(b) Readings from current flow sensor in A along the time in s

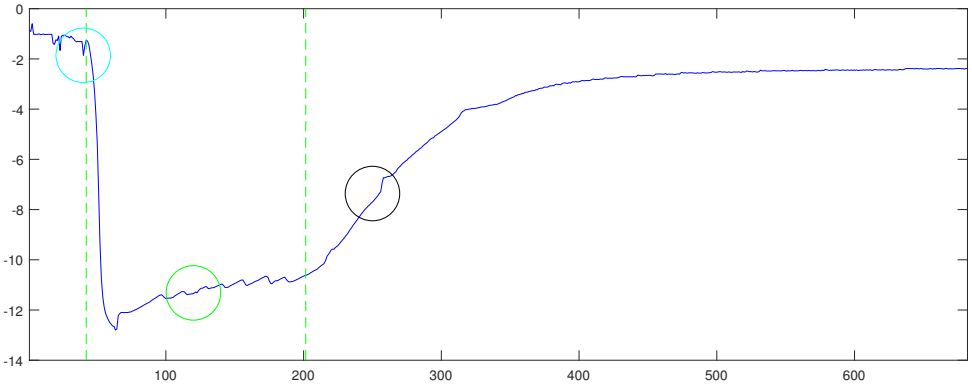

(c) Readings from pressure sensor in 10^3 Pa along the time in s

Figure A.6: Readings from temperature sensor (Top), current flow sensor (middle) and pressure sensor (bottom).
The 5 cent euro coin was grabbed using polystyrene as grip filler. The x-axis is time and the y-axis is temperature, current and pressure, respectively.
The first green dashed line represents the moment when the gripper was activated and the second the time it was turned off. The cyan and green circles represent the following moments: gripper touches the object and gripper is lifted from the table

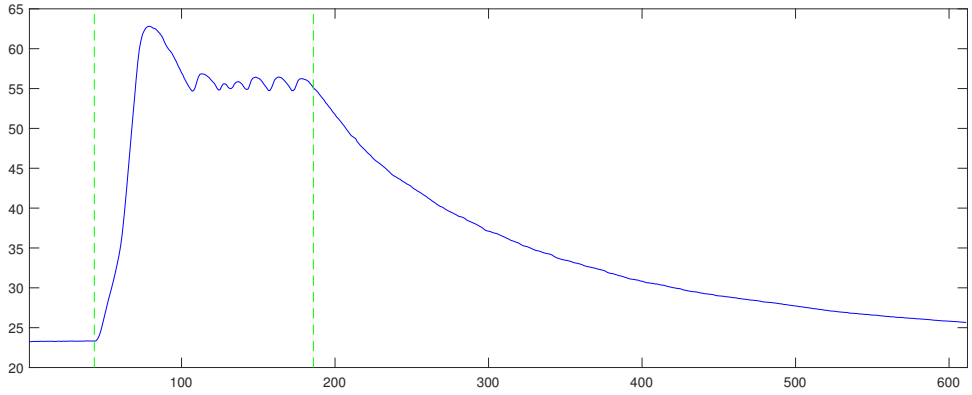

(a) Readings from temperature sensor in °C along the time in s

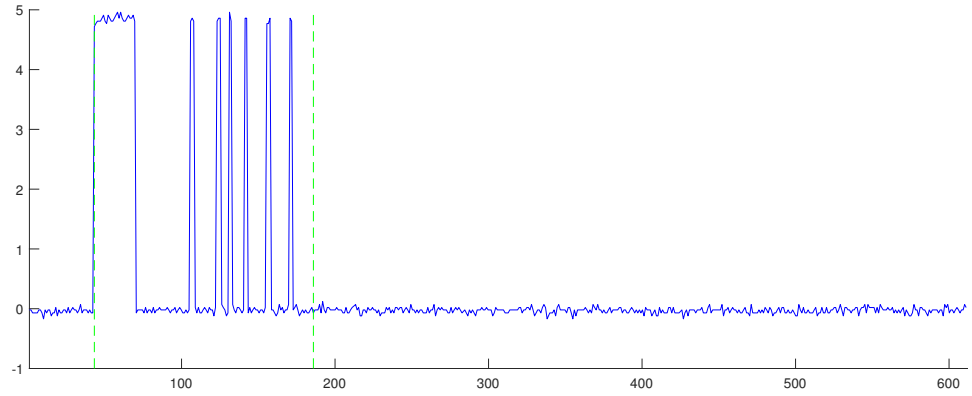

(b) Readings from current flow sensor in A along the time in s

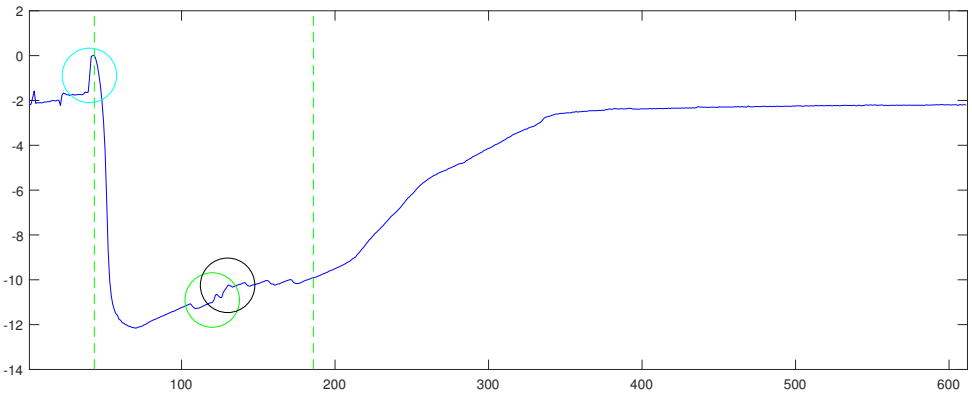

(c) Readings from pressure sensor in 10^3 Pa along the time in s

Figure A.7: Readings from temperature sensor (Top), current flow sensor (middle) and pressure sensor (bottom).
The 50 cent euro coin was grabbed using polystyrene as grip filler. The x-axis is time and the y-axis is temperature, current and pressure, respectively.
The first green dashed line represents the moment when the gripper was activated and the second the time it was turned off. The cyan and green circles represent the following moments: gripper touches the object and gripper is lifted from the table

A.0.2 Couscous as Filler Material

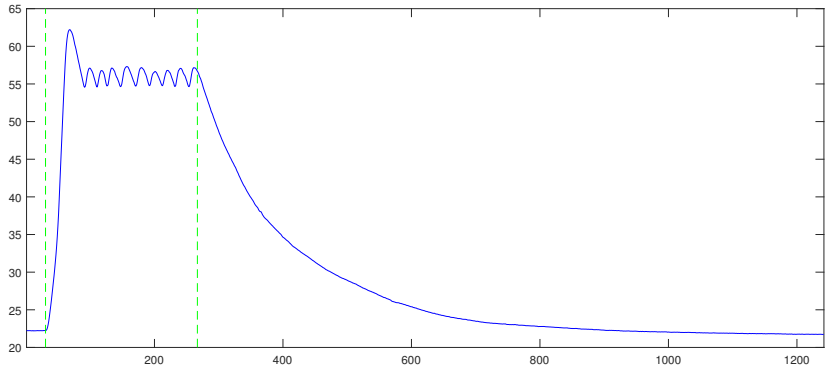

(a) Readings from temperature sensor in ℃ along the time in s

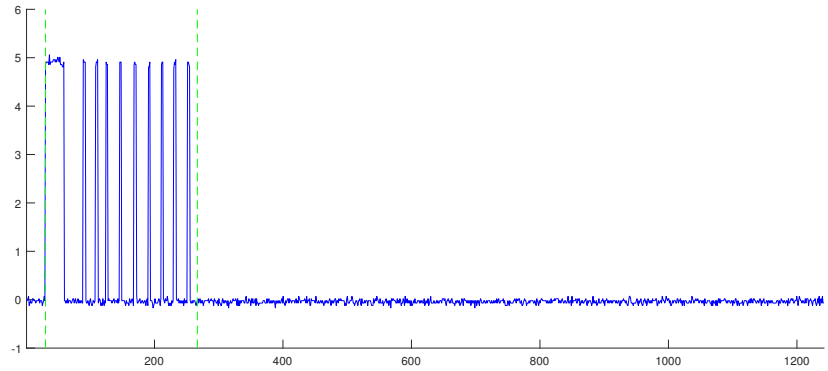

(b) Readings from current flow sensor in A along the time in s

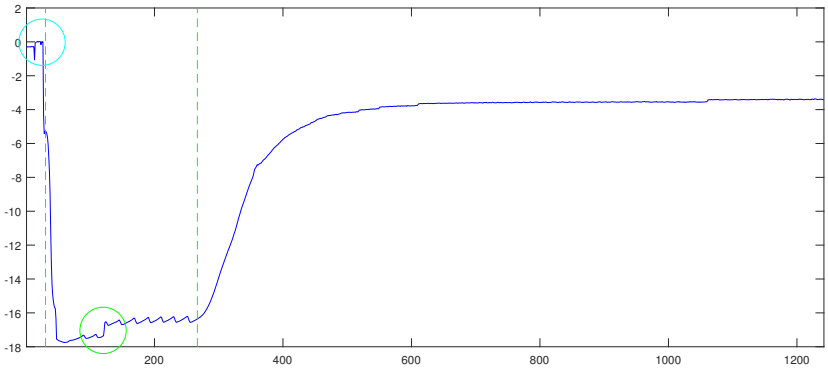

(c) Readings from pressure sensor in 10^3 Pa along the time in s

Figure A.8: Readings from temperature sensor (Top), current flow sensor (middle) and pressure sensor (bottom).
The 50% sized sphere was grabbed using couscous as grip filler. The x-axis is time and the y-axis is temperature, current and pressure, respectively.
The first green dashed line represents the moment when the gripper was activated and the second the time it was turned off. The cyan and green circles represent the following moments: gripper touches the object and gripper is lifted from the table

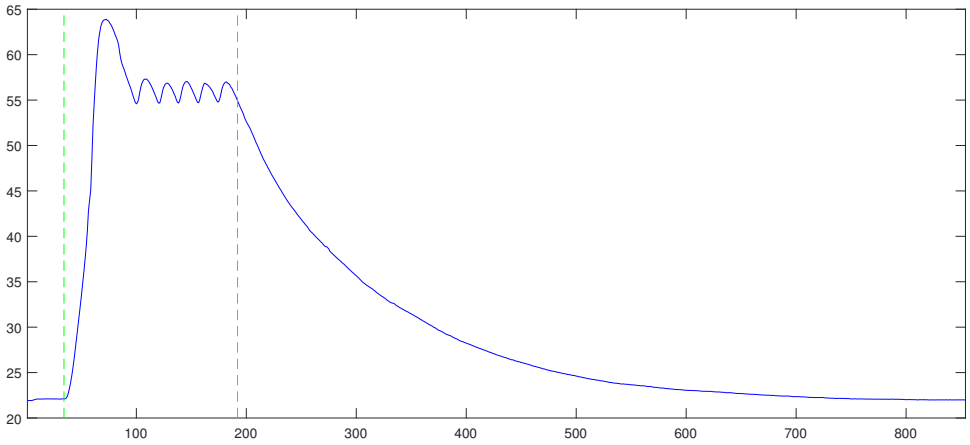

(a) Readings from temperature sensor in ℃ along the time in s

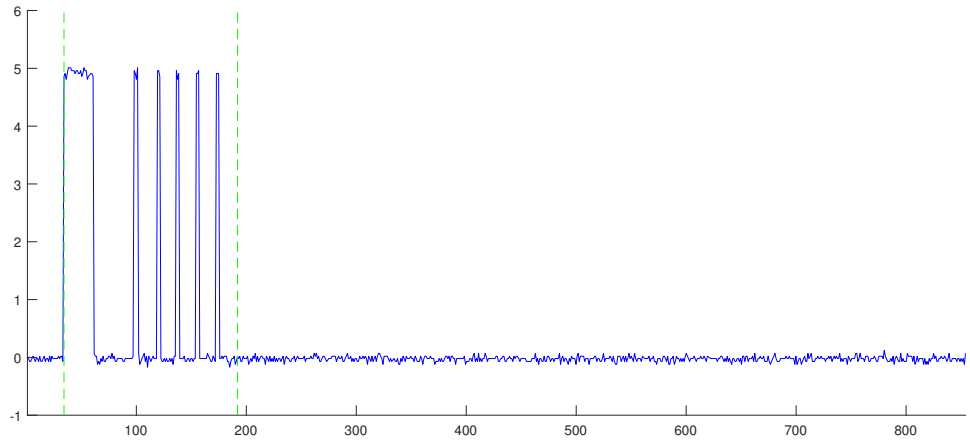

(b) Readings from current flow sensor in A along the time in s

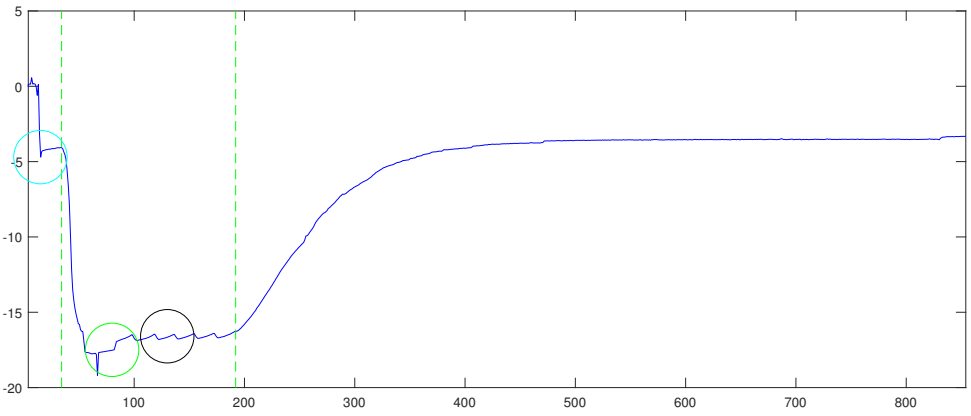

(c) Readings from pressure sensor in 10^3 Pa along the time in s

Figure A.9: Readings from temperature sensor (Top), current flow sensor (middle) and pressure sensor (bottom).
The 75% sized sphere was grabbed using couscous as grip filler. The x-axis is time and the y-axis is temperature, current and pressure, respectively.
The first green dashed line represents the moment when the gripper was activated and the second the time it was turned off. The cyan and green circles represent the following moments: gripper touches the object and gripper is lifted from the table

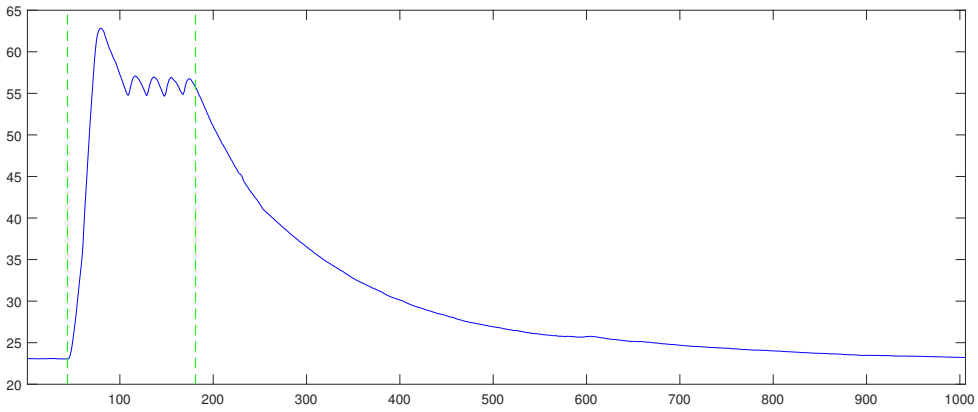

(a) Readings from temperature sensor in ℃ along the time in s

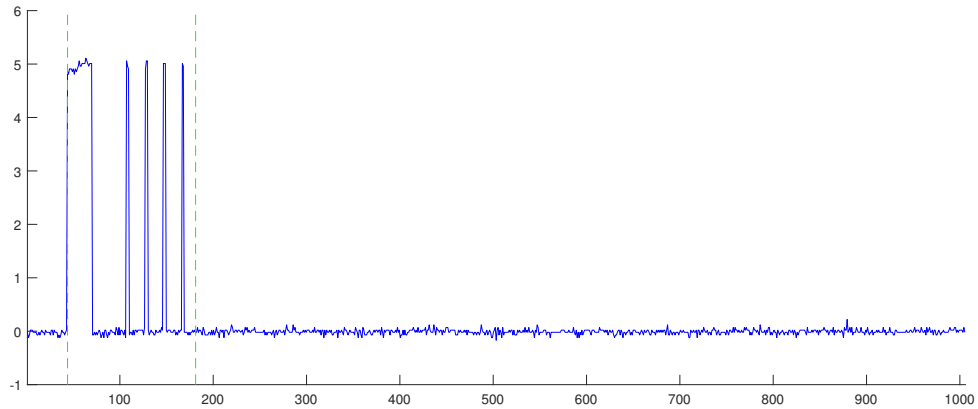

(b) Readings from current flow sensor in A along the time in s

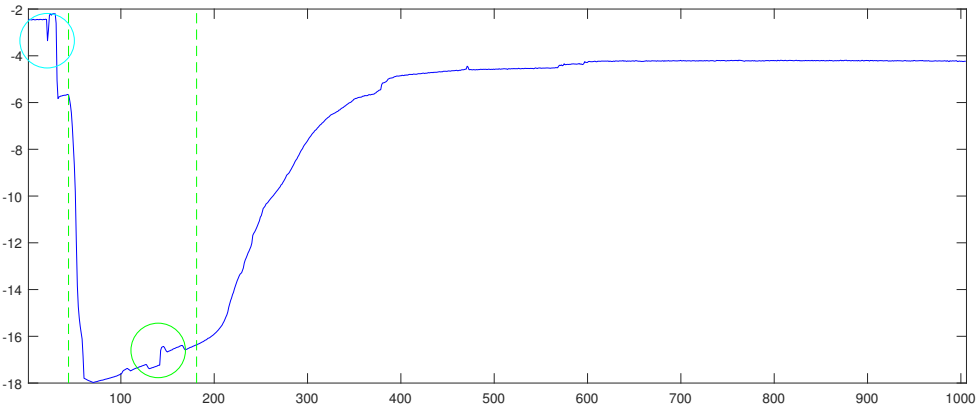

(c) Readings from pressure sensor in 10^3 Pa along the time in s

Figure A.10: Readings from temperature sensor (Top), current flow sensor (middle) and pressure sensor (bottom).
The The 50% sized cube was grabbed using couscous as grip filler. The x-axis is time and the y-axis is temperature, current and pressure, respectively.
The first green dashed line represents the moment when the gripper was activated and the second the time it was turned off. The cyan and green circles represent the following moments: gripper touches the object and gripper is lifted from the table

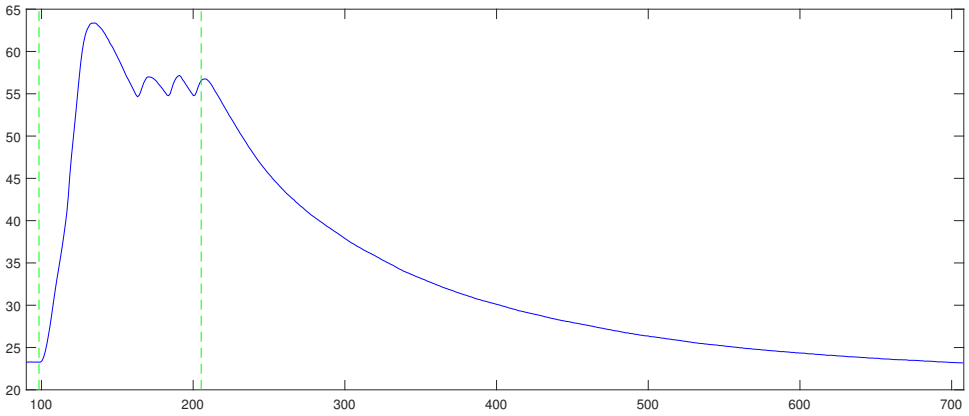

(a) Readings from temperature sensor in ℃ along the time in s

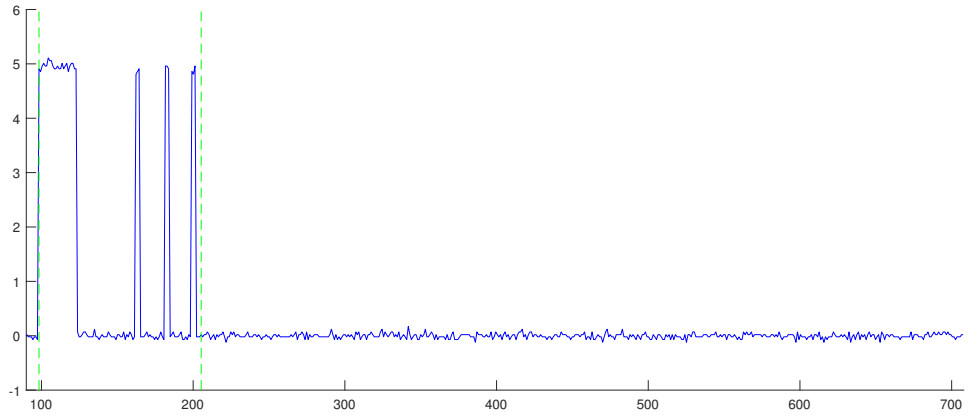

(b) Readings from current flow sensor in A along the time in s

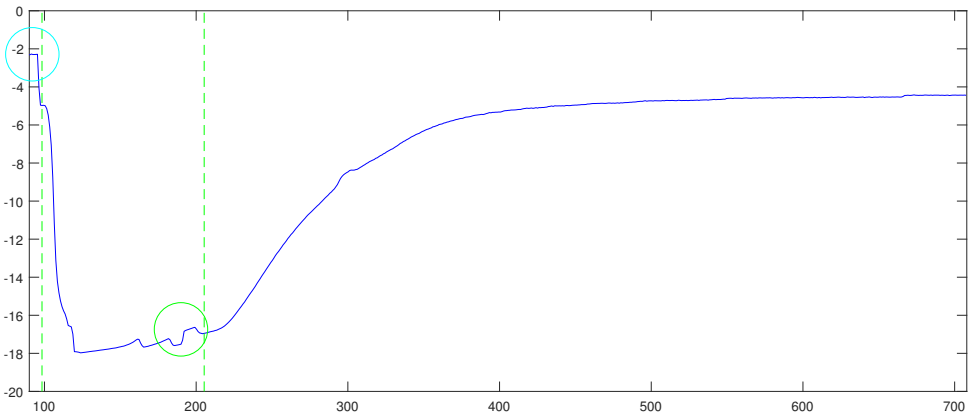

(c) Readings from pressure sensor in 10^3 Pa along the time in s

Figure A.11: Readings from temperature sensor (Top), current flow sensor (middle) and pressure sensor (bottom).
The 50% sized pyramid was grabbed using couscous as grip filler. The x-axis is time and the y-axis is temperature, current and pressure, respectively.
The first green dashed line represents the moment when the gripper was activated and the second the time it was turned off. The cyan and green circles represent the following moments: gripper touches the object and gripper is lifted from the table

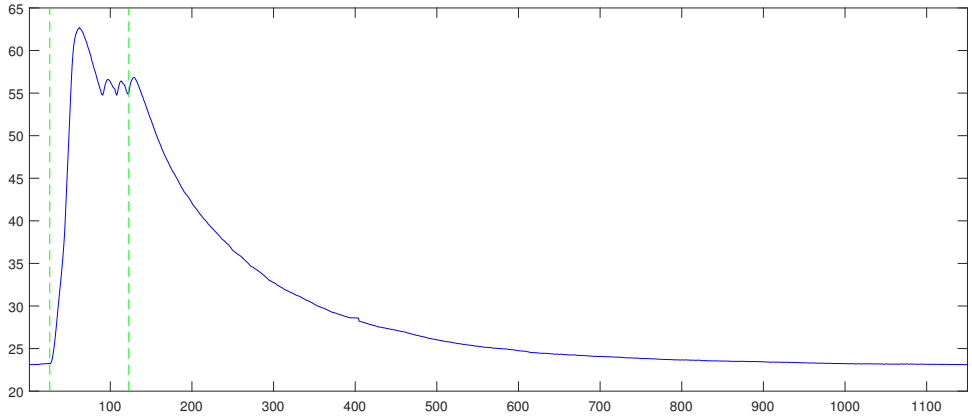

(a) Readings from temperature sensor in °C along the time in s

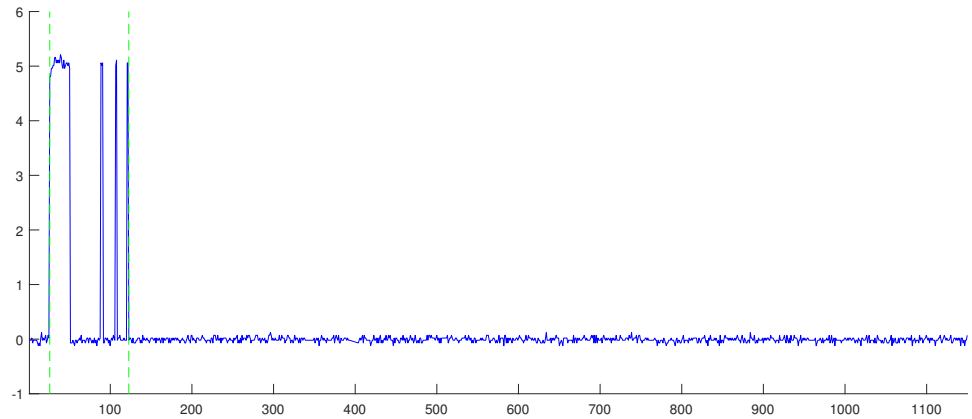

(b) Readings from current flow sensor in A along the time in s

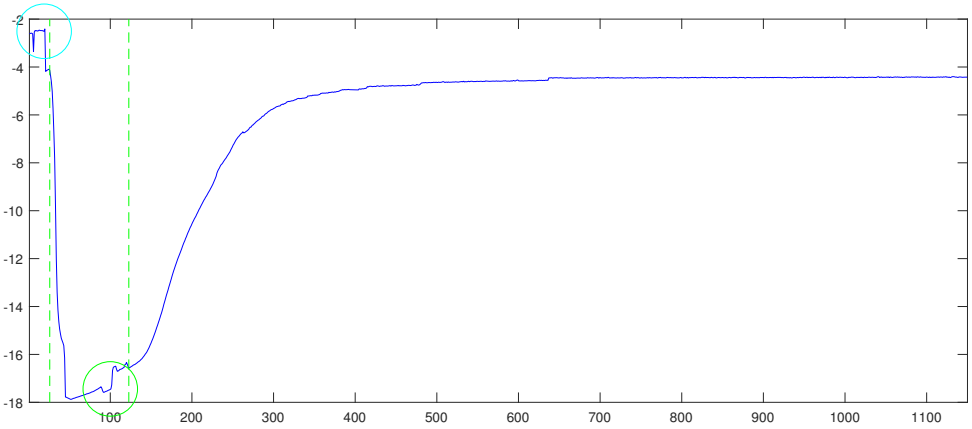

(c) Readings from pressure sensor in 10^3 Pa along the time in s

Figure A.12: Readings from temperature sensor (Top), current flow sensor (middle) and pressure sensor (bottom).
The 75% sized pyramid was grabbed using couscous as grip filler. The x-axis is time and the y-axis is temperature, current and pressure, respectively.
The first green dashed line represents the moment when the gripper was activated and the second the time it was turned off. The cyan and green circles represent the following moments: gripper touches the object and gripper is lifted from the table

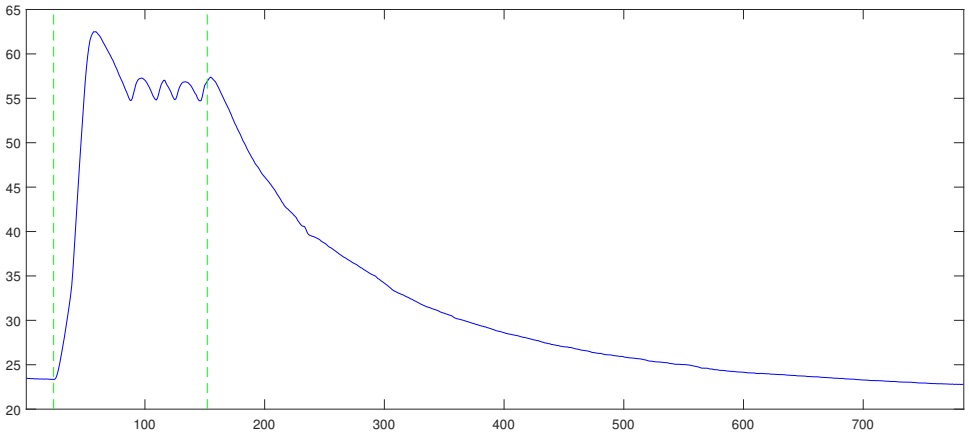

(a) Readings from temperature sensor in ℃ along the time in s

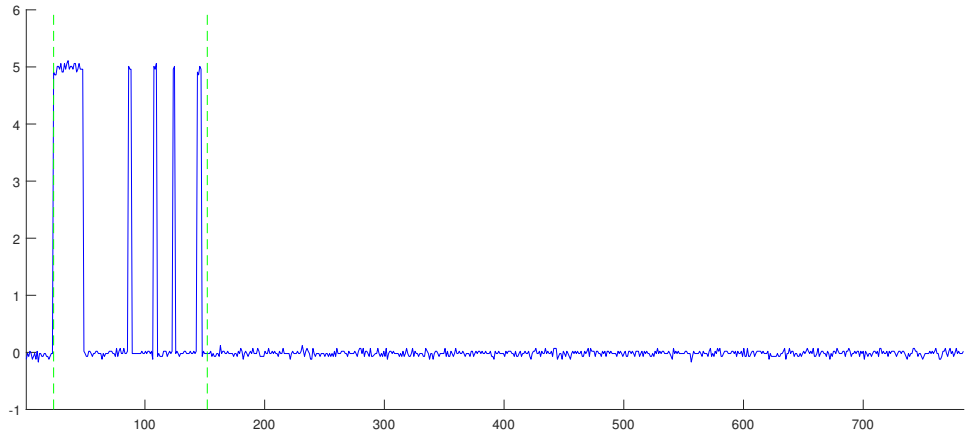

(b) Readings from current flow sensor in A along the time in s

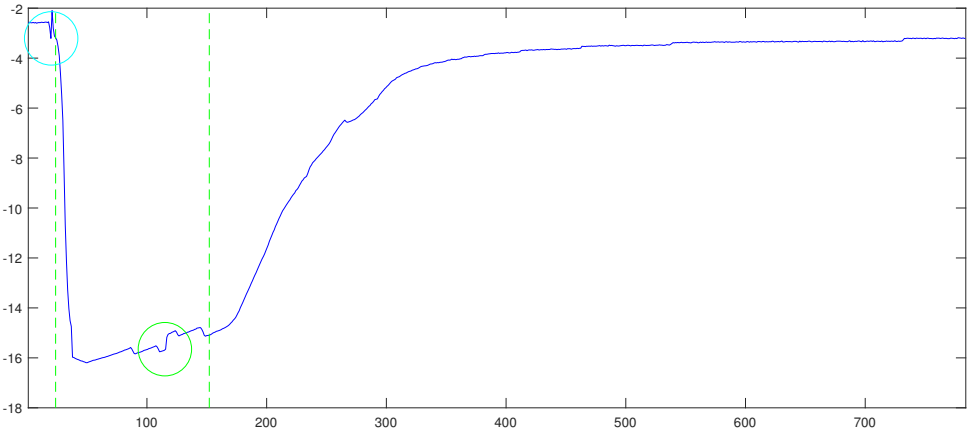

(c) Readings from pressure sensor in 10^3 Pa along the time in s

Figure A.13: Readings from temperature sensor (Top), current flow sensor (middle) and pressure sensor (bottom).
The 5 cent euro coin was grabbed using couscous as grip filler. The x-axis is time and the y-axis is temperature, current and pressure, respectively.
The first green dashed line represents the moment when the gripper was activated and the second the time it was turned off. The cyan and green circles represent the following moments: gripper touches the object and gripper is lifted from the table

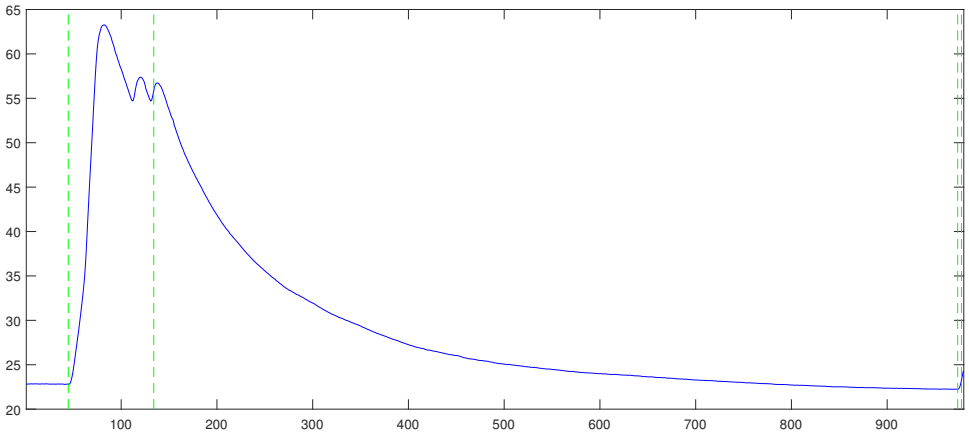

(a) Readings from temperature sensor in ℃ along the time in s

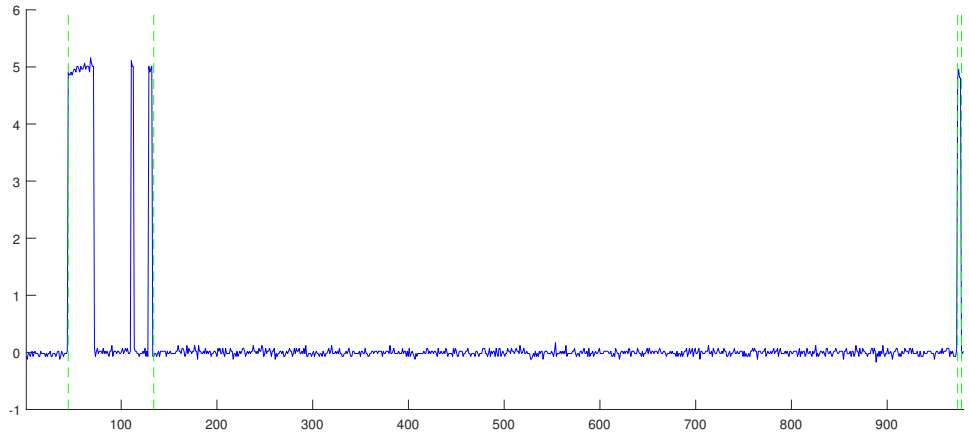

(b) Readings from current flow sensor in A along the time in s

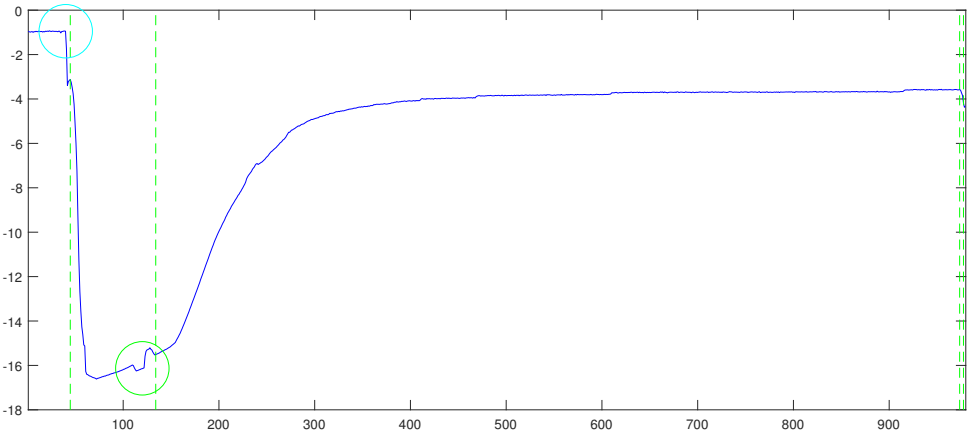

(c) Readings from pressure sensor in 10^3 Pa along the time in s

Figure A.14: Readings from temperature sensor (Top), current flow sensor (middle) and pressure sensor (bottom).
The 50 cent euro coin was grabbed using couscous as grip filler. The x-axis is time and the y-axis is temperature, current and pressure, respectively.
The first green dashed line represents the moment when the gripper was activated and the second the time it was turned off. The cyan and green circles represent the following moments: gripper touches the object and gripper is lifted from the table

A.0.3 Coffee Grain as Filler Material

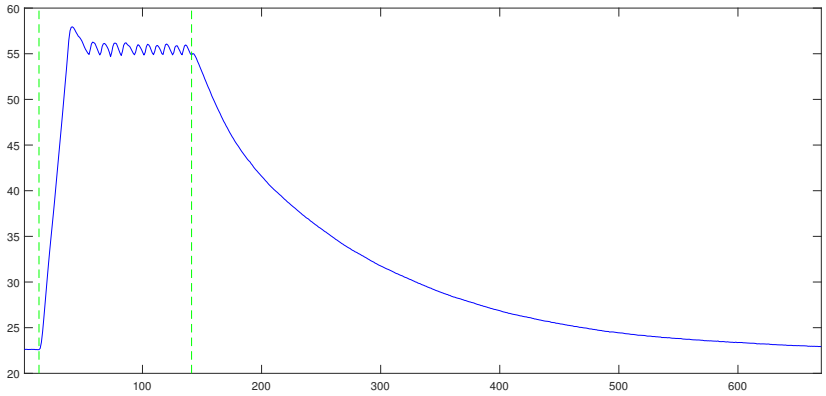

(a) Readings from temperature sensor in ℃ along the time in s

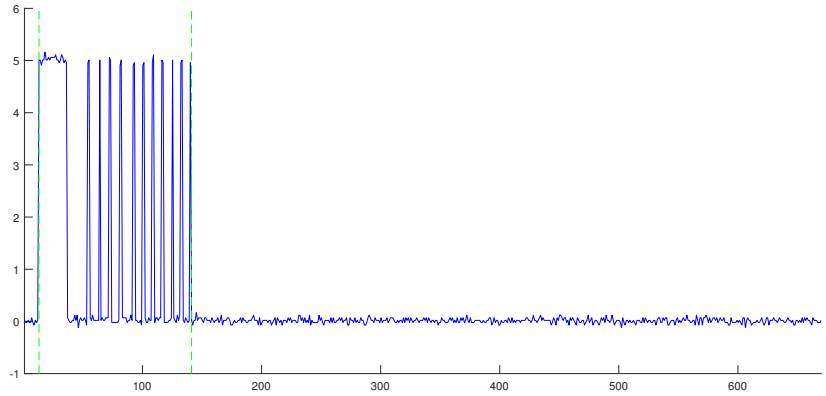

(b) Readings from current flow sensor in A along the time in s

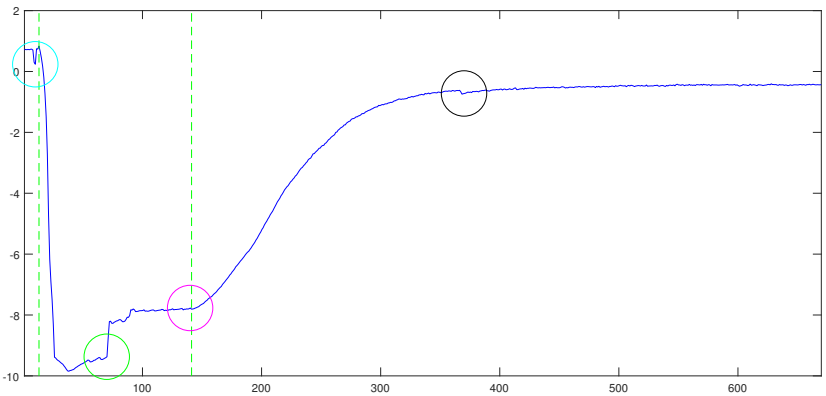

(c) Readings from pressure sensor in 10^3 Pa along the time in s

Figure A.15: Readings from temperature sensor (Top), current flow sensor (middle) and pressure sensor (bottom).
The 50% sized sphere was grabbed using coffee as grip filler. The x-axis is time and the y-axis is temperature, current and pressure, respectively.
The first green dashed line represents the moment when the gripper was activated and the second the time it was turned off. The cyan and green circles represent the following moments: gripper touches the object and gripper is lifted from the table

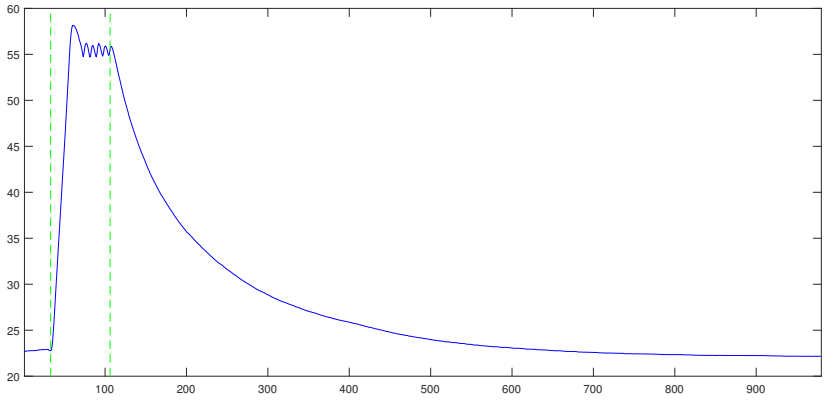

(a) Readings from temperature sensor in ℃ along the time in s

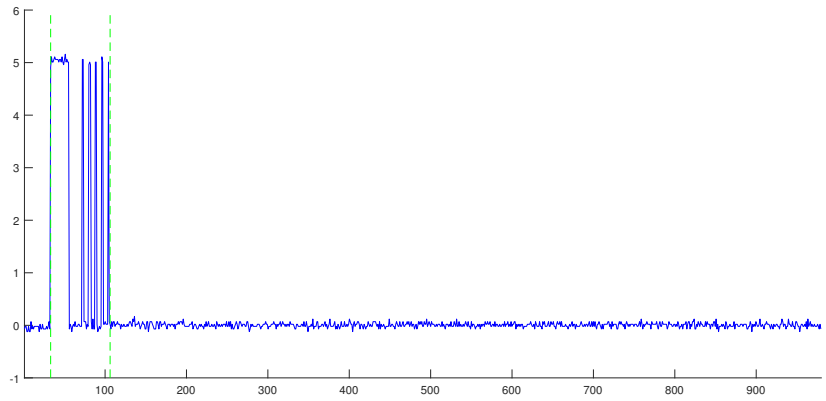

(b) Readings from current flow sensor in A along the time in s

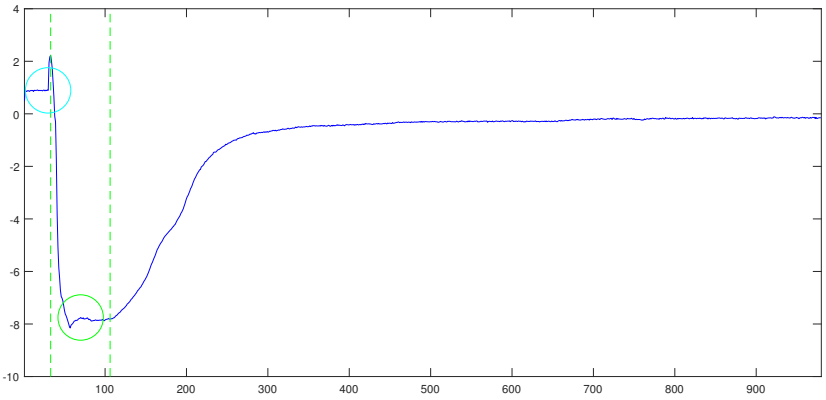

(c) Readings from pressure sensor in 10^3 Pa along the time in s

Figure A.16: Readings from temperature sensor (Top), current flow sensor (middle) and pressure sensor (bottom).
The 75% sized sphere was grabbed using coffee as grip filler. The x-axis is time and the y-axis is temperature, current and pressure, respectively.
The first green dashed line represents the moment when the gripper was activated and the second the time it was turned off. The cyan and green circles represent the following moments: gripper touches the object and gripper is lifted from the table

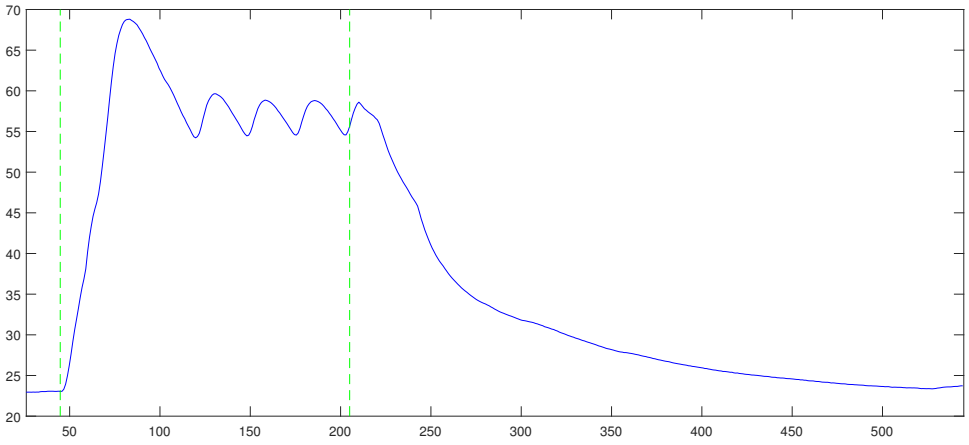

(a) Readings from temperature sensor in ℃ along the time in s

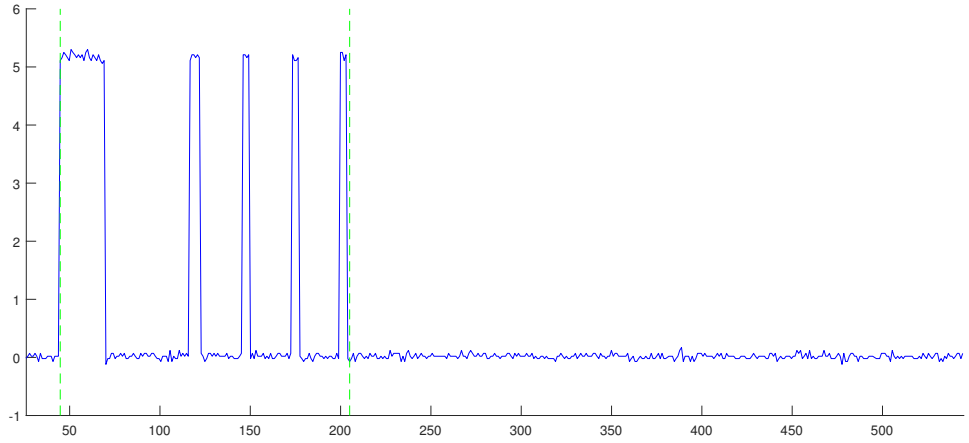

(b) Readings from current flow sensor in A along the time in s

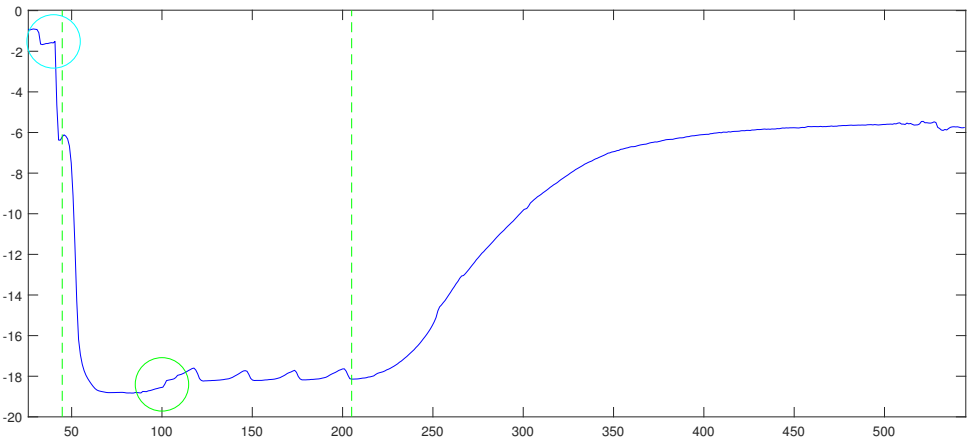

(c) Readings from pressure sensor in 10^3 Pa along the time in s

Figure A.17: Readings from temperature sensor (Top), current flow sensor (middle) and pressure sensor (bottom).
The The 50% sized cube was grabbed using coffee as grip filler. The x-axis is time and the y-axis is temperature, current and pressure, respectively.
The first green dashed line represents the moment when the gripper was activated and the second the time it was turned off. The cyan and green circles represent the following moments: gripper touches the object and gripper is lifted from the table

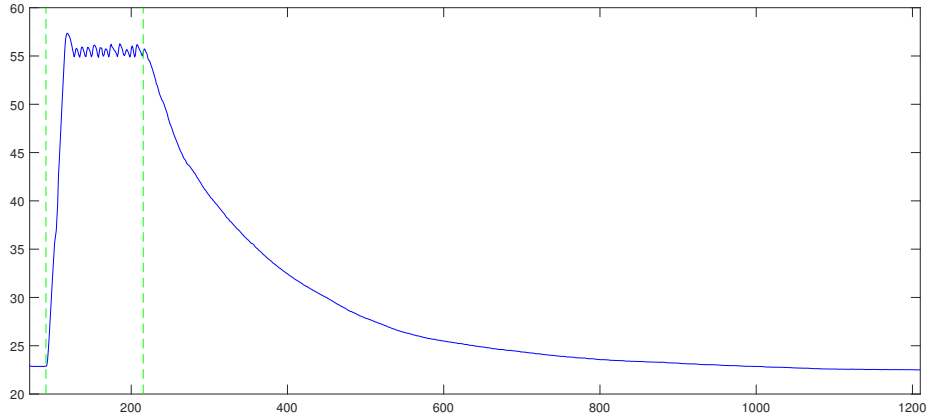

(a) Readings from temperature sensor in ℃ along the time in s

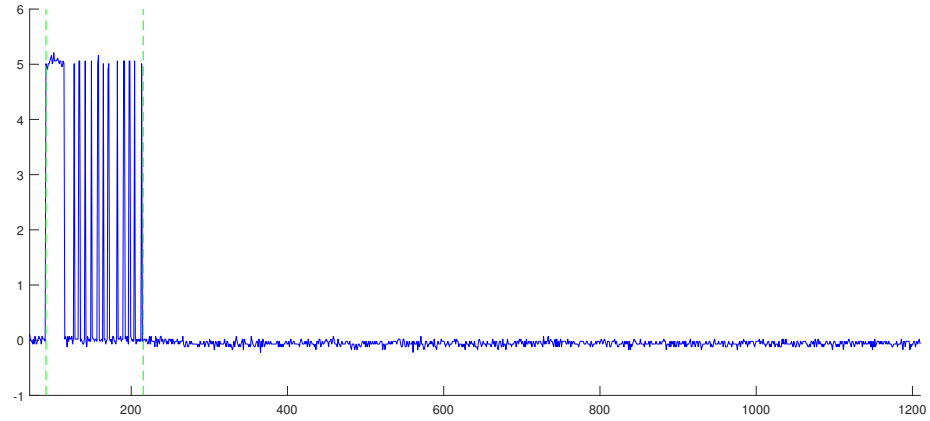

(b) Readings from current flow sensor in A along the time in s

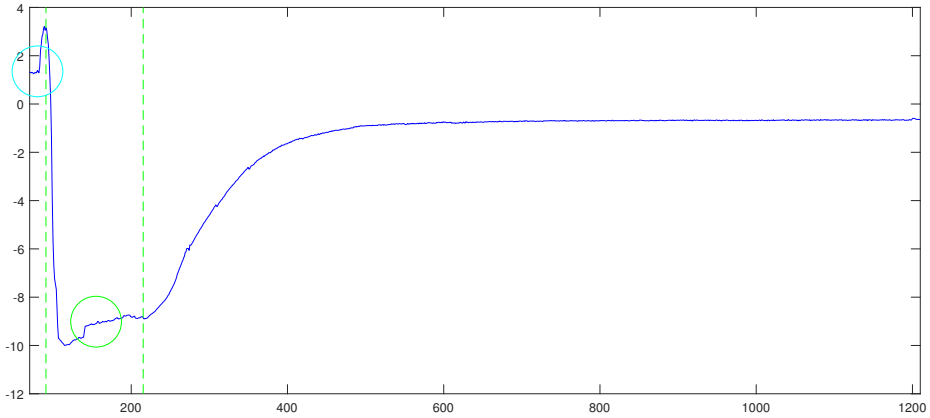

(c) Readings from pressure sensor in 10^3 Pa along the time in s

Figure A.18: Readings from temperature sensor (Top), current flow sensor (middle) and pressure sensor (bottom).
The 75% sized cube was grabbed using coffee as grip filler. The x-axis is time and the y-axis is temperature, current and pressure, respectively.
The first green dashed line represents the moment when the gripper was activated and the second the time it was turned off. The cyan, green and black circles represent the following moments: gripper touches the object, gripper is lifted from the table and piece fells off.

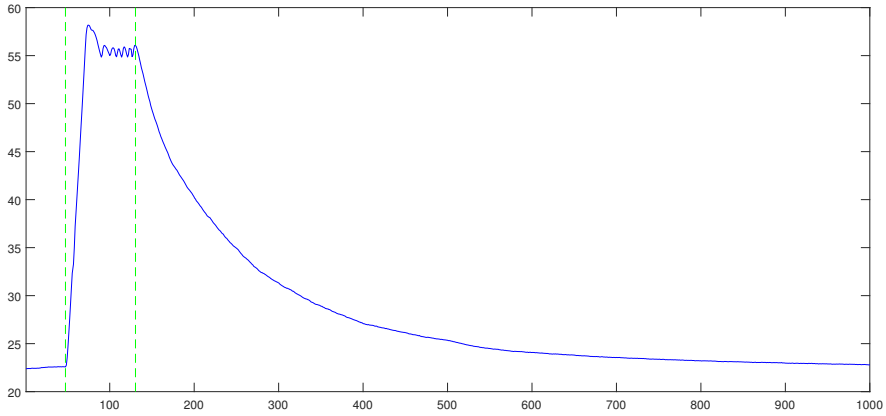

(a) Readings from temperature sensor in ℃ along the time in s

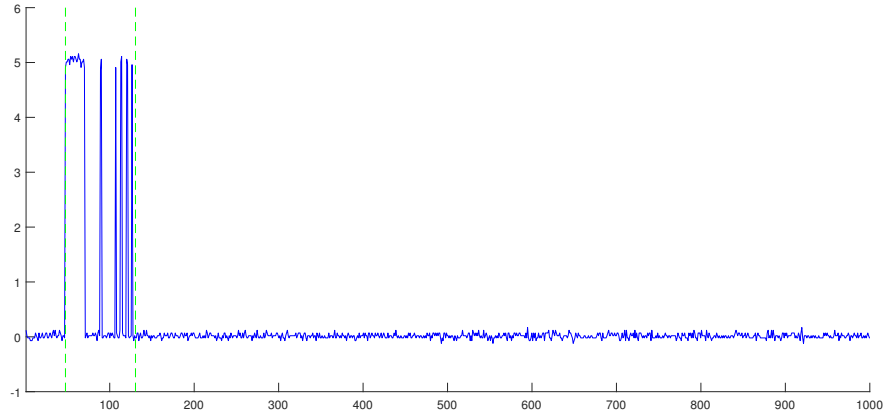

(b) Readings from current flow sensor in A along the time in s

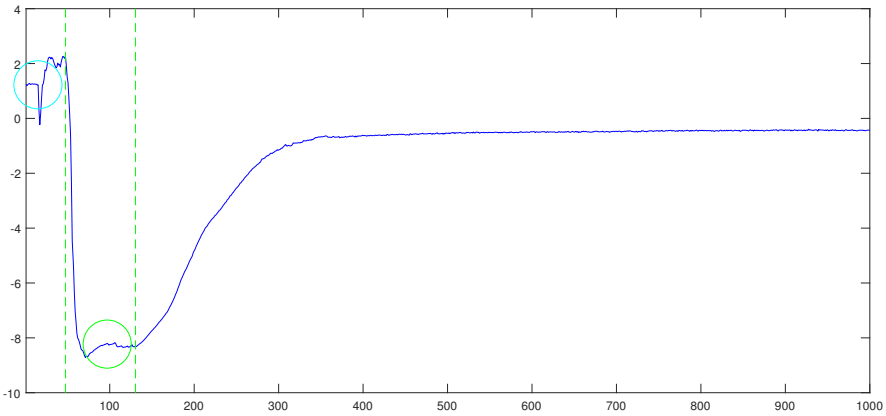

(c) Readings from pressure sensor in 10^3 Pa along the time in s

Figure A.19: Readings from temperature sensor (Top), current flow sensor (middle) and pressure sensor (bottom).
The 50% sized pyramid was grabbed using coffee as grip filler. The x-axis is time and the y-axis is temperature, current and pressure, respectively.
The first green dashed line represents the moment when the gripper was activated and the second the time it was turned off. The cyan and green circles represent the following moments: gripper touches the object and gripper is lifted from the table

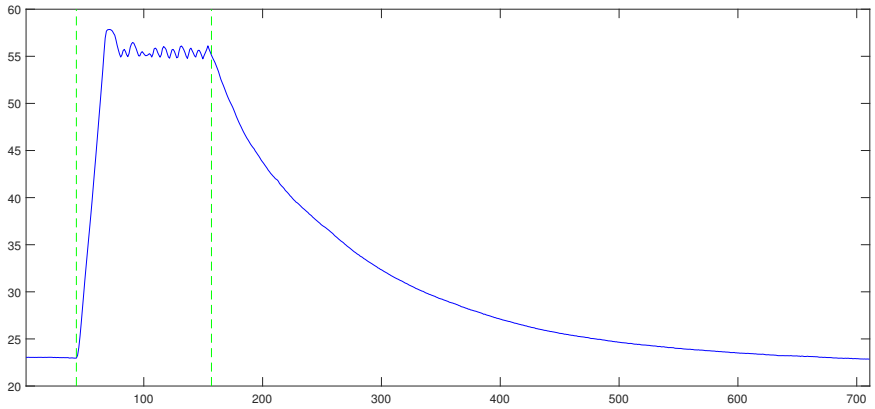

(a) Readings from temperature sensor in °C along the time in s

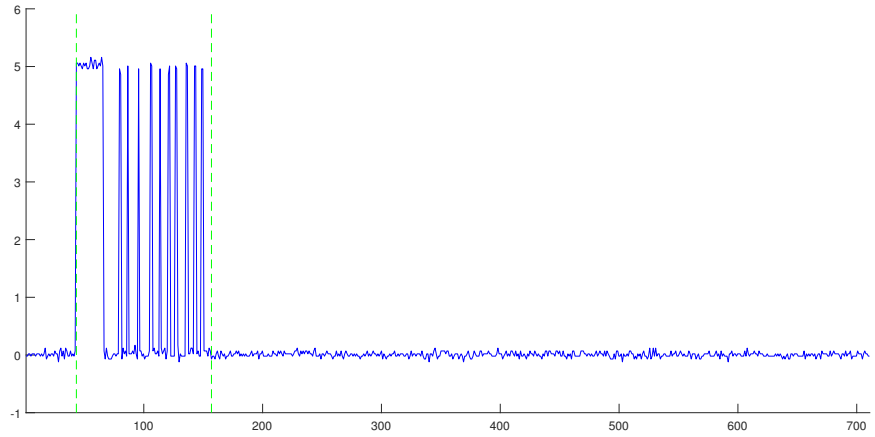

(b) Readings from current flow sensor in A along the time in s

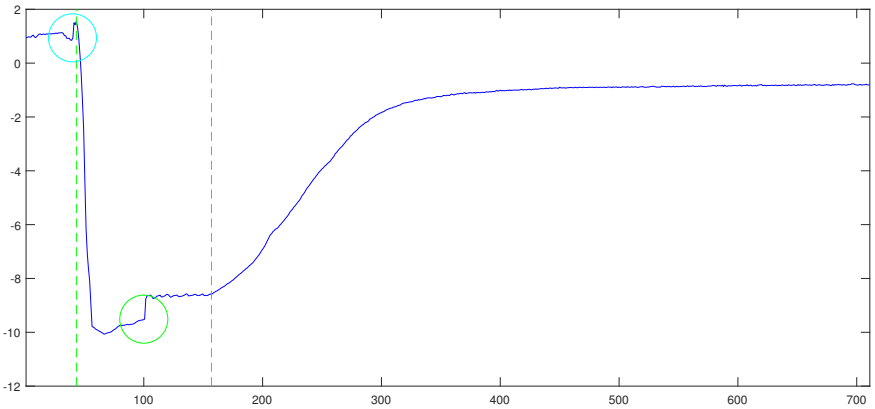

(c) Readings from pressure sensor in 10^3 Pa along the time in s

Figure A.20: Readings from temperature sensor (Top), current flow sensor (middle) and pressure sensor (bottom).
The 75% sized pyramid was grabbed using coffee as grip filler. The x-axis is time and the y-axis is temperature, current and pressure, respectively.
The first green dashed line represents the moment when the gripper was activated and the second the time it was turned off. The cyan and green circles represent the following moments: gripper touches the object and gripper is lifted from the table

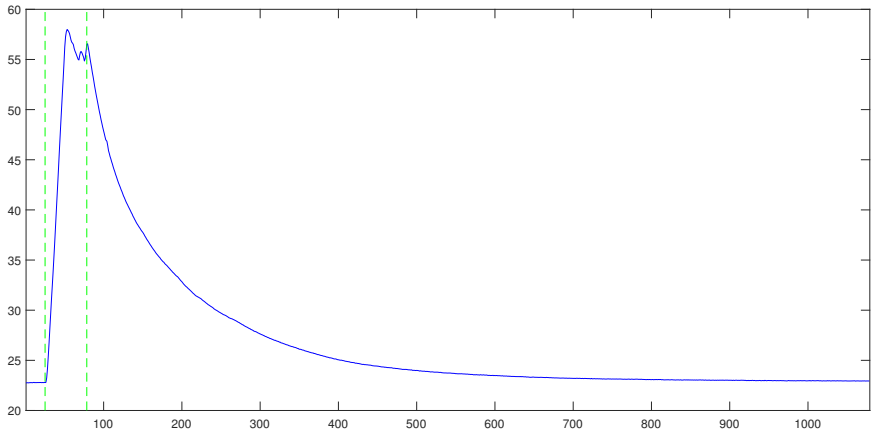

(a) Readings from temperature sensor in ℃ along the time in s

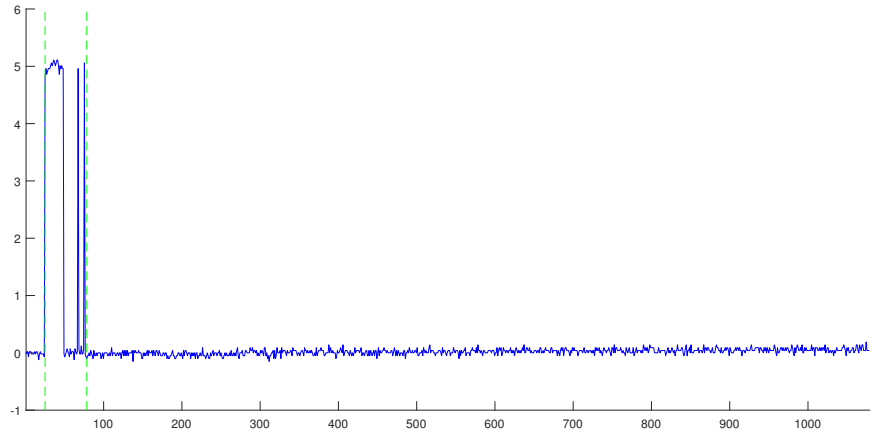

(b) Readings from current flow sensor in A along the time in s

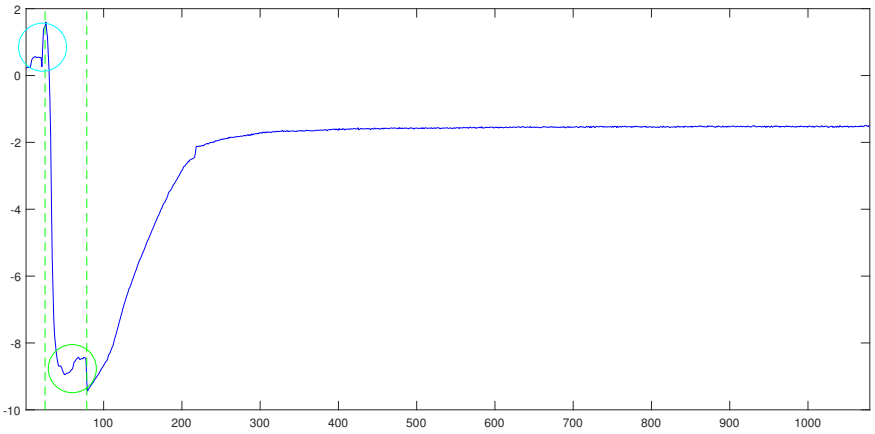

(c) Readings from pressure sensor in 10^3 Pa along the time in s

Figure A.21: Readings from temperature sensor (Top), current flow sensor (middle) and pressure sensor (bottom).
The 50 cent euro coin was grabbed using coffee as grip filler. The x-axis is time and the y-axis is temperature, current and pressure, respectively.
The first green dashed line represents the moment when the gripper was activated and the second the time it was turned off. The cyan and green circles represent the following moments: gripper touches the object and gripper is lifted from the table